Final report

1.1 Project details

Project title	Boosting Economic Electricity STorage (BEEST)
Project identification (program abbrev. and file)	Journalnummer: 64017-0033
Name of the programme which has funded the project	ForskEL
Project managing company/institution (name and address)	DTU Energy (DTU)
Project partners	Blue World Technologies (BWT) Green Hydrogen Systems (GHS)
CVR (central business register)	30060946
Date for submission	15/07/2021

1.2 Short description of project objective and results

1.3 Executive summary

1.4 Project objectives

1.5 Project results and dissemination of results

1.6 Utilization of project results

1.7 Project conclusion and perspective

Annex
Relevant links

1.2 Short description of project objective and results

BEEST has set forward the innovative steps for a gradual transition of the traditional AEC technology towards high conversion efficiencies and production rates while maintaining its reliance on low cost abundant materials. Porous matrix based electrodes are an excellent platform for zero-gap AEC, with the Cathode being rather insensitive to the microstructure of the porous matrix, the main performance driver being the surface area and intrinsic activity of the electrocatalyst. The performance of the Anode on the other hand depends critically on the ability of the porous electrode to promote mass transport of the electrolyte and of the generated O_2 gas.

BEEST har lagt grundlaget for de nødvendige innovative skridt, som forudsættes for en gradvis omlægning af traditionel alkalisk elektrolyse (AEC) mod højere effektivitet og produktionsrater. Dette uden at gå på kompromis med brugen af billige og tilgængelige råmaterialer. Porøse matrix-elektroder har vist sig som en fremragende platform til "nul-gabs" AEC (zero-gap AEC). Mere specifikt, så har katoder vist sig at have lav følsomhed overfor den præcise mikrostruktur, men er derimod stærkt afhængige af elektrodens totale overflade areal og katalysatorens intrinsiske aktivitet. Anoder derimod, afhænger kritisk af deres evne til at fremme massetransporten og dermed udveksling mellem elektrolytten (væske) og den O_2 gas som dannes.

1.3 Executive summary

The overall objective of BEEST was to set forward the innovative steps required for a gradual transition of the traditional AEC technology towards high conversion efficiencies and production rates, while maintaining its reliance on low cost abundant materials, in order to facilitate a stable, flexible, efficient, and highly integrated future Danish energy system relying 100% on renewable energy. Emphasis was placed on the development of 3D porous electrodes for advanced zero-gap AEC, combining large open pores for the escape of the evolved gases and micro- or meso-porosity to increase the electrocatalytically active surface area.

Within the electrocatalyst screening activities in BEEST, we evaluated various synthetic approaches for $Ni_{1-x}Mo_xO_z$ Hydrogen Evolution Reaction (HER) and $Ni_{1-y}Fe_y$ Layered Doube Hydroxide (LDH) Oxygen Evolution Reaction (OER) electrocatalysts. The intrinsic HER activity of $Ni_{1-x}Mo_xO_z$ synthesized hydrothermally, by sol-gel and by co-precipitation, was screened at room temperature in 11.6 M KOH, after reduction in five different temperatures, ranging between 400-800 ºC in steps of 100 ºC, in order to compare the performance of the starting oxide catalyst ($NiMoO_4$) to that of the fully reduced $Ni_{1-x}Mo_x$ alloy, and to assess potential bi-functional benefits in the composite oxide-alloy catalyst produced at intermediate temperatures. Within the uncertainty in the determination of the electrochemically active surface area (ECSA), we found similar intrinsic activity for all the catalysts, regardless of synthesis method and reduction temperature. Amongst the five different synthetic approaches explored for the $Ni_{1-y}Fe_y$ LDH OER catalyst, a mild hydrothermal synthesis at 120 ºC gave both the best intrinsic activity and the best reproducibility at room temperature in 1 M KOH.

One of the underlying hypothesis of BEEST was that 3D extended electrodes can boost electrode performance in comparison to 2D state-of-the-art supports. By testing a broad range of 2D and 3D matrix electrode supports with varying microstructural characteristics under technologically relevant conditions, it was verified that 3D supports generally result in better performance, especially so at higher current densities where bubble escape becomes more important. The difference in performance is quite substantial, resulting in 200-300 mV lower cell voltage for some of the 3D supports vs. the 2D ones at 1 A/cm^2. Controlling the pore size and thickness of the 3D support is nevertheless critical in terms of benefitting from its full potential.

A novel approach to the positioning of two reference electrodes in a zero-gap cell configuration was also developed as a means to gain insight on the contribution of each individual electrode while operating under technologically relevant conditions. A 2D multi-physics simulation model of an AEC was also established in order to gain additional insight on the inner workings of the AEC. The results from these efforts suggest that for technologically relevant KOH concentrations in the electrolyte, the Galvani electric potential drop (ohmic loss) within the cathode is relatively small (even for thick cathodes), resulting in a rather flat overpotential distribution in the cathode. The Anode performance on the other hand is limited to a large extent by transport processes at high current densities. This finding is in line with the outcome from our simulations, and suggests flow field optimization as a critical next step for further optimization of the anode performance, which is currently the main limiting factor in AEC.

This development of a simple and robust method to determine the individual electrode contribution and transport vs. kinetic limitation of the electrodes under realistic conditions is of great advantage for future electrode optimization work, as it enables us to gain faster and deeper insight on the performance (and performance

limitations) and degradation of each individual electrode simultaneously during operation of a zero-gap AEC under technological conditions.

Already at this point, in the study of 3D Ni foam supports, it has become apparent that the Cathode is rather insensitive to the thickness and porosity of the support, whereas the Anode can benefit from the use of relatively thin supports. Nevertheless, additional questions persist in relation to the optimal thickness of the 3D support, porosity, surface area distribution in the volume of the support, etc. More work is clearly required to capture the full potential of 3D porous matrix electrodes.

3D Ni foam supports, hydrothermally coated with $NiMoO_4$, reduced to $Ni_{1-x}Mo_x@MoO_2$ at 550 ºC in 5% H_2, and $Ni_{1-y}Fe_y$ LDH electrocatalysts for HER and OER, respectively, resulted in a combined overpotential of 0.4 V at 1 A/cm^2, overachieving the performance milestone of 0.5 V at 1 A/cm^2 set in BEEST. The hydrothermally produced $Ni_{1-x}Mo_x@MoO_2$ coating was mechanically weak though, but its robustness could be improved by increasing the reduction temperature. Reduction at 650 ºC offered a good compromise between performance and stability.

The hydrothermal approach is nevertheless somewhat challenging in terms of large scale high throughput production of electrodes, since it is a batch process rather than a continuous one, and due to size limitations of hydrothermal reactors. A different approach was thus also developed, based on dip coating of Ni supports using a $NiMoO_4$ containing slurry, employing $NiMoO_4$ nano-powder synthesized via a sol gel route. Due to the very different morphology of the sol gel particles (spherical nanoparticles, as opposed to approx. 10 µm long rods obtained hydrothermally), improved robustness of the coating could be achieved at 550 ºC while maintaining a very high surface area. The optimum coating thickness was evaluated to be approx. 3 µm, resulting in Cathodes with exceptional performance, requiring only 75 mV overpotential for 1 A/cm^2 and 90 mV for 2 A/cm^2.

On the other hand, various attempts to stabilize the $Ni_{1-y}Fe_y$ LDH electrocatalyst (avoiding Fe leaching) were inconclusive, and efforts concentrated in realizing high surface area Anodes with Ni as the electrocatalyst. Although robocasting (3D printing) gave the best results in terms of surface area and performance, dip coating was selected as the route for optimization and scaling up due to its advantages in terms of simplicity and scalability.

BWT concluded that the cost associated with the use of 3D Ni foam as electrode support is acceptable. GHS also concluded that 3D Ni foam based electrodes pose no obstacle for stack integration in terms of in-plane electronic conductivity and welding ability. The dip coating and reduction recipes developed at DTU were shared with BWT who established a pilot scale production for fabrication of such electrodes at larger scale, namely ø30 cm electrodes in quarter-pieces.

Although the low-cost porous electrodes developed by DTU in BEEST met the very ambitious goals set in the project, this performance could not be fully captured upon electrode upscaling. After three iterative improvement cycles of the upscaled Cathodes, their initial performance approached that of the lab scale electrodes, but substantial degradation was observed during continuous operation. The upscaled Anodes showed good stability upon continuous operation, but their performance did not live up to expectations from the lab scale equivalents. Implementation and testing in an industrial stack and system was therefore deemed premature, and the associated project plan was revised. It was decided to assess the durability of the upscaled electrodes under accelerated stress test conditions. This way it was concluded that the $Ni_{1-x}Mo_x$ coating is stable under continuous cathodic polarization, but sensitive to depolarization effects upon discontinuous on/off operation.

GHS has alongside BEEST optimized an in-house method for electrode fabrication on 2D supports. Since work undertaken within BEEST suggested that it is beneficial to employ a 3D porous microstructure for the cathode, GHS attempted to apply

their catalytic coating on the 3D Ni foam used in BEEST. The performance of the 3D Cathode was comparable to that of the 2D one with a similar coating, albeit no optimization of the coating on the 3D support was undertaken, suggesting that there is room for improvement. Stability-wise the 3D Cathode was also proven to be extremely robust under both continuous and discontinuous operation.

BEEST also contributed to a broad range of dissemination activities, among others the organization of the 1st International Conference on Electrolysis (Copenhagen, June 2017, Chaired by DTU Energy), http://www.ice2017.net/Conference, which was a great success with participation of more than 200 people from all over the world, covering both academia and industry. A new conference series dedicated to Electrolysis was thus established, with the 2nd International Conference on Electrolysis being held in Norway (Loen, June 2019), https://www.sintef.no/projectweb/ice2019/, and the 3rd International Conference on Electrolysis planned to take place in Colorado, USA in 2021, but postponed to 2022 because of the global pandemic, https://ice2021.csmspace.com/. BEEST also contributed to the writing of a Book Chapter on "Intermediate Temperature Electrolysers" in Keith Scott (ed.) Electrochemical Methods for Hydrogen Production. Royal Society of Chemistry, 2019, https://pubs.rsc.org/en/content/ebook/978-1-78801-378-9. Furthermore, BEEST results were disseminated through 26 scientific conference contributions and 3 publications in international peer reviewed scientific journals. Drafts for an additional 8 papers have been compiled and will be finalized and submitted for publication within the coming period.

The project results have contributed substantially to the building up of expertise on alkaline electrolysis at DTU Energy. DTU has gained insight in electrocatalysts for HER and OER in alkaline environment and their application in 3D porous electrodes, and has realized methodological improvements in testing zero-gap AEC that offer much greater insight on the inner workings of the AEC performance and degradation characteristics. The latter development, along with a simple multi-physics simulation model of zero-gap AEC, have promoted our understanding of the factors limiting AEC electrode performance. Aspects of the generated results are also integrated in teaching activities.

BWT has also gained precious insight in the field of alkaline electrolysis. The electrode performance and scalability of the developed electrode fabrication method is considered very promising, but further assessment and potential optimization of the electrode stability under varying operating conditions will be required, before demonstration of the technology at industrial scale and subsequent planning of product roll out. A key take-away is the importance of adhesion of the catalyst coating and techniques for improving adhesion will be investigated further. The BEEST project has contributed to improving the GHS electrodes and catalysts and demonstrated the importance of including Universities in the R&D process. GHS will utilise the results gained within electrode support geometry and the driving forces for the electrode performance in order to continuously improve their electrodes.

Although alkaline electrolysis is an established technology, its efficiency at high production rates needs to be improved to reduce the overall levelized cost of hydrogen. Active and stable HER and OER catalysts, based on low-cost abundant materials, are critical for this endeavour. $Ni_{1-x}Mo_xO_z$ has been identified as a good HER candidate, but more work is required to assess its stability upon discontinuous operation. GHS has also developed a well performing non-precious metal HER catalyst that appears to be tolerant to depolarization. A thorough examination of its properties and understanding of its response to electrode potential variations is required for further cathode development. Similarly, $Ni_{1-y}Fe_y$ LDH is indeed an excellent OER catalyst, but further R&D work is required to establish and potentially promote its long-term stability under technologically relevant operating conditions.

Porous matrix based electrodes were proven to be an excellent platform for zero-gap AEC. Within BEEST it was concluded that the Cathode is rather insensitive to the microstructure of the porous matrix, the main performance driver being the surface area and intrinsic activity of the electrocatalyst. Future efforts in cathode development will therefore focus on electrode designs and fabrication methods that can help achieve ultra high surface area cathodes with low-cost catalysts having as high intrinsic activity as possible and sufficient stability under depolarization.
The performance of the anode on the other hand depends critically on the ability of the porous electrode to promote mass transport of the electrolyte and of the generated O_2 gas. As this can also be influenced by the flow field characteristics and the catalyst coating properties, further anode development efforts need to address the topic more holistically. The methodology developed in BEEST that enables to assess experimentally the impact of mass transport on the performance of the anode is an invaluable asset for future development efforts. As the anode constitutes by far the main efficiency loss component at this point, a lot can be gained by its optimization. A combined simulation and experimental approach is required to speed up this complex optimization.

1.4 Project objectives

The overall aim of the project was to develop alkaline electrolysis cells (AEC), which can compete with PEM electrolysis cells (PEMEC) in terms of performance, but at a much lower cost, avoiding the use of expensive and critical raw materials. BEEST intended to set forward the innovative steps required for a gradual transition of the traditional AEC technology towards high conversion efficiencies and power densities, while maintaining its reliance on low cost abundant materials.

Traditional AEC are constructed with a gap-configuration, which implies that there exists a gap of several millimeters between each electrode and the porous diaphragm placed in the electrolyte as a separator, in order to facilitate the removal of the produced gases. This configuration results in a large ohmic drop in the electrolyte, limiting power density and conversion efficiency. PEMEC on the other hand can be operated at much higher current densities since they are built with a zero-gap configuration, with the electrodes in direct contact with the separator and made porous to allow access of the electrolyte and exit of bubbles. Exploiting the full potential of the zero-gap configuration requires that the massive solid electrodes currently used in conventional AEC are replaced by porous electrodes that allow the escape of the produced gasses through their structure. The point of departure in BEEST was that three-dimensional porous electrodes with a bi-modal porosity distribution are ideal for this purpose, combining both large open pores for the escape of the evolved gases and micro- or meso-porosity to drastically increase the electrocatalytically active surface area.

The project objectives (at project start) were:

- To develop 3D porous electrodes for AEC, enabling the transition to an advanced zero-gap configuration.
- To prove cell performance of 2 A cm^{-2} at maximum 2 V (like the PEM electrolyzer bench-mark).
- To make an oxygen evolution electrode capable of operating at 1 A cm^{-2} with a kinetic overvoltage below 400 mV.
- To make a hydrogen evolution electrode capable of operating at 1 A cm^{-2} with a kinetic overvoltage below 100 mV.
- To show a cell durability of 100 h with a decay of less than 10 µV h^{-1}.
- To upscale the developed porous electrodes to a size of 270 cm^2.
- To implement and test the upscaled electrodes in AEC stacks at GreenHydrogen.
- To explore novel alkaline electrolysis cell concepts by combining the developed 3D porous electrodes with advanced separators.
- To develop manufacturing routes for future electrode production.
- To assess the impact of the developed technologies in different business cases.
- To contribute to the arrangement of an international conference on electrolysis in Copenhagen in 2017.

Most of the objectives were indeed met. During the progress of BEEST, BWT and GHS decided in fact to raise the level of ambition with respect to electrode upscaling and testing in a stack, targeting electrodes of a size of 707 cm^2. Nevertheless, the performance and robustness of the upscaled electrodes did not live up to expectations, rendering implementation and testing in an industrial stack premature. This objective was thus revised and increased emphasis was placed on the assessment of the developed electrodes under accelerated stress test conditions. Table 1 below provides an overview of BEEST's Milestones and status by June 1st 2021.

Table 1: *List of Milestones organized by WP and associated success status*

WP1: Catalyst screening	**Status**
M1.1 Selection of electrocatalyst compositions to be tested (M4, DTU)	✓
M1.2 Selection of electrocatalyst compositions to be used for electrode development (M11, DTU)	✓
WP2: Matrix electrodes & WP3: Bonded electrodes (*joint milestones for WP2 and WP3*)	
M2.1 First functional porous electrode (M16, DTU)	✓
M2.2 An oxygen evolution electrode capable of 1 A cm^{-2} at an overvoltage of 0.4 V (M22, DTU)	✓
M2.3 An hydrogen evolution electrode capable of 1 A cm^{-2} at an overvoltage of 0.1 V (M21, DTU)	✓
WP4: Electrode upscaling	
M4.1 Identification of manufacturing technique(s) (M24, BWT)	✓
M4.2 Electrode technology selected (M26, BWT)	✓
M4.3 A full size electrode successfully fabricated (M36, BWT)	✓
WP5: Integration and testing	
M5.1 Successful integration of the new porous electrodes in a GHS cell (M37, GHS)	✓
M5.2 Performance and durability screening of at least 3 zero-gap cells for 350 h each completed (M44→M46, GHS)	✓
M5.3 Durability testing of selected set of electrodes for 1500 h completed (M44→M48, GHS)	✓
WP6: Dissemination	
M6.1 Date and overall plan for workshop/thematic day (M21, DTU)	✓
M6.2 At least eight publications to international peer reviewed scientific journals (M12, M24, M36, DTU)	✗
M6.3 At least six international conference presentations (M12, M24, M36, DTU)	✓

Milestones M2.2 and M2.3 were very ambitious, but nevertheless achieved. During the electrode development efforts, there was no established method to determine the individual electrode overpotential contributions while testing in a zero-gap configuration and under technologically relevant conditions. Therefore, the combined overpotential of both electrodes was used as an indicator of the combined success of M2.2 and M2.3. Efforts were also directed towards covering this methodological gap, as it was realized that it would be very valuable to be able to distinguish the two electrode contributions under real life operation, in terms of speeding up both electrode performance and durability optimization. A simple method was indeed identified, able to provide also insight on the contribution of ionic transport processes (versus charge transfer processes) within the electrodes. Furthermore, it became clear during the electrode development work, that a parallel effort of simulating the processes taking place inside the AEC is important in terms of under-

standing the limiting factors and providing a direction for further cell development. This was initiated within BEEST and was indeed proven very useful.

Challenges were of course observed. The literature on electrocatalysts is immense, and often difficult to compare and deduce conclusions for technological development, due to lack of harmonized testing protocols, testing conditions being far from technological ones, and lack of prolonged durability assessment. Nevertheless, the most interesting groups of materials were identified. Catalyst fabrication was found to critically affect their performance, with certain fabrication methods offering poor reproducibility, thereby challenging catalyst screening and selection. Bonded electrode development was challenged by lack of suitable binders, therefore emphasis was placed on the matrix electrode development line. Mechanical robustness of catalyst coatings under harsh technological conditions is critical but often overlooked in the literature. This required adjustments to the manufacturing process. Electrode up-scaling proved more challenging than anticipated, due to difficulties in obtaining catalyst powders from commercial suppliers matching the quality of lab scale synthesized powders, and due to lack of specialized equipment required for certain steps of the manufacturing process. Such equipment can become available, but additional longterm durability data of the developed electrodes is required before the necessary investment is justified. As the performance and robustness of the upscaled electrodes did not live up to expectations from the lab scale electrodes, implementation and testing in an industrial stack was abandoned and increased emphasis was placed on the assessment of the developed electrodes under accelerated stress test conditions in single cell tests. The aforementioned challenges absorbed more efforts than originally anticipated and resulted in somewhat suppressed focus on scientific dissemination through publications to international peer reviewed journals. M6.2 was thus not achieved, with 3 publications realized within the course of the project, instead of 8 that were planned. The material for an additional 8 publications is nevertheless available and efforts in concluding those are ongoing.

1.5 Project results and dissemination of results

The main activities and technical results in the project are described below, organized by WP for convenience.

WP1: Catalyst screening

WT 1.1 Literature review

It is difficult to accurately compare published data between publications due to varying experimental conditions, as well as differences in the presented figures of merit. The overpotential at 10 mA/cm^2 is the most commonly used figure of merit, typically with the current being normalized to the projected geometrical electrode area, but occasionally with respect to the electrochemically active surface area (ECSA), which is more appropriate in terms of identifying the intrinsic activity of the electrocatalyst.

In recent academic papers, the electrolyte used is commonly NaOH (aq) or KOH (aq) at concentrations of either 0.1 M or 1.0 M, with 1 M KOH (aq) being the most common. The experiments are generally conducted at room temperature. However, in older publications, conditions are often closer to relevant technological conditions, such as temperatures in the range of 50-90°C, and concentrations of up to 6-10 M KOH (aq). Consequently, much published data are not necessarily representative of performance in real systems.

It is unfortunately common in the majority of recent publications, that stability aspects are only vaguely covered and often under conditions less harsh than in real systems. When addressed, it is often under relatively mild conditions (temperature, KOH concentration, polarization), for relatively short duration (10-48 h) and with lacking post-operando characterization. Consequently, most of the novel materials in research literature are still far away from any real applications.

Due to the outlined variations in activity estimates and experimental conditions, literature data is best used to elucidate activity trends and as a starting point for further material development. Moreover, there is a strong need for validation of investigated and developed materials under technological conditions and over prolonged periods of time to assess durability.

An overview of notable electrocatalyst materials, organized by material class, is provided in Tables 2 and 3 for HER and OER, respectively, using the overpotential at 10 mA/cm^2, η_{10}, (unless otherwise specified) and the Tafel slope as figures of merit. A more detailed report of the electrocatalyst literature review carried out in BEEST is provided as Appendix 1.

Table 2: *Reviewed HER performance for electrode materials at ambient and near-ambient temperature. Data for several entries is associated with a large degree of uncertainty with regards to precise overpotentials, either due to data being represented by graphs, or by data referring to reference potentials other than the Reversible Hydrogen Evolution potential at non-standard conditions. Not all materials are labelled with accurate stoichiometry. The "a"-prefix denotes amorphous phase.*

** Is presented as a Cobalt, but clearly contains phosphorous.*

Material	η_{10}	Tafel slope	[KOH/NaOH]	Year
	mV	mV dec^{-1}		
PGM				
Pt/C 20%	10	34	1 M	2016
Pt/C	13	35	1 M	2017
Pt/C	34	34	1 M	2016

Pt	90	32	1 M	2015
Ni / RuO_2	175	-	1 M	2010
Sulfides				
Ni-Ni_3S_2	50	-	1 M	1990
a-NiS_x	50	106.8	28 wt%	2003
a-NiS_xCo_y	50	94.3	28 wt%	2003
NiS / NiS_2	60	99	1 M	2016
a-NiS_x	85	-	1 M	1984
Ni-MoS_2	98	60	1 M	2016
Ni / Ni-FeS	110	62	6 M	1997
NiS	130	83	1 M	2016
Ni_3S_2	223	-	1 M	2015
Phosphides				
Co(P) *	20	42.6	1 M	2017
$NiCoP_2$	87	59	1 M	2017
Ni_5P_4	150	53	1 M	2015
CoP	158	58	1 M	2017
CoP	209	129	1 M	2014
FeP	218	146	1 M	2014
Nickel-molybdenum				
$MoNi_4$ / MoO_2	15	30	1 M	2017
$MoNi_4$ / MoO_2	17	36	1 M	2017
$MoNi_4$ / MoO_2	28	36	1 M	2017
NiMo-NW	30	86	1 M	2016
Ni-Mo	34	-	1 M	2014
MoO_2	55	66	1 M	2015
Ni-Mo	70	-	2 M	2013
Raney Nickel				
Ni-Al	15	-	30 wt%	2013
Ni-Al-Mo	150	150	38 wt%	2011
Ni-Al-Mo	<60	99	1 M	2004
Ni-Al	<50	121	1 M	1993
Other				
Co-Mo-B	66	67	1 M	2017
Ni-Sn	80	86	30 wt%	2016
$NiFeO_x$	88	-	1 M	2015
NiSe	96	120	1 M	2015
MoC_x	151	59	1 M	2015
Mo_2C	190	54	1 M	2012
MoB	225	59	1 M	2012

Table 3: *Reviewed OER catalysts. GC = glassy carbon (electrode), + C = mixed with carbon, CFP = carbon fibre paper. Publications labelled their investigated materials differently, and the listed 'Material' is not always stoichiometrically accurate, but resembles what is used in the given publication.*

Material	Support	η_i	Tafel slope	[KOH / NaOH]	Year
		mV	mV dec^{-1}		
Perovskites		***@ 1 mA cm^{-2}***			
$Ba_{0.5}Sr_{0.5}Co_{0.8}Fe_{0.2}O_3$	GC	330	-	0.1 M	2011
$Ho_{0.5}Ba_{0.5}CoO_3$	GC + C	330	-	0.1 M	2013
$Pr_{0.5}Ba_{0.5}CoO_3$	GC + C	330	-	0.1 M	2013
$Ba_{0.5}Sr_{0.5}Co_{0.8}Fe_{0.2}O_3$	GC + C	360	-	0.1 M	2013
$Sm_{0.5}Ba_{0.5}CoO_3$	GC + C	360	-	0.1 M	2013
$Gd_{0.5}Ba_{0.5}CoO_3$	GC + C	370	-	0.1 M	2013
$La_{0.5}Ca_{0.5}FeO_3$	GC	390	-	0.1 M	2011
$LaCoO_3$	GC + C	410	-	0.1 M	2013
$La_{0.5}Ca_{0.5}CoO_3$	GC	420	-	0.1 M	2011
$LaCoO_3$	GC	450	-	0.1 M	2011
$LaNiO_3$	GC	450	-	0.1 M	2011
Spinels		***@ 100 mA cm^{-2}***			
$NiCo_2O_4$	Graphite	184	-	1 M	2011
La-Co_3O_4	Ni support	230	55	1 M	2007
$NiFe_{1.2}Cr_{0.8}O_4$	Ni support	285	40	1 M	2006a
$CoFe_{1.2}Cr_{0.8}O_4$	Ni support	312	42	1 M	2002
$MnFe_{1.4}Cr_{0.6}O_4$	Ni support	330	35	1 M	2006
$NiFe_2O_4$	Ni support	352	40	1 M	2006a
$NiFe_{1.5}V_{0.5}O_4$	Ni support	380	40	1 M	2010
$NiFeVO_4$	Ni support	400	40	1 M	2010
$CuFe_{1.2}Cr_{0.8}O_4$	Ni support	428	50	1 M	2007
Hydroxides	***@ GC***	**@ 10 mA cm^{-2}**			
G-CoFeW	GC	223	37	1 M	2016
NiFeMn-LDH	GC	262	47	1 M	2016
Ni-Fe	GC + C	262	49.7	1 M	2017
NiFeCr-6:2:1	GC	280	131	1 M	2018
$Ni_{0.75}V_{0.25}$	GC	300	50	1 M	2016
NiFe-3:1	GC	322	144	1 M	2018
FeCo-LDH	GC	331	85	1 M	2016
$Ni_{0.75}Fe_{0.25}$	GC	335	64	1 M	2016
Hydroxides	***@ Foam***	**@ 10 mA cm^{-2}**			
G-CoFeW	Au/Ni foam	191	-	1 M	2016
NiFeV-LDH	Ni foam	192	42	1 M	2018
$Ni_{0.8}Co_{0.2}Fe_{0.1}$-LDH	Ni foam	220	42	1 M	2015
Ni-Fe	Ni foam	244	32	1 M	2016

FeCo-LDH	Au/Ni foam	279	-	1 M	2016
Ni-Fe/$NiCo_2S_4$	Ni foam	201 @60mAcm^{-2}	46.3	1 M	2017
Ni-Fe	Ni foam	260 @60mAcm^{-2}	57.7	1 M	2017
Sulfides		**@ 10 mA cm^{-2}**			
NiS_x	Ni foam	180	96	1 M	2016
$Fe_{17.5\%}$-Ni_3S_2	Ni foam	214	42	1 M	2018
$Ni(Fe)S_2$	GC + C	230	42	1 M	2017
Ni_3S_2	Ni foam	287	82	1 M	2018
$Fe_{0.1}$-NiS_2	Ti mesh	231 @100mAcm^{-2}	43	1 M	2016
$NiCo_2S_4$	Ni foam	306 @60mAcm^{-2}	56.8	1 M	2017
NiS_2	Ti mesh	420 @100mAcm^{-2}	83	1 M	2016
Selenides		**@ 10 mA cm^{-2}**			
$CoNi_2Se_4$	CFP	160	72	1 M	2017
$Ni_xFe_{1-x}Se_2$	Ni foam	195	28	1 M	2016
$NiSe_2$	Ni foam	241	54	1 M	2016
NiSe	Ni foam	253	45	1 M	2016
$Ni_{0.85}Se$	Graphite	302	81	1 M	2016
NiSe	Ni foam	270 @20mAcm^{-2}	64	1 M	2015
Other		**@ 10 mA cm^{-2}**			
NiTe	Ni foam	262	74	1 M	2018
$CoTe_2$	Ti mesh	340 @50mAcm^{-2}	67	1 M	2018
Ni_2P	GC	290	47	1 M	2015
RuO_2	Ti mesh	278 @100mAcm^{-2}	61	1 M	2016
IrO_x	Ni foam	347	107	1 M	2018
RuO_2	GC + C	350	90.3	1 M	2017

Looking through the available literature, some trends present themselves for both the cathodic HER and the anodic OER.

In terms of HER, nickel-molybdenum systems generally come out on top. Although the Ni-Mo system has seen increasing interest, questions remain in terms of stability and active sites. The degree of Mo leaching or oxidation on depolarization is a possible concern. Furthermore, the active sites and optimal catalyst structure remain far from understood. Although alternative interesting catalysts exist besides Ni-Mo and platinum, such as amorphous nickel-sulfide, and perhaps cobalt-phosphide, it was decided to pursue the Ni-Mo system as it consistently shows good activity across most published literature.

The OER is more complex, but the current prevailing trend in literature is to prepare nickel-iron-containing materials. Initially as pristine nickel-iron-hydroxides such as the Ni-Fe-LDH, and more recently in the form of e.g. sulfides or selenides, which generally present even higher activity. What is most critically lacking currently, is information on the behavior under technological conditions, and the possible adverse effects of iron leaching. It seems prudent to pursue a plain oxide/hydroxide nickel-iron structure before looking into sulfurized versions of the material. Even among spinel structures, the mixed Ni-Fe-spinels display good activity. A further trend is the positive effects of introducing chromium to the Ni-Fe catalysts. This appears to improve activity of Ni-Fe based catalysts, both when prepared as

spinels, as LDH, or in a less specified manner, even if it is a result of Cr-leaching and increased effective surface area.

WT 1.2 Electrocatalyst testing

Within the electrocatalyst screening activities in BEEST, we evaluated a diverse range of synthesis methods for $Ni_{1-x}Mo_x$ alloys and $Ni_{1-y}Fe_y$ LDH. The as-synthesized electrocatalysts were tested in the same way as thin-film electrodes. This facilitates a fair comparison between the different synthesis methods, supressing effects of electrode microstructure. The intrinsic activity of the electrocatalysts was evaluated by normalizing to their ECSA, and compared to state-of-the-art Ni.

$Ni_{1-x}Mo_x$ alloys were synthesized in three different ways, hydrothermally, by a sol-gel method, and by co-precipitation, resulting in substantially different powder morphology, as shown in Figure 1. Hydrothermal synthesis results in 10-15 µm long beams with an approx. square cross section of 0.2-1 µm edge length. Sol-gel and co-precipitation on the other hand result in spherical nanoparticles of 100- 200 nm and 100-700 nm diameter, respectively.

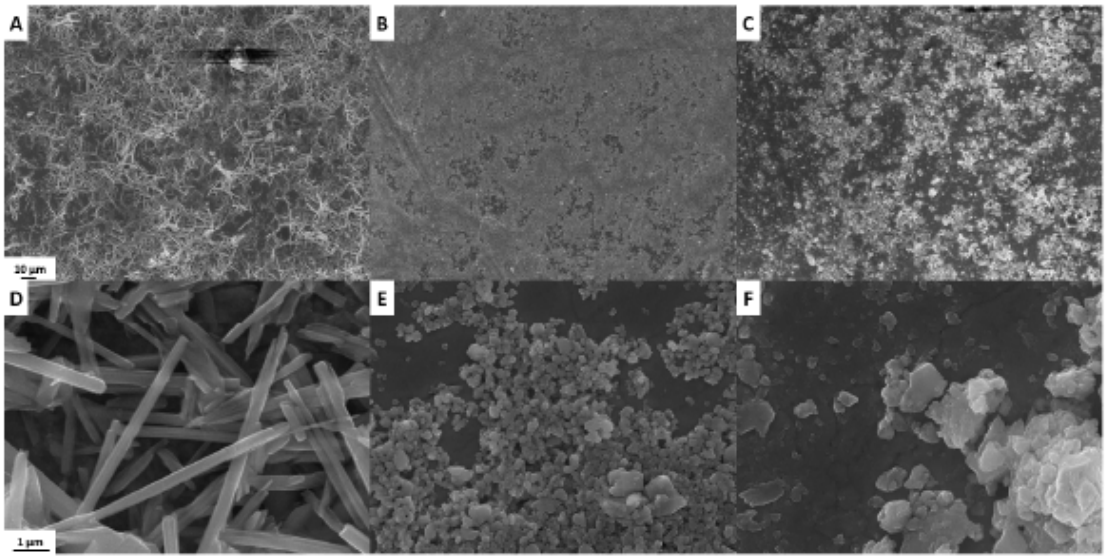

Figure 1: *SEM micrographs of $NiMoO_4$ powders synthesized by hydrothermally (A, D), by a sol-gel method (B, E), and by co-precipitation (C, F).*

As the reduction of $NiMoO_4$ to $Ni_{1-x}Mo_x$ in sensitive to pO_2 and T, with the possible formation of intermediate oxides and ordered alloys, this was followed in-situ by X-Ray Diffraction under controlled temperature in 5% H_2 and 3% H_2O (balance Ar). Broadly speaking, a similar behaviour was observed for all three powder types, consisting of $NiMoO_4$ and other oxides and amorphous contributions originally, forming mainly $NiMoO_4$ when heated to 400 ºC, gradually being reduced to mixtures of $NiMoO_{4-\delta}$ and $Ni_{1-x}Mo_x$ up to 600 ºC, above which only $Ni_{1-x}Mo_x$ alloys are detected. This behaviour was confirmed also by SEM of electrodes reduced at different temperatures in 5% H_2 and 3% H_2O (balance Ar), as shown in Figure 2.

Figure 2: *SEM micrographs of hydrothermally produced $NiMoO_4$ powders reduced in 5% H_2 and 3% H_2O (balance Ar) at 400 ºC (A), 600 ºC (B), and 800 ºC (C).*

The intrinsic HER activity of $Ni_{1-x}Mo_x$ alloys synthesized by the three approaches mentioned, was screened at room temperature (ca. 20 ºC) in 11.6 M KOH, after reduction of the thin film electrodes (produced by drop casting of a small amount of catalyst powder on Ni foil) in five different temperatures, ranging between 400-800 ºC in steps of 100 ºC, in order to compare the performance of the starting oxide catalyst ($NiMoO_4$) to that of the fully reduced $Ni_{1-x}Mo_x$ alloy, and to assess potential bi-functional benefits in the composite oxide-alloy catalyst produced at intermediate temperatures. Within the uncertainty in the determination of the ECSA, we found similar intrinsic activity for all the catalysts, regardless of synthesis method and reduction temperature, as shown in Figures 3-5. This dependene of the performance on ECSA is clearly observed in Figure 6, showing the decrease in η_{10} with respect to the increasing surface area enhancement. Interestingly, the slope of the data matches the anticipated Tafel slope of Ni (100-125 mV/dec). This is anticipated for thin film electrodes, with catalysts of similar intrinsic activity, where the performance is indeed dominated by the actual surface area.

This performance is in fact similar to that of fresh Ni. However, we find that the performance of Ni degrades in the first minutes of electrolysis, something that has also been reported in the literature. Such degradation was not observed for the $Ni_{1-x}Mo_x$ electrocatalysts.

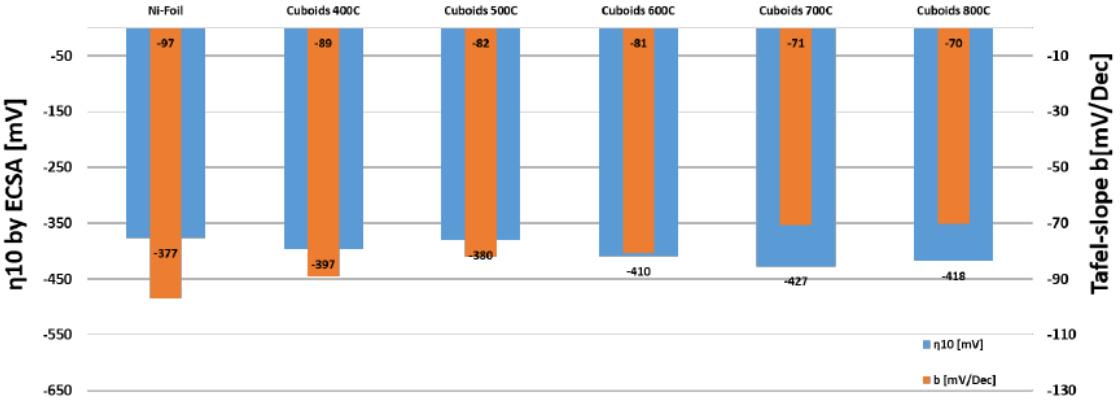

Figure 3: *The overpotential (blue) at an intrinsic current density of 10 mA/cm² (η_{10}) and the corresponding Tafel-slopes (orange) of $Ni_{1-x}Mo_x$ electrocatalysts synthesized hydrothermally and reduced at five different temperatures in comparison to the best achieved fresh Ni-foil test. The tests were conducted in 11.6 M KOH at room temperature.*

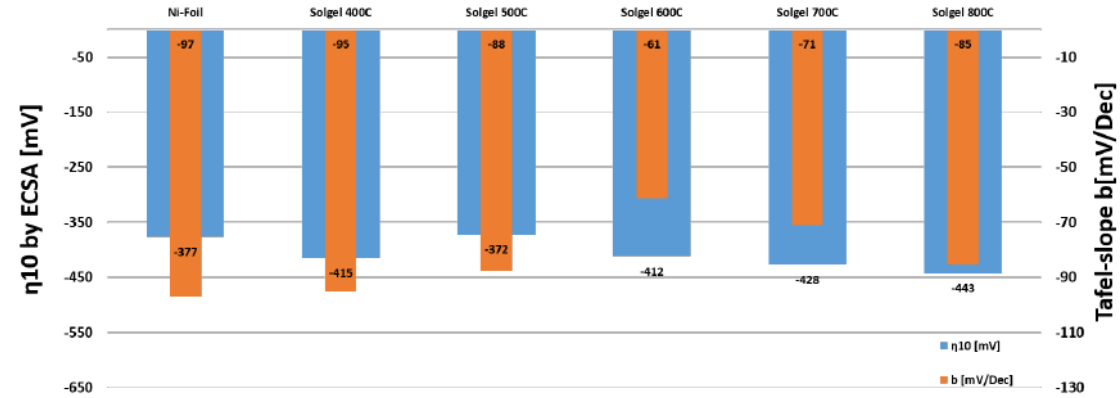

Figure 4: *The overpotential at an intrinsic current density of 10 mA/cm² (η_{10}) and the corresponding Tafel-slopes of $Ni_{1-x}Mo_x$ electrocatalysts synthesized by a sol-gel method and reduced at five different temperatures in comparison to the best achieved fresh Ni-foil test. The tests were conducted in 11.6 M KOH at room temperature.*

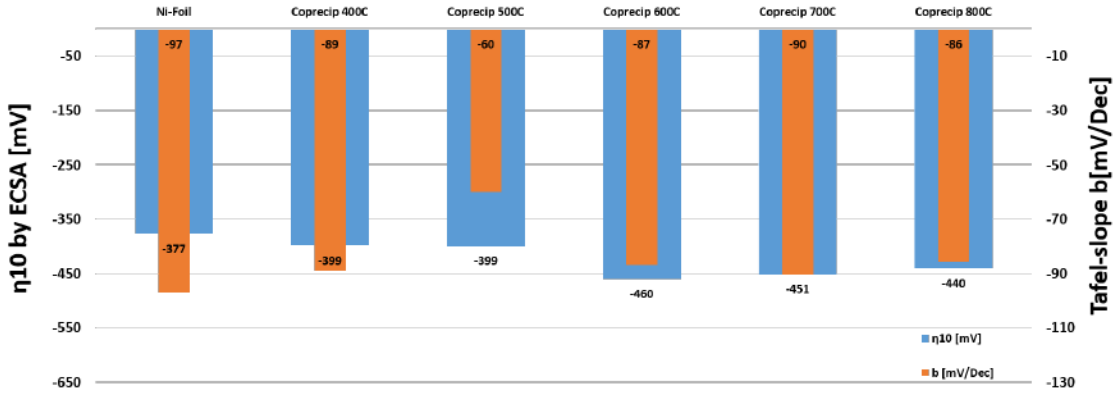

Figure 5: *The overpotential at an intrinsic current density of 10 mA/cm² (η_{10}) and the corresponding Tafel-slopes of $Ni_{1-x}Mo_x$ electrocatalysts synthesized by co-precipitation and reduced at five different temperatures in comparison to the best achieved fresh Ni-foil test. The tests were conducted in 11.6 M KOH at room temperature.*

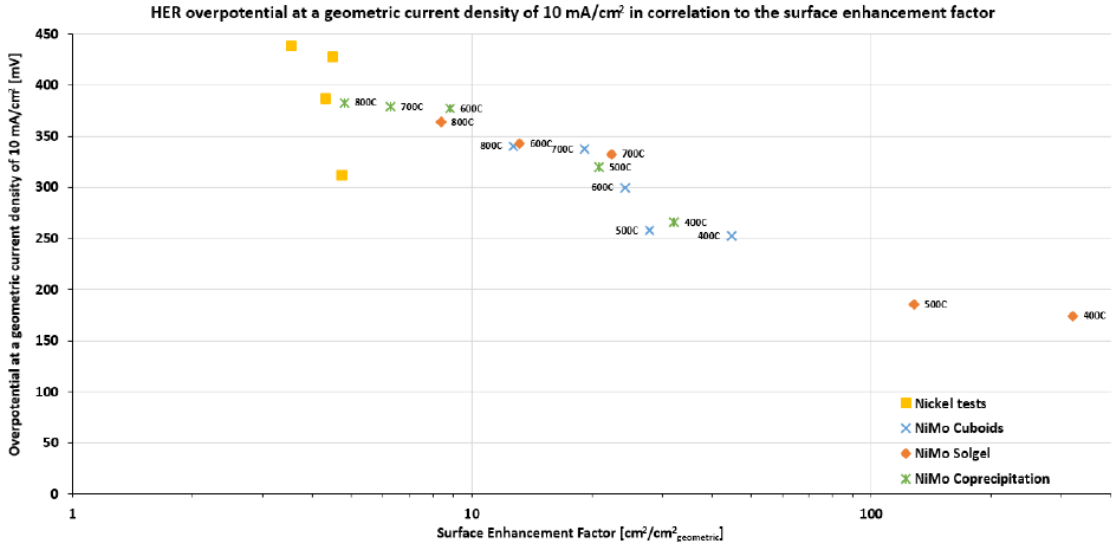

Figure 6: *The HER overpotential at a geometric current density of 10 mA/cm² (η_{10}) for the 15 different $Ni_{1-x}Mo_x$ electrocatalysts and of pure Ni foil tests with respect to the surface enhancement factor. The tests were conducted in 11.6 M KOH at room temperature.*

The development of $Ni_{1-y}Fe_y$ LDH OER electrocsatalysts for the anode has been less conclusive. We have observed, in accordance with literature, a notable intrinsic performance gain from NiFe LDH relative to Ni in 1 M KOH, and confirmed that high ECSA can be achieved by hydrothermal synthesis. We have also faced reproducibility issues though with the hydrothermal synthesis, which triggered a more careful examination of synthetic approaches. Figure 7 compares the intrinsic activity of $Ni_{1-y}Fe_y$ LDH to that of Ni for the different synthetic approaches explored.

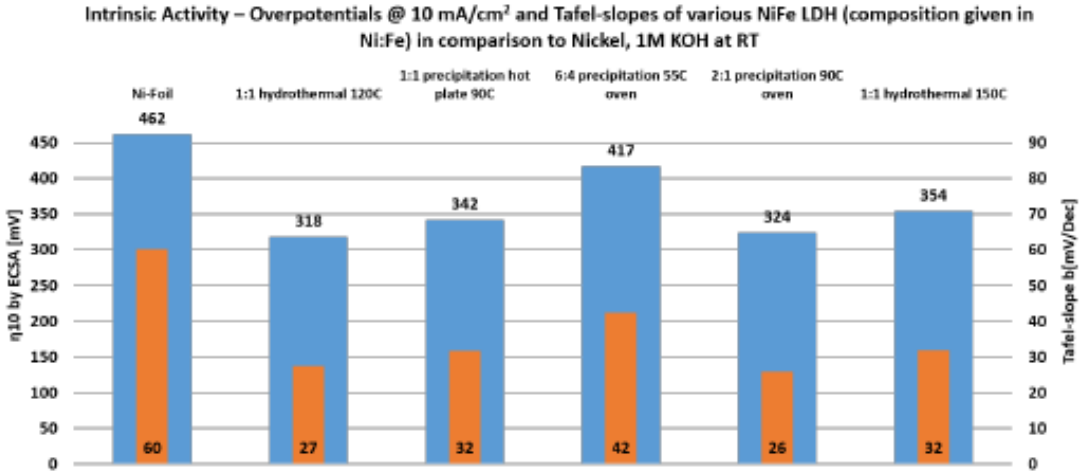

Figure 7: *The overpotential at an intrinsic current density of 10 mA/cm² (η_{10}) and the corresponding Tafel-slopes of $Ni_{1-y}Fe_y$ LDH electrocatalysts synthesized by different approaches in comparison to Ni. The tests were conducted in 1 M KOH at room temperature (to facilitate comparison with literature).*

The mild hydrothermal synthesis at 120 ºC gave both the best intrinsic activity and the best reproducibility, and was thus selected for electrode fabrication and testing in WP2. One of the main concerns with the use of $Ni_{1-y}Fe_y$ LDH is their stability under technologically relevant conditions. This was addressed to some extent in WP2 and is discussed later on in this report.
More detailed information on the electrocatalyst screening efforts carried out in BEEST can be found in Appendix 2.

WP2: Matrix electrodes

Electrodes for zero-gap configuration need to be porous to facilitate the escape of evolved gases from their back side. One of the underlying hypothesis of BEEST was that 3D extended electrodes can boost electrode performance in comparison to 2D state-of-the-art supports. 2D and 3D matrix electrode supports with varying microstructural characteristics were selected and tested, in order to assess this hypothesis. Figure 8 provides a collection of micrographs of the different supports that were examined, and Figure 9 provides an overview of their performance in symmetric zero-gap AEC tests at 80 ºC, 1 bar, and 20 wt% KOH (pre-electrolyzed). The tests were carried out with 10 cm^2 size cells, in a flow cell under continuous and separate flows of anolyte and catholyte of 75 Nml/min.

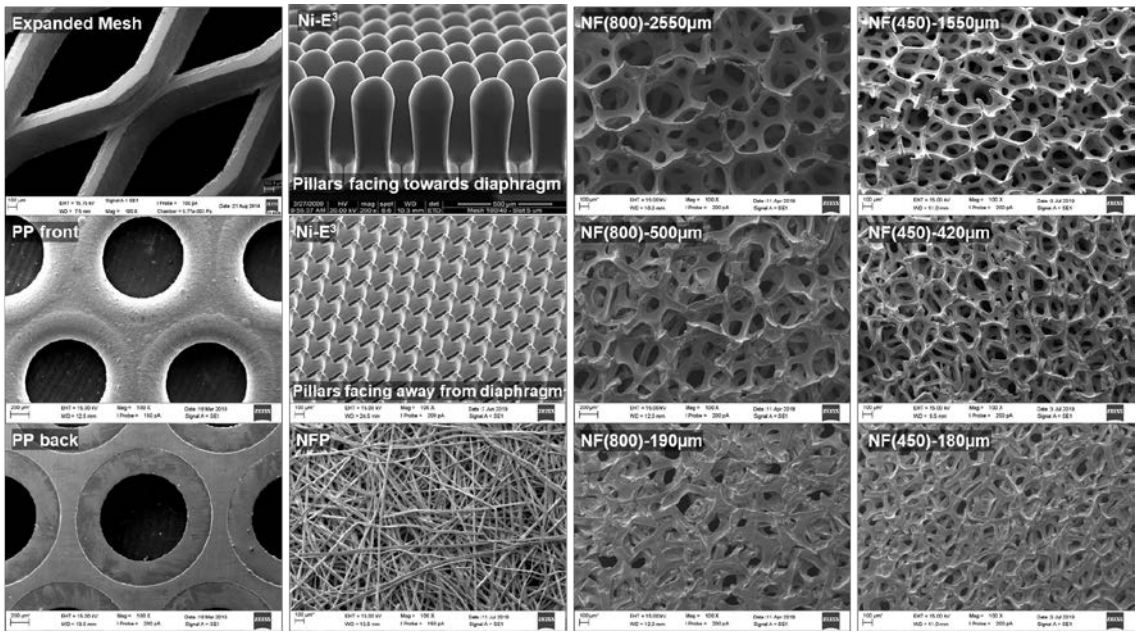

Figure 8: *SEM micrographs of 2D (Expanded Mesh, Perforated Plate (PP)) and 3D (Ni-E^3, Ni felt paper (NFP), and Ni foams (NF) of pore diameter 800 or 450 µm, having a thickness of 2550 and 1550 µm, respectively, as received, or compressed to ca. 450 µm and 200 µm) supports examined in BEEST.*

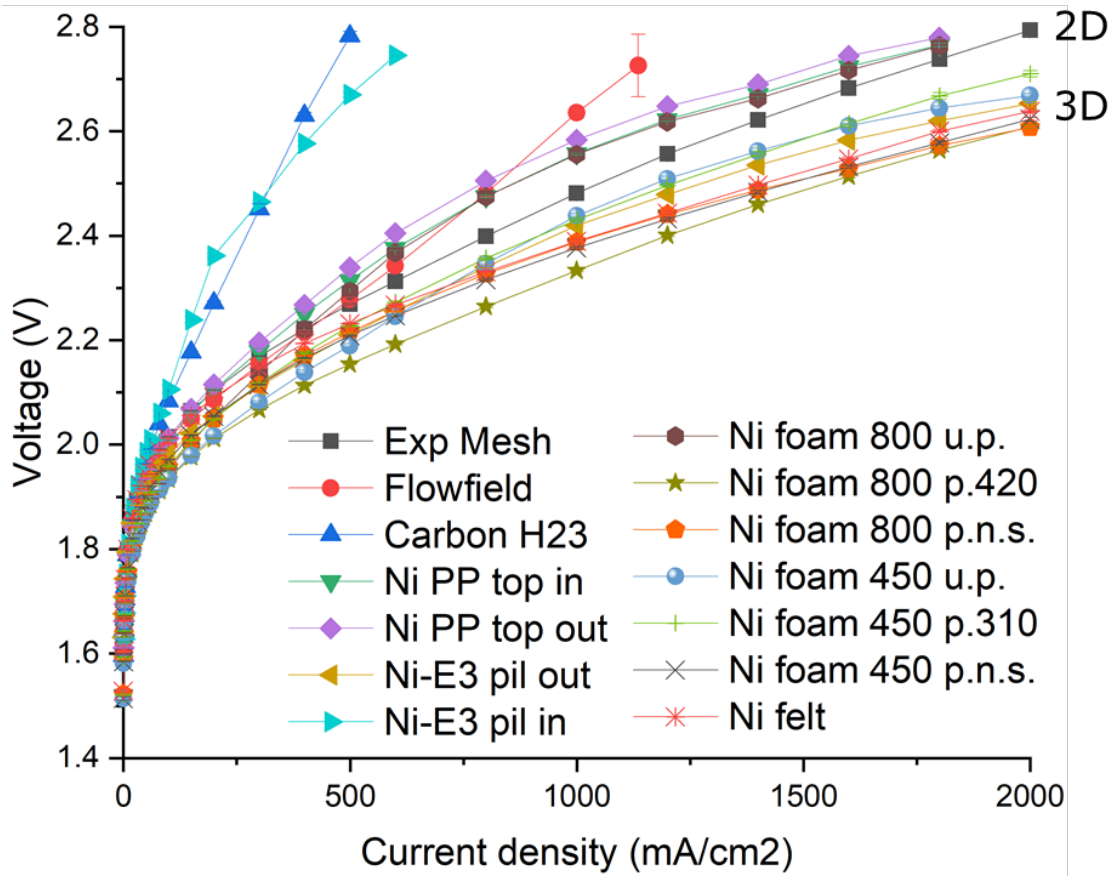

Figure 9: *I-V curves of symmetric AEC cells comprising different 2D or 3D porous supports as electrodes and a 132 µm microfiltration membrane as diaphragm. The tests were carried out in a flow cell under continuous and separate flows of anolyte and catholyte of 75 Nml/min, and at 80 ºC, 1 bar, and 20 wt% KOH (pre-electrolyzed).*

As can be seen from Figure 9, 3D supports generally result in better performance, especially so at higher current densities where bubble escape becomes more important. The difference in performance is quite substantial, resulting in 200-300 mV lower cell voltage for some of the 3D supports vs. the 2D ones at 1 A/cm^2. For a

fair comparison between different support topologies, the surface area of the supports should be kept similar. The surface area of the different supports was estimated from the value of the double layer capacitance of the cathode, determined by electrochemical impedance spectroscopy during operation at 0.5-1 A/cm^2. The 3D supports tested had ca. 2x higher surface area than the 2D supports. This is a relatively small difference, considering that approx. 10x larger surface area would be required to account for the measured improvement in performance. This suggests that the 3D topology is indeed advantageous.

An interesting observation is that compressing the Ni foam 3D supports is important in terms of achieving improved performance, especially for the coarser foam. This can be seen more clearly in Figure 10, where the I-V of the coarse and fine Ni-foam based cells is compared at different levels of compression of the original foam structure.

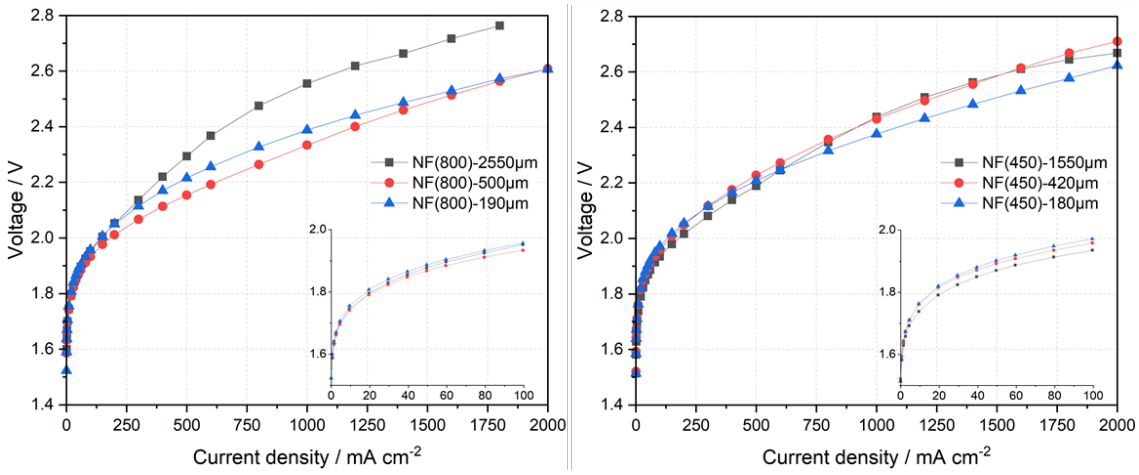

Figure 10: *I-V curves of symmetric AEC cells comprising coarse or fine Ni-foam supports at different levels of compression as electrodes and a 132 µm microfiltration membrane as diaphragm. The tests were carried out in a flow cell under continuous and separate flows of anolyte and catholyte of 75 Nml/min, and at 80 ºC, 1 bar, and 20 wt% KOH (pre-electrolyzed).*

Several questions arise in relation to these observations; the most pressing one relates to whether the improvement is similar for both cathode and anode, or whether one of the electrodes benefits less or perhaps even performs worse when shifting its topology from 2D to 3D. In order to address this question, we need to be able to separate the contribution of each one of the two electrodes while operating the AEC under relevant operating conditions and in a zero-gap configuration.

A novel approach to the positioning/utilization of reference electrodes in a zero-gap cell configuration was thus explored as a means to gain insight on the contribution of each individual electrode while operating under technologically relevant conditions. A 2D multi-physics simulation model of an AEC was also established as a means to support this effort and in order to gain additional insight on the inner workings of the AEC. This model suggested that for technologically relevant KOH concentrations in the electrolyte, the Galvani electric potential drop (ohmic loss) within the cathode is relatively small (even for thick cathodes), resulting in a rather flat overpotential distribution in the cathode. This opens up the possibility to place a reference electrode in the flow channel behind the cathode to measure its overpotential without disturbing the current flow or ohmic contribution (and gas separation ability) of the diaphragm in a zero-gap configuration. This possibility was assessed using the configuration shown in Figure 11, with a relative hydrogen reference electrode (RHE_1) placed in between Cathode and Anode, and a second reference electrode (RHE_2) placed behind the Cathode, in an open holder (flushed with N_2) used for electrode screening at room temperature and in absence of electrolyte flow. As

can be seen in the same Figure, the overpotential measured with either RHE is identical up to a current density of at least 100 mA/cm^2.

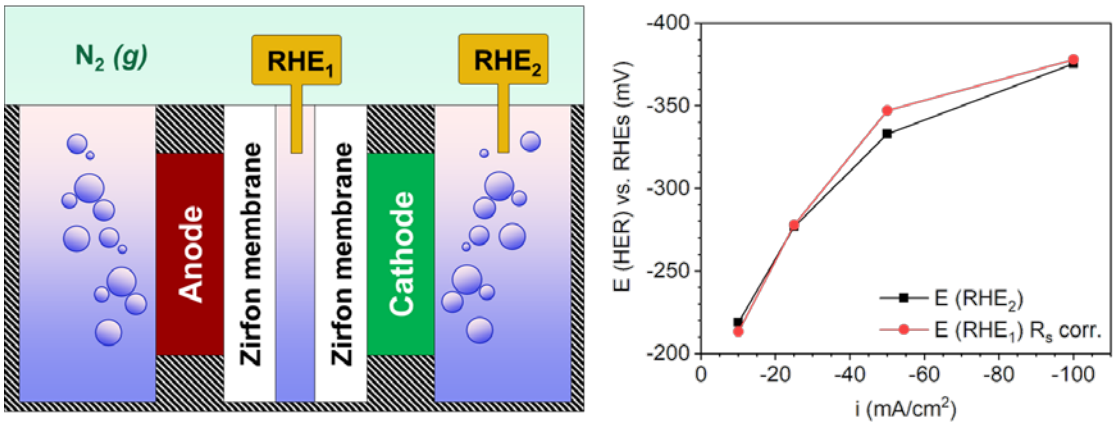

Figure 11: *Comparison of cathodic overpotential measured under zero-gap configuration with the use of RHE$_1$ placed in between the Cathode and Anode (conventional placement) relative to that measured with the use of RHE$_2$ placed behind the Cathode.*

Following this encouraging result, we placed relative hydrogen reference electrodes behind the Cathode (RC) and Anode (RA) at the corresponding electrolyte inlets of the flow cell used for AEC testing, as shown in Figure 12. The same Figure provides a schematic representation of the potential distributions across the AEC.

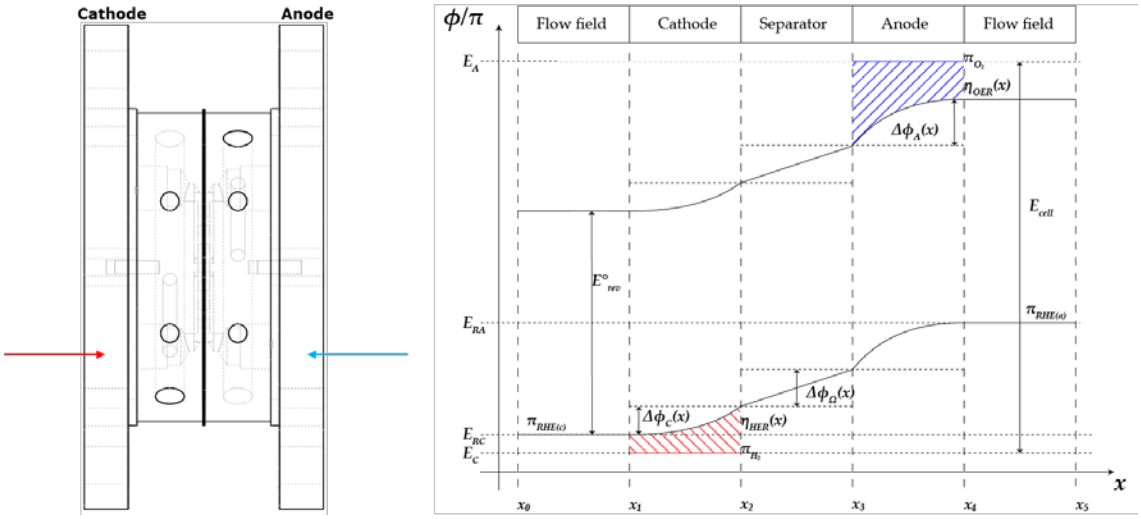

Figure 12: *Placement of reference electrodes in flow-cell for zero-gap AEC testing, and schematic illustration of potential distributions across the cell.*

The potential difference measured between RA and RC corresponds to the Galvani drop across the entire AEC. Subtracting the contribution of the diaphragm (which can be determined by EIS), we can deduce the combined Galvani drop in the two electrodes. Assuming the drop in the Cathode to be negligible (as Figure 11 and multi-physics simulations suggest), we can assess the Galvani drop in the Anode. This offers critical insight concerning the inner workings of the Anode, allowing us to assess the significance of transport versus reaction kinetics.

Figure 13 shows a comparison of the performance of fine (450 µm pore diameter) Ni-foam electrodes either un-compressed, 1500 µm, or compressed to 300 µm, measured in the flow cell at 80 ºC in either 30 or 5 wt% KOH (with a 500 µm Zirfon Perl diaphragm). Besides their I-V response, the Galvani drop through the cell is also plotted, as measured by the potential difference between RA and RC, as well as the individual electrode potentials versus the RHE reference electrodes positioned behind them. As expected, the performance in 5 wt% KOH is far inferior to

that in 30 wt% KOH, due to increased transport losses, both in the diaphragm and in the electrodes. This is clearly illustrated in the Galvani drop across the cell, as measured by the potential difference between RA and RC. Interestingly, compressing the Cathode from 1500 to 300 µm (while maintaining the Anode uncompressed), makes no difference to the I-V response of the AEC or the Galvani drop across the entire AEC, suggesting that the Galvani drop in the Cathode is indeed negligible. Compressing the Anode from 1500 to 300 µm, on the other hand, has a pronounced effect on the I-V response and the Galvani drop of the AEC. The overpotential of the cathode, as measured relative to the RHE that is placed behind it, corresponds to the overpotential at the back side of the Cathode. As the Galvani drop can be considered negligible for the Cathode, the measured value is indicative of the rather homogeneous overpotential prevailing at the Cathode. The overpotential of the Anode, on the other hand, has a pronounced distribution, due to the substantial Galvani drop in the Anode. The value measured directly versus the RHE that is placed behind the Anode corresponds to the minimum anodic overpotential prevailing at the back side of the Anode. The maximum overpotential prevailing at the Anode/Diaphragm interface can be derived from the full cell voltage by subtracting the Cathodic overpotential and the ohmic loss in the diaphragm (determined by EIS).

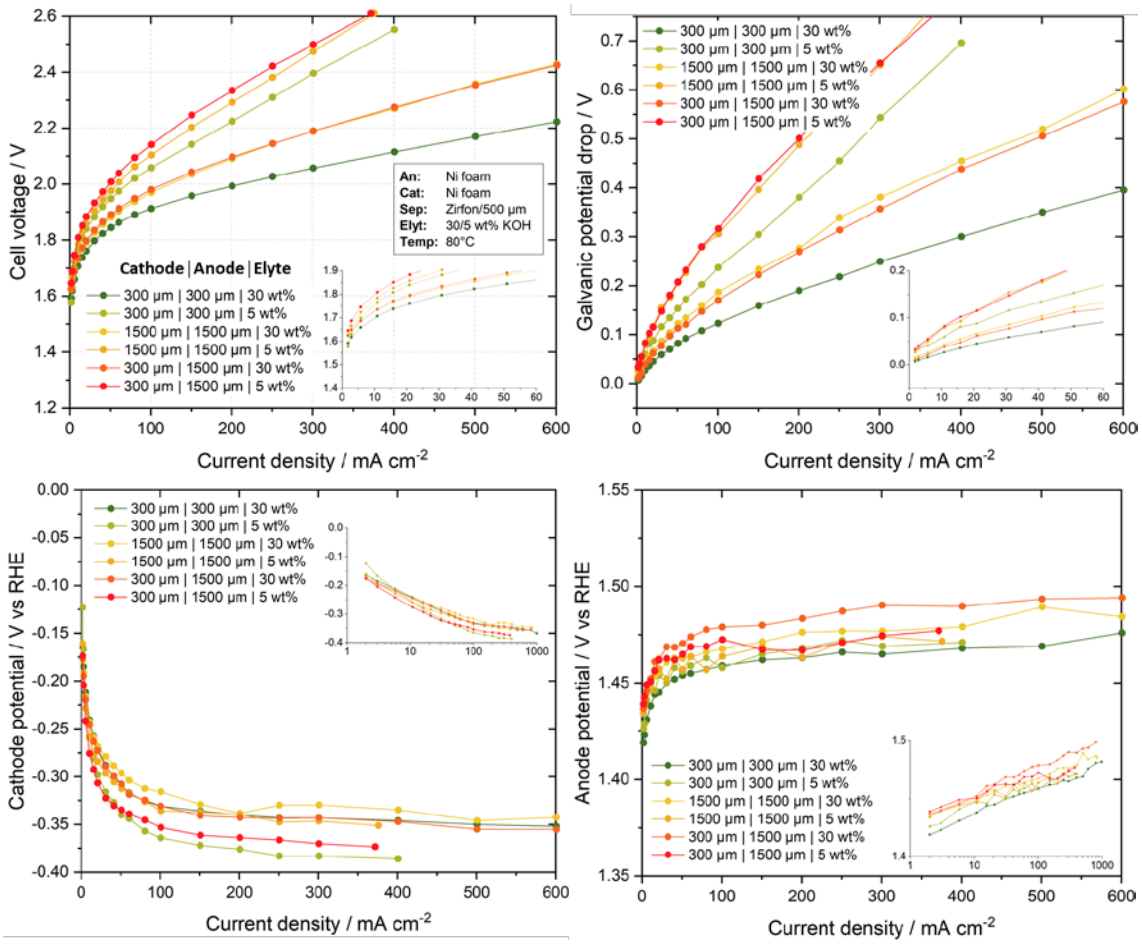

Figure 13: *I-V response, Galvani drop, and individual electrode potentials (vs. RHE placed behind the electrodes) of fine Ni-foam electrodes either un-compressed, 1500 µm, or compressed to 300 µm, measured in the flow cell at 80 ºC in either 30 or 5 wt% KOH (with a 500 µm Zirfon Perl diaphragm).*

This development of a simple and robust method to determine the individual electrode contribution and transport vs. kinetic limitation of the electrodes under realistic conditions is of great advantage for future electrode optimization work, as it enables us to gain faster and deeper insight on the performance (and performance

limitations) and degradation of each individual electrode simultaneously during operation of a zero-gap AEC under technological conditions.
Already at this point, in the study of 3D Ni foam supports, it has become apparent that the Cathode is rather insensitive to the thickness and porosity of the support, whereas the Anode can benefit from the use of relatively thin supports. Nevertheless, additional questions persist in relation to the optimal thickness of the 3D support, porosity, surface area distribution in the volume of the support, etc. More work is clearly required to capture the full potential of 3D porous matrix electrodes.

3D Ni foam was originally chosen as a support for matrix electrode development, on the basis of their improved performance compared to 2D supports in the symmetric cell screening of different supports reported above. The hydrothermal approach of synthesizing the $NiMoO_4$ and $Ni_{1-y}Fe_y$ LDH electrocatalysts selected in WP1 is also suitable for directly growing the catalyst particles on the support. This method was thus selected for electrode fabrication, with the Cathode further reduced in 5% H_2 and 3% H_2O (balance Ar) at 550 ºC to form $Ni_{1-x}Mo_x@MoO_2$@Ni foam. Characteristic micrographs of the fabricated electrodes are shown in Figure 14, along with the performance of a zero-gap AEC comprising those and a 132 μm thick microporous diaphragm, measured in a flow cell at 60 ºC and 20 wt% KOH. The performance of this cell is compared to that of zero-gap AEC employing uncoated Ni PP (2D) and Ni foam (3D) supports, measured in a flow cell at 80 ºC and 20 wt% KOH. The performance of the cell with loaded catalysts shows a drastic improvement compared to that of the uncoated supports, despite the fact that it was measured at 20 ºC lower temperature. Subtracting the ohmic loss in the diaphragm (ca. 100 mV), as determined by EIS, suggests that the combined overpotential of the two electrodes was 0.4 V at 1 A/cm^2, exceeding the performance target set in M2.2 and M2.3 (combined overpotential of 0.5 V at 1 A/cm^2).

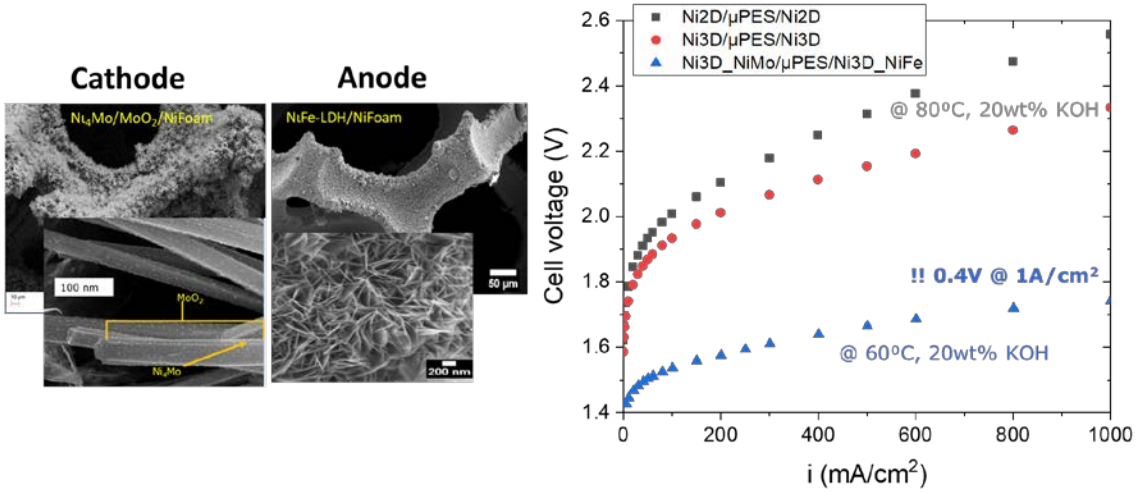

Figure 14: *Characteristic micrographs of the fabricated Ni foam electrodes, hydrothermally coated with $Ni_{1-x}Mo_x@MoO_2$ and $Ni_{1-y}Fe_y$ LDH electrocatalysts, along with the performance of a zero-gap AEC comprising those and a 132 μm thick microporous diaphragm, measured at 60 ºC and 20 wt% KOH (blue) and compared to the performance of a zero-gap AEC comprising uncoated 2D (black) and 3D (red) Ni supports, measured at 80 ºC and 20 wt% KOH.*

Despite the fact that a target value for electrode stability was not set as a Milestone in the project, efforts were undertaken to assess the stability of the developed electrodes. While mounting and testing the cell it became apparent that catalyst particles fall off from the electrodes and enter the electrolyte stream. Post mortem SEM-EDS analysis (Figure 15) of the tested set of electrodes showed indeed that most of the $Ni_{1-x}Mo_x@MoO_2$ rods are detached from the Cathode, albeit leaving behind a layer of $Ni_{1-x}Mo_x$ on the surface of the Ni foam. Furthermore, Fe particles were

found on the surface of the Cathode, which suggests that Fe is leaching out from the $Ni_{1-y}Fe_y$ LDH electrocatalyst of the Anode, permeates through the microporous diaphragm and deposits on the Cathode. Fe-rich particles were also found present on the Anode, despite the fact that the LDH coating appears still present.

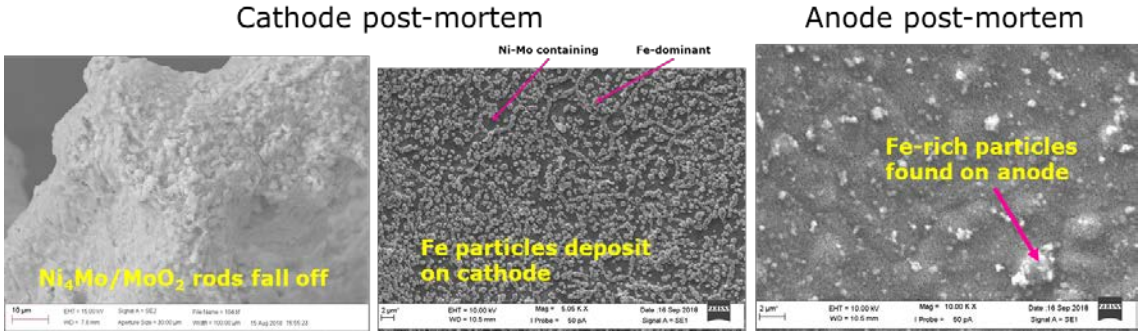

Figure 15: *Post mortem SEM-EDS analysis of the set of $Ni_{1-x}Mo_x@MoO_2$ and $Ni_{1-y}Fe_y$ LDH electrodes, whose performance in shown in Figure 14.*

Based on these findings it was decided that it is important to work on improving the electrode stability. The electrocatalyst screening efforts in WP1 suggested that fully reducing $NiMoO_4$ to $Ni_{1-x}Mo_x$ does not influence the intrinsic HER performance of the electrocatalyst and has a relatively small impact on decreasing surface area if the reduction temperature is not raised far above 600 ºC. On the other hand, a more robust coating could be expected by increasing the reduction temperature, due to improved necking of the catalyst particles/rods and adhesion to the Ni support. A series of Cathodes were thus fabricated hydrothermally and reduced sintered at 600, 650, and 700 ºC, to assess the impact on the performance and robustness of the coating. Indeed, reducing at 650 ºC was found to provide a good compromise between performance and stability. Figure 16 shows the long-term performance of a zero-gap AEC comprising a $Ni_{1-x}Mo_x$ coated Ni foam Cathode, reduced at 650 ºC, and a bare Ni foam Anode, measured at 80 ºC in 20 wt% KOH with a 132 µm microporous diaphragm. SEM micrographs of the as produced Cathode and post-mortem are also shown in the same Figure. The two Ni foam electrodes were originally tested uncompressed for 1 day (black curve), then the cell was taken apart, the electrodes pressed, and the cell was remounted and operated for 19 days (red curve). There was no sign of catalyst particle loss during operation or during electrode pressing. As can be seen from Figure 16 there was also no detectable loss in performance after 19 days of operation under continuous polarization. The cell was in fact found to perform significantly better after compression of the electrodes, but this is an effect that we associate with the Anode. Compared to the bare Ni foam Cathode (Figure 14), the performance of the fully reduced $Ni_{1-x}Mo_x$ coated Ni foam Cathode is approx. 200 mV improved at 0.5 A/cm^2. EDS and XRD analysis of the as produced electrode confirmed that the original $NiMoO_4$ rods grown hydrothermally are fully reduced to $Ni_{1-x}Mo_x$, albeit still maintaining their shape. Post-mortem SEM analysis confirms that the coating remains intact after testing, despite the mechanical stress induced upon pressing the electrode.

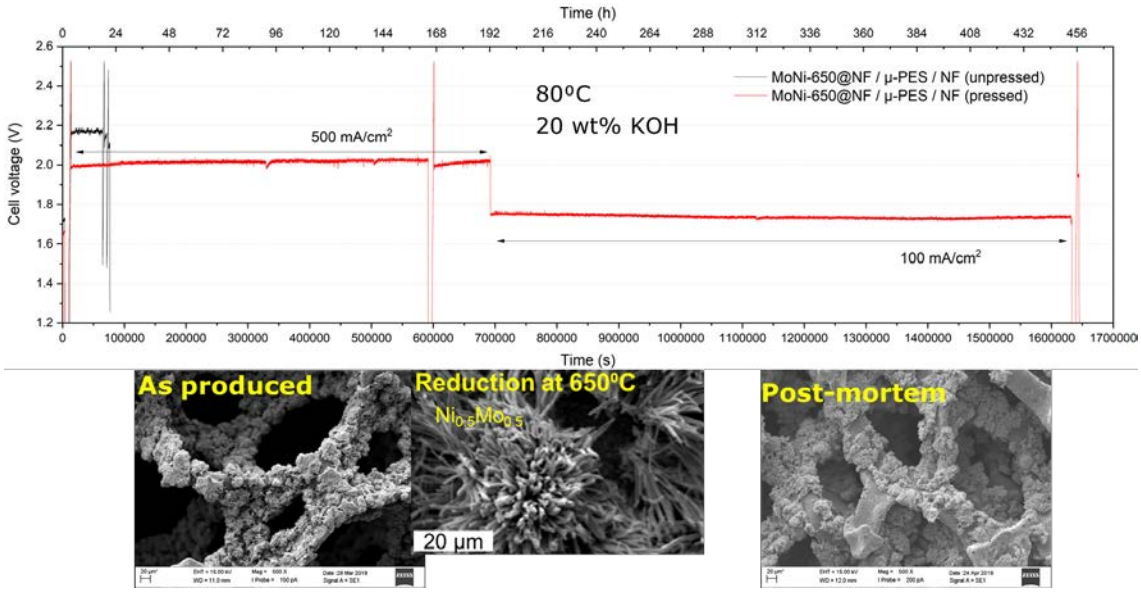

Figure 16: *Long-term performance of a zero-gap AEC comprising a $Ni_{1-x}Mo_x$ coated Ni foam Cathode, reduced at 650 ºC, and a bare Ni foam Anode, measured at 80 ºC in 20 wt% KOH with a 132 µm microporous diaphragm, and SEM micrographs of the as produced Cathode and post-mortem.*

A method was thus developed for the fabrication of well performing and durable $Ni_{1-x}Mo_x$ coated 3D Ni matrix Cathodes. The hydrothermal approach for synthesizing and growing the catalyst on the Ni matrix is nevertheless somewhat challenging in terms of large scale high throughput production of electrodes, since it is a batch process rather than a continuous one, and due to size limitations of hydrothermal reactors. A different approach was thus also explored, based on dip coating of Ni supports (Figure 17) using a $NiMoO_4$ containing slurry, employing the $NiMoO_4$ nano-powder synthesized via the sol gel route in WP1. Both 3D Ni foam and 2D Ni PP were used as supports. Due to the very different morphology of the sol gel particles (spherical nanoparticles, as opposed to approx. 10 µm long rods obtained hydro-thermally), we also expected improved robustness of the coating. The influence of reduction temperature on performance and robustness was thus examined in the range 400-550 ºC. It was concluded that full reduction is achieved at 550 ºC while maintaining a very high surface area.

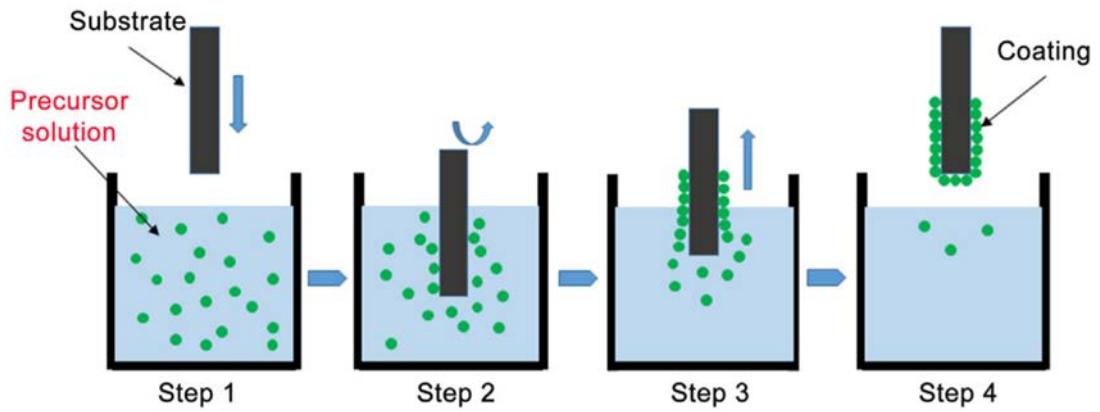

Figure 17: *Schematic illustration of dip coating process.*

The adhesion of the coating was substantially better on Ni foam, which was then selected for assessing the effect of coating thickness on the Cathode performance. The coating thickness was gradually increased by increasing the number of dip coating repetitions from one to ten. As can be seen in Figure 18, five repetitions (5L) were found to offer the optimum coating thickness, which was evaluated to be approx. 3 μm. It should also be stressed that the dip coated Cathodes show excellent performance, requiring only 75 mV overpotential for 1 A/cm^2 and 90 mV for 2 A/cm^2 in the best case. This Cathode fabrication approach offers thus a very promising path for large scale electrode production. Before this step is taken up though, it is important to thoroughly assess the long-term stability of this electrode and its ability to withstand fast cycling and deep depolarizations.

The Anode development work focused on two directions; stabilizing the $Ni_{1-y}Fe_y$ LDH electrocatalyst and increasing the surface area of the Ni support. Efforts on stabilizing the $Ni_{1-y}Fe_y$ LDH electrocatalyst (avoiding Fe leaching) involved reducing the amount of Fe substitution and adding a third element. Unfortunately, these efforts were inconclusive, with poor reproducibility of the obtained catalyst performance. This remains in fact a hot topic in the literature, with some recent studies suggesting that the catalyst stability depends on multiple parameters, such as the Fe content, the thickness of the nanoplatelets, the KOH concentration in the electrolyte, the current density, the ability of the cell configuration to sustain a certain level of Fe in solution, etc. As the resources available for catalyst development were insufficient to trace this multi-parametric landscape, this route was abandoned and efforts were concentrated in realizing high surface area electrodes with Ni as the electrocatalyst.

Different methods to coat 2D and 3D supports were explored, including screen printing, robocasting, and dip coating, employing NiO nanoparticles in different slurry formulations and processing parameters that resulted in different thicknesses of the coating. It was nevertheless concluded that the determining factor for the resulting surface area was the temperature of reduction of the NiO coating. After screening different temperatures in the range 400-725 ºC, a reduction temperature of 550 ºC was selected as a compromise between surface area and robustness of the coating. Although robocasting (3D printing) gave the best results in terms of surface area and performance, dip coating was selected as the route for optimization and scaling up due to its advantages in terms of simplicity and scalability.

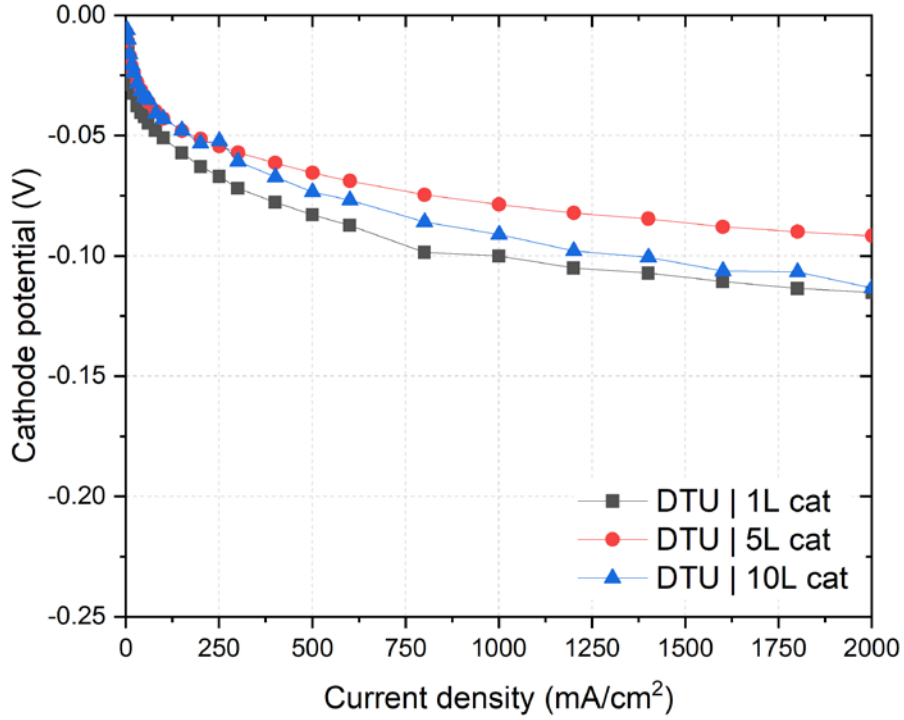

Figure 18: *Performance of $Ni_{1-x}Mo_x$ dip coated Ni foam Cathodes with 1, 5, or 10 dip coating repetitions, reduced at 550 ºC and measured at 80 ºC in 30 wt% KOH with a 132 µm microporous diaphragm.*

Anodes with optimized Ni coatings were thus fabricated following the developed dip coating recipe on 2D Ni PP support and 3D coarse Ni foam (compressed to 500 µm). These were tested in zero-gap AEC with corresponding $Ni_{1-x}Mo_x$ dip coated Cathodes (on 2D Ni PP and 3D Ni foam, respectively), using a 132 µm microporous diaphragm at room temperature and 80 ºC in 30 wt% KOH. Figure 19 shows the I-V performance curves and long-term durability results for these sets of electrodes. The cell with the 3D Ni foam electrodes performed slightly better at room temperature, whereas the cell with the 2D Ni PP performed slightly better at 80 ºC, showing a cell voltage of 1.93 V at 1 A/cm^2, including IR-drop. Both sets of electrodes showed very stable performance.

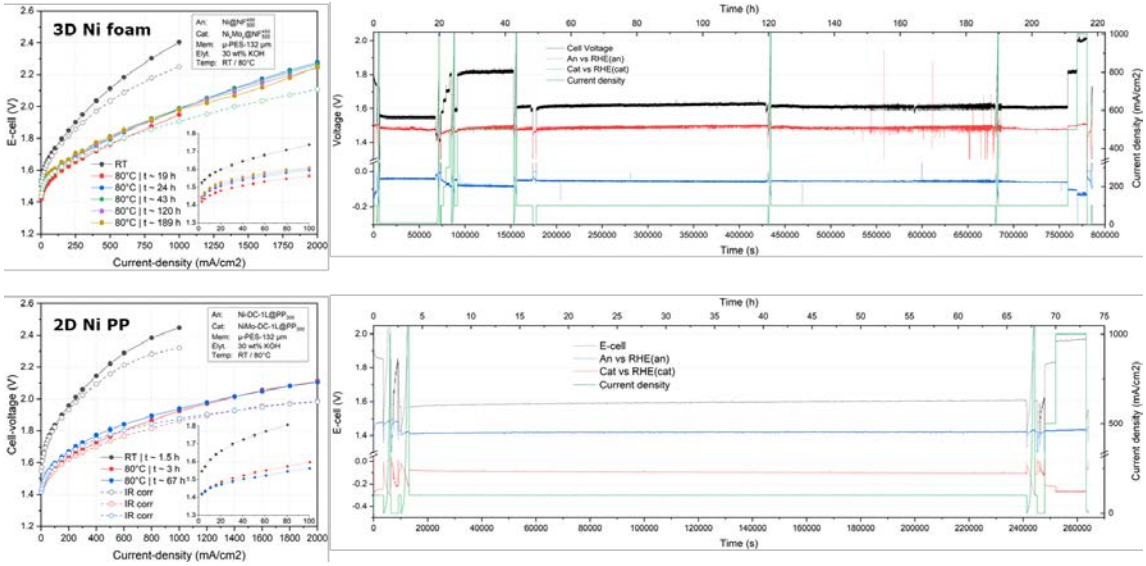

Figure 19: *Performance and durability test of 3D Ni foam and 2D Ni PP dip coated with $Ni_{1-x}Mo_x$ and Ni catalyst layers for the Cathode and Anode, respectively. The measurements were carried out in the flow cell at room temperature and 80 ºC in 30 wt% KOH with a 132 µm microporous diaphragm.*

More insight can be gained by comparing the individual contributions of each electrode, measured by the use of the reference electrode approach described previously. As can be seen in Figure 20, the performance of the 3D Ni foam based Cathode, dip coated with $Ni_{1-x}Mo_x$, is excellent and far superior than that of the corresponding 2D Ni PP Cathode, requiring an overpotential of only 100 mV to support a current density of 1 A/cm^2, in comparison to more than 250 mV required by the 2D based electrode. As discussed earlier, this is primarily an effect of a better coating achieved on the Ni foam and secondarily an effect of the 3D microstructure of the support. Despite the much better performance of the 3D Cathode, the 3D electrode based AEC underperforms the 2D one. This suggests that the 2D Anode must perform substantially better than the 3D one. Deducing the Anode potential from the measured signal of the Anode versus the RHE placed behind it, requires the addition of the Galvani drop measured between the two RHEs (corrected for the IR-drop in the diaphragm). As can be seen in Figure 20, the Galvani drop is substantially smaller in the case of the 2D Anode, resulting in an overpotential of less than 400 mV at 1 A/cm^2, as opposed to 600 mV for the 3D Anode. This difference overcompensates for the difference in Cathode performance, resulting in the slightly better overall performance of the 2D based cell. Furthermore, this suggests that the Anode performance is limited to a large extent by transport processes at high current densities. This finding is in line with the outcome from our multi-physics electrode simulations, and suggests flow field optimization as a critical next step for further optimization of the anode performance, which is currently the main limiting factor in AEC.

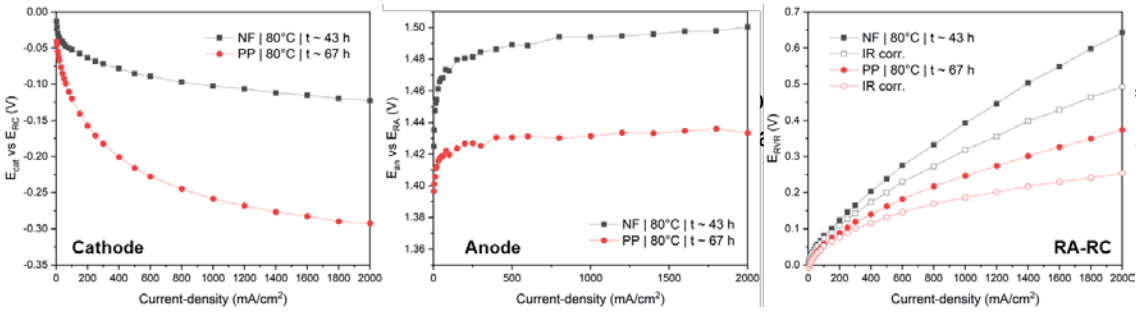

Figure 20: *Individual electrode potentials (vs. RHE placed behind the electrodes) and Galvani drop for the 3D Ni foam and 2D Ni PP based AEC of Figure 19, measured at 80 ºC in 30 wt% KOH.*

Based on these results, the best performance can be expected from an AEC employing the 3D Cathode and 2D Anode. This was therefore the electrode combination that was selected for upscaling in WP4.

WP3: Bonded electrodes

In parallel to the work on matrix electrodes, a study on bonded electrodes was also planned. Bonded electrodes are made from catalyst particles bonded together in a 3D porous structure by means of a binder. As the project developed and the concept of bonded electrodes was considered in more detail it was decided to prioritize the matrix electrodes line for the following reasons:

1) Bonded electrodes is the dominating technology for gas diffusion elecrodes, which are used in fuel cells. Bonding of small catalyst particles, or conducting support particles carrying the catalyst on the surface, leads to quite compact structures with fine pores accessible to gasses. For alkaline electrolyzers though with flooded electrodes and with bubble formation, this concept is much less obvious as bubbles are easily trapped in the structure unless the total catalyst layer is extremely thin.

2) The electronic conductance through the catalyst layer along percolating pathways of particles can be expected to be poor compared to a matrix structure like nickel foam. The contact between the particles is hampered by the limited contact areas between spherical or spherical-like particles. Moreover, the polymeric binder, which is not electron conducting, will form insulating domains.
3) Matrix based electrodes are typically significantly stronger and work well as self suported free-standing layers easy to handle and process.
A completed study of the bonded electrodes line would in a sense have made the project more comprehensive overall, but that would have been at the cost of part of the work on matrix electrodes. The discontinuation of the work on bonded electrodes was decided with the perspective of getting the most out of the technology that was deemed most promissing.

WP4: Electrode upscaling

BWT has been following closely the electrode development work performed by DTU in order to assess scalability potential and to align efforts towards a direction with promising potential for industrial production.
In this context, BWT investigated the cost associated with the use of 3D Ni foam as electrode support. Alantum, that is the supplier of Ni foam to DTU, requests a small-sample fee of 1.666 $/m^2 for less than 45 m^2 which is prohibitive, as opposed to a bulk cost of about 70-90 $/m^2. A Chinese vendor was identified, providing a relevant 6 m^2 sample at 70$/m^2. This material was shared with DTU for performance qualification, and a strip was supplied to GHS for electronic conductivity testing.
Figure 21 shows a comparison of the performance of the Ni foam obtained by BWT (pore diameter 1200 µm / compressed to 500 µm) in relation to other Ni foams and the Ni PP previously tested by DTU within the support screening efforts, in a zero-gap symmetric cell configuration in the flow cell at 80 ºC and 20 wt% KOH. As can be seen, the performance of the foam obtained by BWT falls within the range of foams employed by DTU, that show some variation with thickness and pore diameter.

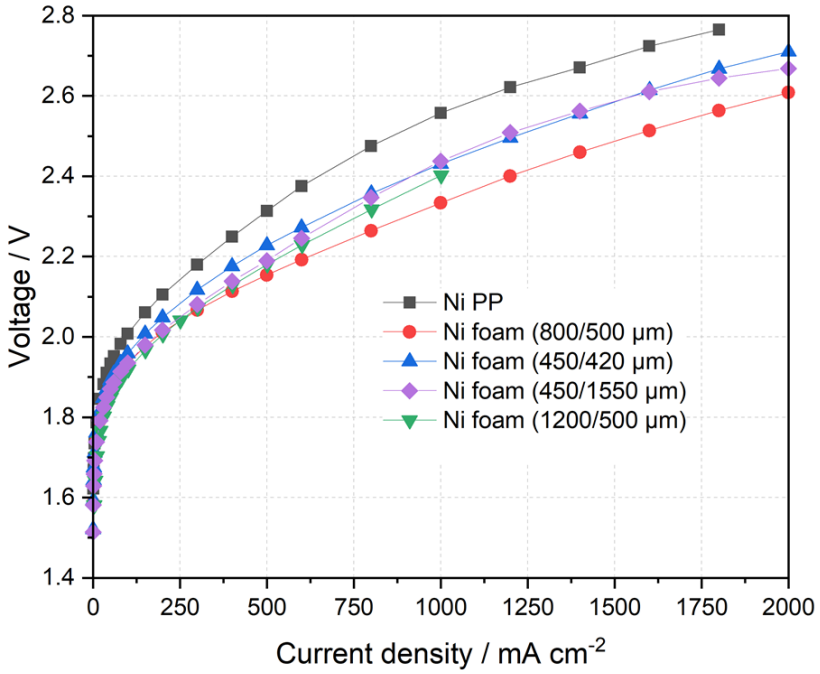

Figure 21: *Performance of the Ni foam obtained by BWT (ø1200 µm / 500 µm) in relation to other Ni foams and the Ni PP previously tested by DTU in a zero-gap symmetric cell configuration in the flow cell at 80 ºC and 20 wt% KOH.*

Employing the hydrothermal route established at DTU for electrode fabrication is feasible at BWT but not considered attractive for industrial production, partly because the pressurized vessel required inherently implies a batch process, and partly due to challenges in obtaining a reproducible and homogeneous coating in preliminary upscaling attempts. Dip coating with oxides and subsequent sintering/reduction was thus selected as process path for upscaling.

Electrode development work by DTU in WP2 pointed to Ni-foam and Ni PP as the preferred Cathode and Anode supports, respectively. Furthermore the studies of various electrode surface layers deposited onto the substrate has pointed to prioritising surface-enhancing coatings of Ni and $Ni_{1-x}Mo_x$ on the Anode and Cathode, respectively.

The dip coating and reduction recipes developed at DTU were shared with BWT who established a pilot scale production for fabrication of such electrodes at larger scale, namely ø30 cm electrodes in quarter-pieces. A commercial $NiMoO_4$ powder was obtained for the first batch of $Ni_{1-x}Mo_x$ based Cathodes. The resulting performance was assessed by DTU and found to be substantially inferior to that of the corresponding DTU Cathodes. As a careful repetition of the process (batch 2) did not yield any substantial improvement, BWT decided to produce a batch of $NiMoO_4$ nanopowder in house following the sol gel synthesis established at DTU. This led to a 3rd batch of Cathodes with much improved performance, albeit still somewhat inferrior to that of the corresponding DTU Cathodes. A comparison of the performance of the last two batches of Cathodes produced at BWT versus the ones produced at DTU is shown in Figure 22. The same Figure also shows the performance evolution of the BWT b3 Cathode over 236 h of continuous operation, where substantial degradation was observed.

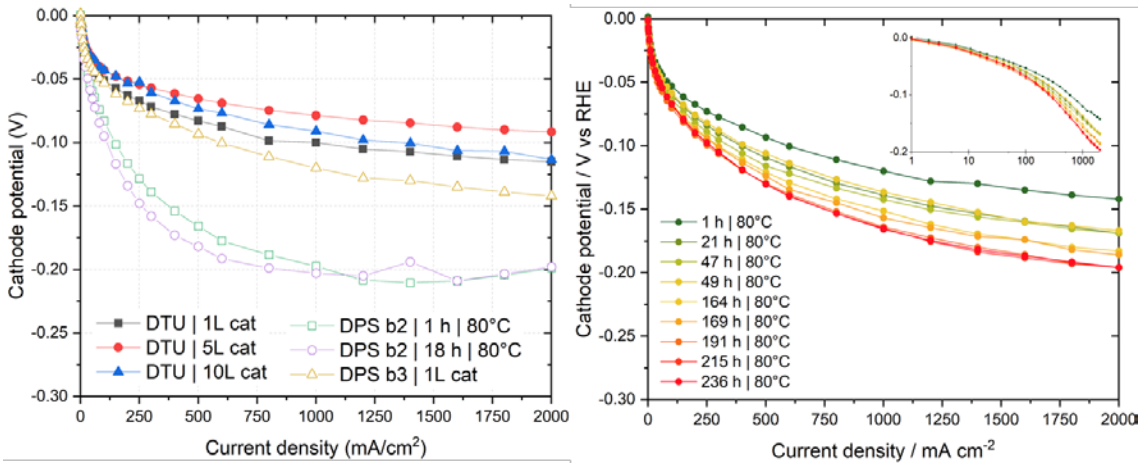

Figure 22: *(Left) Cathode potentials (vs. the RHE placed behind the Cathode) for the 3D Ni foam Cathodes dip coated with $Ni_{1-x}Mo_x$ produced at BWT and DTU, measured at 80 ºC in 30 wt% KOH. (Right) Performance evolution of BWT b3 Cathode over 236 h of continuous operation.*

The performance of the upscaled Anode is shown in Figure 23. After correcting for a shift of the reference electrode RA, the performance of the Anode does not appear to change over time, when assessed in terms of its polarization (maximum overpotential). Mass transport losses seem to improve over time though, suggesting improved wetting of the Anode and more facile release of evolved O_2. The performance as such though, with 520 mV at 1 A/cm^2, is inferrior to what was observed on nominally similar Anodes produced at DTU, showing 400 mV at 1 A/cm^2. Still this performance is an improvement compared to non-coated Ni PP, which requires an overpotential of 650 mV to deliver 1 A/cm^2 at the same conditions.

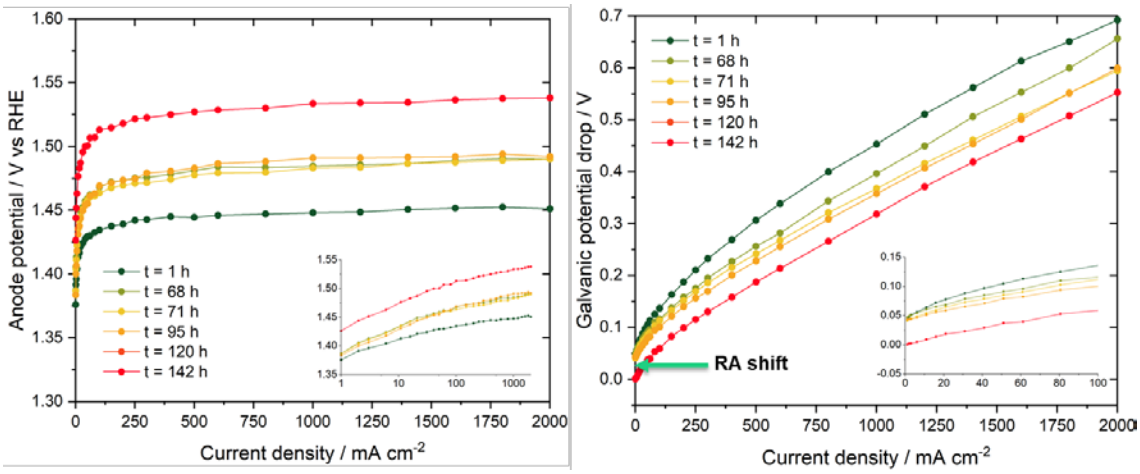

Figure 23: *Anode potential (vs. the RHE placed behind the Anode) for the 2D Ni PP Anode dip coated with Ni by BWT and Galvani potential drop across the AEC, measured at 80 ºC in 30 wt% KOH over 142 h of continuous operation.*

WP5: Integration and testing

One important consideration in WP5 related to the possibility to integrate the developed 3D Ni foam electrodes in a technological AEC stack. The main concerns were associated with the in-plane electronic conductivity of the porous support and the possibility to weld it to the interconnect/bipolar plate. GHS measured the electronic conductivity of a long strip of Ni foam supplied by BWT, and confirmed that the in-plane electronic conductance is sufficient for implementation in their stack. Furthermore, welding on the interconnect plate was successfully carried out. It was thus concluded that 3D Ni foam based electrodes pose no obstacle for stack integration.

Although the low-cost porous electrodes developed in BEEST met the very ambitious goals set in the project, this performance could not be fully captured upon electrode upscaling. After three iterative improvement cycles of the upscaled Cathodes, their initial performance approached that of the lab scale electrodes, but substantial degradation was observed during continuous operation. The upscaled Anodes showed good stability upon continuous operation, but their performance did not live up to expectations from the lab scale equivalents. Implementation and testing in an industrial stack and system was therefore deemed premature, and the associated project plan was revised.

Within WP2, the robustness of the $Ni_{1-x}Mo_x$ catalytic coating produced hydrothermally was improved by increasing the reduction temperature. It was decided to implement this approach for the Cathodes that were produced by BWT and to assess their performance and durability under accelerated stress test conditions. Figure 24 shows the performance of the catalytic coating when tested at the GHS 25 cm^2 accelerated test setups operating at 800 mA/cm^2 and at 120 °C. The Figure shows two samples of the BWT produced $Ni_{1-x}Mo_x$ catalytic coating, after further reduction at 600 °C by DTU. The first 72 h the samples are operated continuously and after a I-U curve the cell is switched off and on repeatedly with 2 h on and 2 h off periods. It is noted that within the first period of continuous operation, the electrode activates by approx. 100 mV, with part of the activation associated with the first on/off cycle. After the subsequent 3 on/off cycles though gradual degradation is observed, and after 10-20 on/off cycles the cell voltage has increased by approximately 150-200 mV. Figure 24 includes also a sample with the GHS in-house developed coating on a 2D substrate tested under identical operating conditions. This shows also approx. 50 mV of activation during the original continuous operation,

but more importantly no sign of degradation upon the subsequent 320 h of repeated on/off cycles.

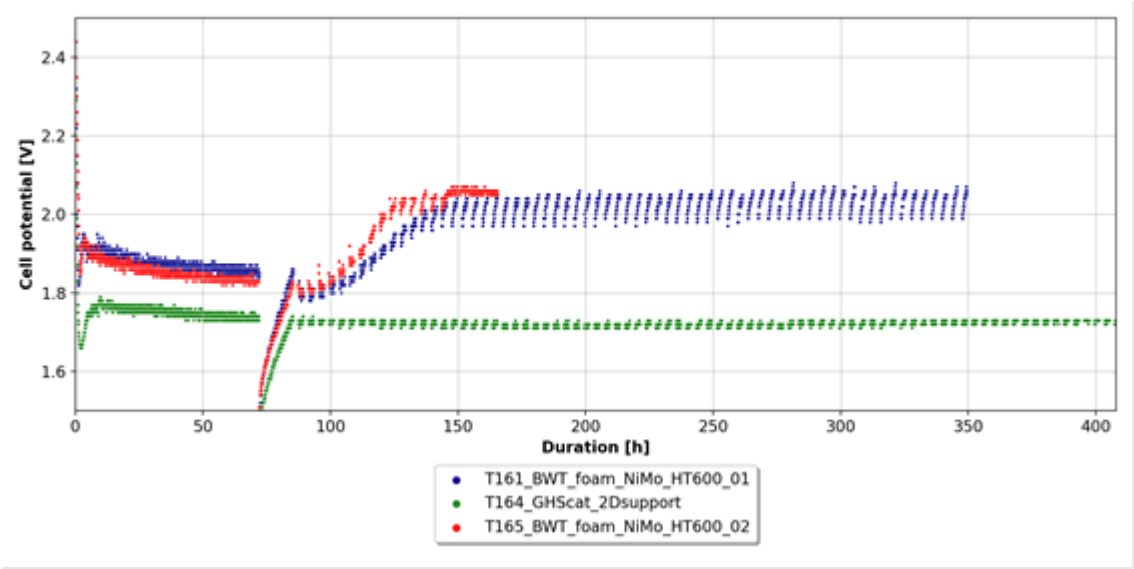

Figure 24*: Accelerated stress test of the 3D Ni foam Cathodes dip coated with $Ni_{1-x}Mo_x$ by BWT and re-reduced at 600 ºC by DTU, measured at 120 ºC in 40 wt% KOH over 72 h of continuous operation at 800 mA/cm² and an additional 80-270 h of repeated on/off cycles of 2 h duration each. A sample with the GHS in-house developed Cathode coating on a 2D substrate tested under identical operating conditions is also included for comparison. All tests employed the same separator and uncoated 2D Ni anode.*

After operation the samples were investigated by SEM-EDS, the results of which as shown in Figure 25. It can be observed that a large part of the $Ni_{1-x}Mo_x$ catalytic coating seems to have disappeared during operation in the test cell. These results, when also combined with the electrochemical performance presented in Figure 24, suggest that the $Ni_{1-x}Mo_x$ coating is stable under continuous cathodic polarization, but sensitive to depolarization effects upon discontinuous on/off operation.

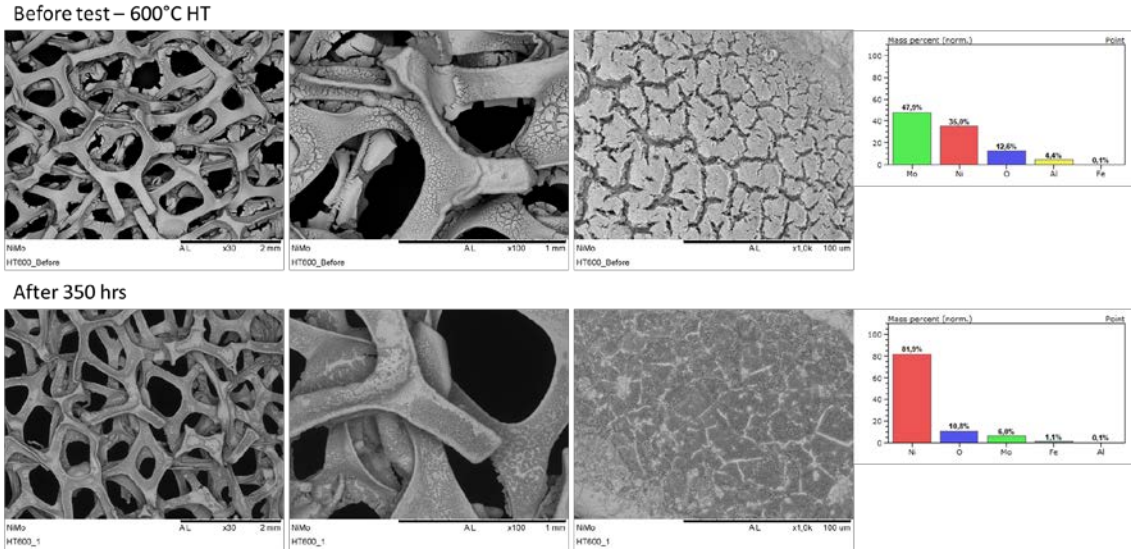

Figure 25: *SEM pictures and EDS measurements of the $Ni_{1-x}Mo_x$ catalytic coating before and after the test shown in Figure 24.*

Furthermore, work within WP2 suggested that it is likely beneficial to employ a 3D porous microstructure for the cathode. GHS has alongside BEEST optimized an in-house method for electrode fabrication on 2D supports, resulting in comparable performance to the best 3D Ni foam based $Ni_{1-x}Mo_x$ Cathodes developed in BEEST. GHS attempted to apply their catalytic coating on the 3D Ni foam used in BEEST, to assess a potential further improvement of the electrode performance. The perfor-

mance and durability of this electrode was also explored under accelerated stress test conditions, and is shown in Figure 26 for a period of more than 1500 h. The performance of the 3D Cathode was comparable to that of the 2D one with a similar coating (see Figure 25), albeit no optimization of the coating on the 3D support was undertaken, suggesting that there is room for improvement. Stability-wise the 3D Cathode was also proven to be very robust under both continuous and discontinuous operation.

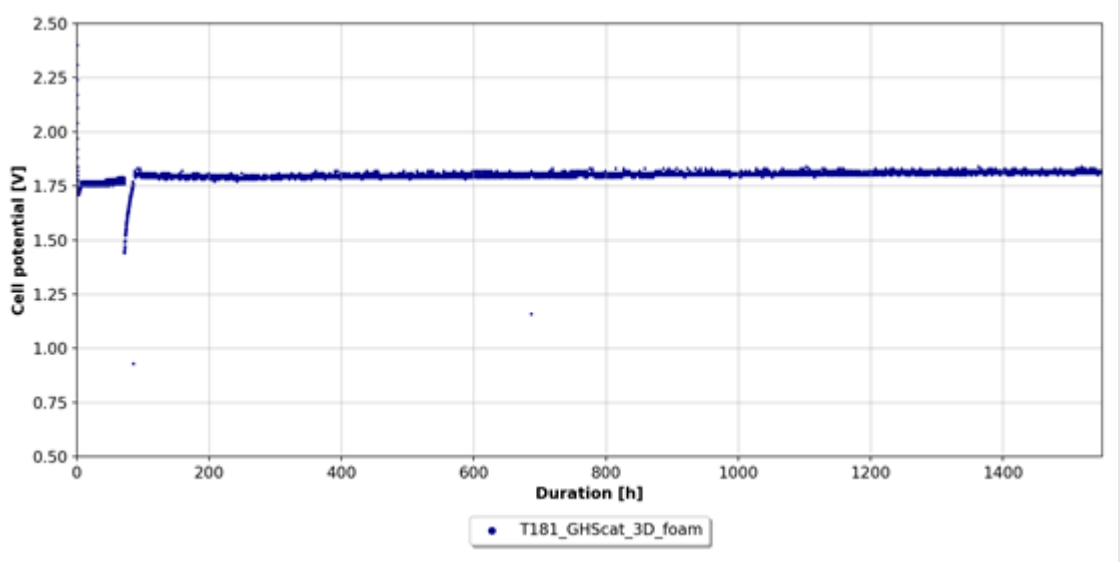

Figure 26: *Accelerated stress test of the 3D Ni foam Cathode with the GHS in-house developed coating, measured at 120 ºC in 40 wt% KOH over 72 h of continuous operation at 800 mA/cm² and an additional ca. 1500 h of repeated on/off cycles of 2 h duration each.*

WP6: Dissemination

A broad range of dissemination activities were undertaken in the project.

BEEST contributed to the organization of the 1st International Conference on Electrolysis (Copenhagen, June 2017, Chaired by DTU Energy), http://www.ice2017.net/Conference, which was a great success with participation of more than 200 people from all over the world, covering both academia and industry. It was thus decided to continue this event, thereby developing a new conference series dedicated to Electrolysis. The 2nd International Conference on Electrolysis, held in Norway (Loen, June 2019), https://www.sintef.no/projectweb/ice2019/, was also very successful. The 3rd International Conference on Electrolysis was planned to take place in Colorado, USA in 2021, but has been postponed to 2022 because of the global pandemic, https://ice2021.csmspace.com/. Two webinars were nevertheless held in June 2021 to bring the community together. The alkaline session was chaired by DTU.

At a national level, a workshop/thematic day on "Low temperature (<200 ºC) fuel cell and electrolysis technologies" was realized in November 2017 in collaboration with the Danish Electro-chemical Society, http://www.electrochemistry.dk/images/Programfolder_2017.pdf. BEEST was represented with an oral presentation (C. Chatzichristodoulou, M. R. Kraglund, J. O. Jensen, M. B. Mogensen. Advanced Alkaline Electrolysis. Electro-chemical Science and Technology Conference, Danish Electrochemical Society, Lyngby 2-3 November 2017)

BEEST also contributed to the writing of a Book Chapter on “Intermediate Temperature Electrolysers”, J.O. Jensen, C. Chatzichristodoulou, E. Christensen, N. J. Bjerrum and Q. Li. in Keith Scott (ed.) Electrochemical Methods for Hydrogen Production. Royal Society of Chemistry, 2019 (https://pubs.rsc.org/en/content/ebook/978-1-78801-378-9).

Furthermore, BEEST results were disseminated through 26 scientific conference contributions; 22 oral presentations and 4 posters:

1. M. R. Kraglund, M. Carmo, D. Aili, G. Schiller, E. Christensen, A. Friedrich, D. Stolten, J. O. Jensen. Alkaline membrane electrolysis with PEM-level electrochemical performance. First International Conference on Electrolysis (ICE2017), Copenhagen, 12-15 June 2017 (oral by Kraglund).

2. C. Chatzichristodoulou, M. R. Kraglund, J. O. Jensen, M. B. Mogensen. Advanced Alkaline Electrolysis. Electrochemical Science and Technology Conference, Danish Electrochemical Society, Lyngby 2-3 November 2017 (oral by Chatzichristodoulou)

3. J. O. Jensen. How can we maintain the excellent performance of the PEM electrolyzer without the use of platinum group metals? 233rd Electrochemical Society Meeting, Seattle, WA, May 13-17, 2018 (invited talk)

4. J. O. Jensen. Material issues of fuel cells. 2018 Wind2H Summer School. North University of China, Taiyuan, 4-5 June 2018 (oral)

5. M. R. Kraglund, M. Carmo, D. Aili, E. Christensen, J. O. Jensen. Alkaline electrolysis with efficient electrodes and ion-solvating membranes. 22nd World Hydrogen Energy Conference (WHEC2018). Rio de Janeiro, 17-22 June, 2018 (oral)

6. J. O. Jensen, M. R. Kraglund, D. Aili, M. Carmo, L. N. Cleemann, E. Christensen, Q. Li. A key to cost efficient electrolyzers. 22nd World Hydrogen Energy Conference (WHEC2018). Rio de Janeiro, 17-22 June, 2018 (oral)

7. J. O. Jensen. Electrolysis at DTU Energy. Talk at Aquahydrex, Louisville, Denver, Colorado 1. October 2018 (invited talk).

8. J. O. Jensen, M. R. Kraglund, D. Aili, A. K. Reumert, M. Carmo, L. N. Cleemann, E. Christensen, Q. Li. Alkaline Electrolysis with an Ion-solvating Membrane. Americas International Meeting on Electrochemistry and Solid State Science (AiMES 2018), 234rd Electrochemical Society Meeting, Cancun, Mexico, September 30 – October 4, 2018 (oral)

9. J. O. Jensen, D. Aili, C. Chatzichristodoulou, E. Christensen, A. Nikiforov, N. J. Bjerrum, M. B. Mogensen, M. R. Kraglund, L. N. Cleemann, and Q. Li. Low temperature electrolysis, yet at higher temperature. 2nd International Conference on Electrolysis (ICE2019), Loen, Norway, 9-13 June 2019 (oral)

10. A. Reumert, M. Kraglund, L. Cleemann, and J.O. Jensen. Electrode improvements for zero gap alkaline polymer electrolyte membrane electrolysis cells. 2nd International Conference on Electrolysis (ICE2019), Loen, Norway, 9-13 June 2019 (oral)

11. M. R. Kraglund, D. Aili, J. Tavacoli, C. Chatzichristodoulou, and J. O. Jensen. Polysulfone-polyvinylpyrrolidone blend membranes in alkaline electrolysis. 2nd International Conference on Electrolysis (ICE2019), Loen, Norway, 9-13 June 2019 (oral)

12. D. Aili, M. R. Kraglund, J. Tavacoli, C. Chatzichristodoulou and Jens Oluf Jensen. Ion-solvating membrane supported high-rate alkaline water electrolysis. EMEA

workshop 2019, Ion Exchange Membranes for Energy Applications. Bad Zwischenahn, Gernamy 25-27 June 2019 (oral)

13. Christodoulos Chatzichristodoulou, S. Pitscheider, N. Seselj, P. Khajavi, M. Lualdi, H. L. Frandsen, C. Gadea, J. Tavacoli, F. Gellrich, R. Kiebach, M. B. Mo-gensen, Microstructural optimization of gas diffusion electrodes for high temperature and pressure alkaline electrolysis. 2nd International Conference on Electrolysis (ICE2019), Loen, Norway, 9-13 June 2019 (oral)

14. C. Chatzichristodoulou, J. Döhn, H. Frandsen, M. Kraglund, J. Tavacoli, P. Khajavi, R. Kiebach, M. Mogensen, J. Jensen, Advancing alkaline electrolysis cell performance by electrode microstructural optimization and high temperature operation. 2nd International Conference on Electrolysis (ICE2019), Loen, Norway, 9-13 June 2019 (poster)

15. F. Gellrich, S. Pitscheider, N. Seselj, J. Tavacoli, C. Gadea, P. Khajavi, M. Kraglund, X. Georgolamprou, M. Traulsen, R. Kiebach, M.B. Mogensen, C. Chatzichristodoulou, Activity and stability of high performance elec-trocatalysts for hydrogen and oxygen evolution in Alkaline Water Electrolysis. 2nd International Conference on Electrolysis (ICE2019), Loen, Norway, 9-13 June 2019 (poster)

16. N. Seselj, S.Pitscheider, F. Gellrich, C. Gadea, P. Khajavi, R. Kiebach, M. Traulsen, K. Brodersen, T. Molla, H.L. Frandsen, M.B. Mogensen, C. Chatzichristodoulou, Optimization and upscaling of porous ceramic separators and full cells for high temperature alkaline electrolysis. 2nd International Conference on Electrolysis (ICE2019), Loen, Norway, 9-13 June 2019 (poster)

17. J. O. Jensen, M. R. Kraglund, D. Aili, A. K. Reumert, E. Christensen, Q. Li, and L. N. Cleemann. Ion-solvating membranes as a new approach towards high rate alkaline electrolyzers. Seminar at Korea Institute of Science and Technology (KIST). Seoul, South Korea, 11 November 2019 (Invited talk)

18. J. O. Jensen, M. R. Kraglund, M. Carmo, G. Schiller, S. A. Ansar, D. Aili, E. Christensen and J. O. Jensen. Ion-solvating membranes as a new approach towards high rate alkaline electrolyzers. NTNU Team Hydrogen Annual Workshop. NTNU, Trondheim, Norway, 2-3 December 2019 (Invited talk)

19. Alexander Reumert. Electrode improvements for zero gap alkaline water electrolysers. DTU Energy's annual PhD symposium, 17 January 2020 (oral)

20. Florian Gellrich, Spectroelectrochemistry - combining two worlds to increase the understanding of alkaline water electrocatalysts. DTU Energy's annual PhD symposium, 17 January 2020 (poster)

21. J. O. Jensen, et al. The renaissance of alkaline electrolysis. 3rd Industry Workshop on Advanced Alkaline Electrolysis. Fraunhofer IFAM, Dresden 1 October 2020. (Invited talk)

22. Florian Gellrich, Characterizing high-performing electrocatalysts for the industrial alkaline water electrolysis. DTU Energy's annual PhD symposium on 5 February 2021 (oral)

23. J. O. Jensen, M. R. Kraglund, A. K. Reumert, F. Gellrich, V. Baj, C. Chatzichristodoulou, Q. Li, and D. Aili. Perspectives on Alkaline Electrolysis. Catching up with Performance. 29th Topical Meeting of the International Society of Electrochemistry, Mikulov, Czech Republic 18-21 April 2021. (Invited talk)

24. J. O. Jensen, M. R. Kraglund, D. Serhiichuk, Y. Xia, V. Baj, Q. Li, L. N. Cleemann and D. Aili. Membranes for Alkaline Electrolysis. Jeju 6th International Conference on Advanced Electromaterials (ICAE 2021) Jeju, Korea 9-12 November 2021 (Invited talk)

25. J. O. Jensen, M. R. Kraglund, F. Gellrich, C. Chatzichristodoulou, Q. Li, L. N. Cleemann and D. Aili. Renaissance of Alkaline Electrolysis. International Workshop on Hydrogen Production Technology through Water Electrolysis. Side event for International Hydrogen Fuel Cell Vehicle Congress (FCVC), Shanghai, 8-10 June 2021(Invited talk)

26. J. O. Jensen et al. Perspectives of alkaline electrolysis for large scale water electrolysis. Future Energy Solutions Conference. Green Electrification and Hydrogen Economy. Lappeenranta University of Technology, Finland, 13-15 September 2021 (Invited talk)

Additionally, 3 talks were accepted for 237th Electrochemical Society Meeting, Montreal, Canada, 10-15 May 2020, but the event was cancelled due to the pandemic

1. C. Chatzichristodoulou, M. R. Kraglund, X. Georgolamprou, S. Pitscheider, N. Seselj, F. Gellrich, C. Gadea, P. Khajavi, R. Kiebach, H. L. Frandsen, J. O. Jensen, and M. B. Mogensen. Advanced Alkaline Electrolysis Cells for the Production of Sustainable Fuels and Chemicals. 237th Electrochemical Society Meeting, Montreal, Canada, 10-15 May 2020 (oral, event cancelled)

2. C. Chatzichristodoulou, M. R. Kraglund, X. Georgolamprou, S. Pitscheider, N. Seselj, F. Gellrich, C. Gadea, P. Khajavi, R. Kiebach, H. L. Frandsen, J. O. Jensen and M. B. Mogensen. Advanced Alkaline Electrolysis Cells for the Production of Sustainable Fuels And Chemicals. Electrochemical Society fall meeting, Prime 2020, Honolulu, US, 4-9 October, 2020 (oral, event cancelled)

3. F. Gellrich, M. R. Kraglund, A. K. Reumert, X. Georgolamprou, M. L. Traulsen, J. O. Jensen, M. B. Mogensen, and C. Chatzichristodoulou. The Role of Surface Area and Stability of High Performing Electrocatalysts in Alkaline Water Electrolysis. Electrochemical Society fall meeting, Prime 2020, Honolulu, US, 4-9 October, 2020 (oral, event cancelled)

Finally, BEEST results have been disseminated through 3 publications in international peer reviewed scientific journals:

1. M. R. Kraglund, M. Carmo, G. Schiller, S. A. Ansar, D. Aili, E. Christensen and J. O. Jensen. Ion-solvating membranes as a new approach towards high rate alkaline electrolyzers. Energy Environ. Sci., 2019, 12, 3313-3318. DOI: 10.1039/c9ee00832b

2. H. Li, M. R. Kraglund, A. K. Reumert, X. Ren, D. Aili, J. Yang. Poly(vinyl benzyl methylpyrrolidinium) hydroxide derived anion exchange membranes for water electrolysis. J. Mater. Chem. A, 2019, 7, 17914-17922. DOI: 10.1039/C9TA04868E

3. D. Aili, M. R. Kraglund, J. Tavacoli, C. Chatzichristodoulou and J. O. Jensen. Promoting electrolyte uptake of polysulfone membranes for advanced alkaline water electrolysis. J. Membr, Sci. 2020, 598, 117674. DOI: 10.1016/j.memsci.2019.117674

In addition to the above listed journal publications, we have compiled drafts for an additional 8 papers, with the following tentative titles:

1. F. Gellrich et al. Intrinsic activity of $Ni_{1-x}Mo_xO_z$ electrocatalysts for HER in alkaline environment.

2. F. Gellrich et al. NiMo – An operando Raman investigation of the stability of molybdenum oxide supported $Ni_{1-x}Mo_x$ Alkaline HER electrocatalysts

3. M. R. Kraglund et al. Measuring individual electrode overpotentials and Galvani potential drop across the electrodes in zero-gap AEC.

4. F. Gellrich et al. NiFe LDH – On the dynamic stability of NiFe LDH Alkaline OER electrocatalyst under industrially relevant conditions on cell level and by operando X-ray diffraction

5. M. R. Kraglund et al. 3D porous supports for AEC electrodes. Opportunity or hype?

6. C. Chatzichristodoulou et al. Design principles for advanced AEC electrodes – a combined experimental and simulation based approach.

7. M. R. Kraglund et al. Ultra high performance, scalable, and robust $Ni_{1-x}Mo_xO_z$ based cathodes for zero-gap AEC

8. A. Reumert, F. Pouregreshi, D. Aili, J. O. Jensen, S. Sunde, F. Seland. Unraveling a mysterious conductivity decrease in a zero-gap alkaline water electrolyzer: Membrane poisoning by catalyst capping agents.

These draft papers will be finalized and submitted for publication within the coming period, and BEEST (EUDP) will be acknowledge for supporting the effort.

1.6 Utilization of project results

DTU

Alkaline elctroysis is a R&D field of high priority at DTU Energy. The project results have contributed substantially to the building up of expertise on alkaline electrolysis at DTU Energy. As stated repeatedly, the need for an affordable electrolyzer technology, which is fully scalable to the multi-GW or even TW scale is undeniable and the gain from a higher performance obvious, both from a resource and a business perspective. At DTU Energy we are convinced that we can make a difference by developing improved electrodes, membranes/separators and cells. BEEST is the first large generic alkaline electrode project at the department and the encouraging results benefit the further development of several branches of the technology (diaphragm-based, AEM-based and high-temperature cells).

More specifically, DTU has gained insight in electrocatalysts for HER and OER in alkaline environment and their application in 3D porous electrodes, and has realized methodological improvements in testing zero-gap AEC that offer much greater insight on the inner workings of the AEC performance and degradation characteristics. The latter development, along with a simple multi-physics simulation model of zero-gap AEC, have promoted our understanding of the factors limiting AEC electrode performance. These results will be used in further development and demonstration efforts that are discussed in the next section.

The $Ni_{1-x}Mo_xO_z$ based Cathodes developed in BEEST show excellent performance, comparable or even better than commercial precious metal based Cathodes, and the fabrication method developed is suitable for large scale production. It is therefore worth assessing the possibility of obtaining IPR. As the associated effort and cost is substantial, DTU has been waiting to gain some insight on the long-term stability of these Cathodes before proceeding. The long-term testing results at DTU and GHS suggest that the stability of these electrodes depends on the operating mode (continuous/discontinuous) and system design (protective voltage during shut down). The possibility to protect the generated IPR in relation to the Cathode fabrication will be assessed prior to scientific journal publications, and further R&D efforts will be pursued in the direction of promoting the stability of the Cathode under diverse operational modes.

Aspects of the generated results are also integrated in teaching activities. For example, a simple continuum version of the multi-physics porous electrode model developed in BEEST has been included as an exercise in the “Advanced Electrochemistry” Course #47514 offered to MSc and PhD students at DTU. The approach of ECSA determination of Ni electrodes, based on electrochemical impedance spectroscopy, that was developed in the project is also introduced in lab exercises offered in “Energy Technologies” Course #47205 and in the “H_2 Production and Storage” Course #47309.

Finally, the broadening of the range of skills has eased the establishment of new collaborative contacts. Besides working with Green Hydrogen Systems, DTU Energy is now coordinating national and international (Horizon 2020) projects on development of advanced alkaline technology. Formal collaboration has been inititated with Nel Hydrogen (NO) and one more potential manufacturer of entire systems.

BWT

At this time any utilization of the project results by BWT depends 100% on the lead of GHS in implementation of the electrodes developed by DTU and scaled up by BWT. No separate marketing of the technology is planned to attract other customers due to the limited documentation of merits available.

So far the project has not resulted in commercial interest for samples or product based on the project activities at BWT, specifically the electrodes that have been scaled up at BWT. The technology and specific electrode designs are, however, further developed and considered for implementation in another project (EEEHy; funded by IFD), targeting operation at elevated temperature and pressure (150 ºC, 30 bar). This will assist in further maturation of the electrode technology and will provide useful knowledge on electrode stability under accelerated degradation conditions. The electrode performance and scalability of the electrode fabrication is very promising, but further assessment and potential optimization of the electrode stability under varying operating conditions will be required, before demonstration of the technology at industrial scale and subsequent planning of product roll out.
The work by BWT has not led to any patentable results.

GHS

The electrodes and catalysts are key components of the electrolysers and therefore of vital strategic importance as well as of crucial importance in order to reduce the cost of green hydrogen to a level where it can become competitive with hydrogen from fossil sources.
GHS will utilise the results gained within substrate geometry and the driving forces for the catalyst performance in order to continuously improve electrode performance.
Additionally, the new knowledge regarding the Galvani-drop is to be exploited in order to reduce the performance loss due to concentration differences.
A key take-away is the importance of adhesion for the catalyst coating and techniques for improving adhesion will be investigated further.
The BEEST project has contributed to improving the GHS electrodes and catalysts and demonstrated the importance of including Universities in the R&D process.

1.7 Project conclusion and perspective

The long-term vision behind the BEEST project was to establish highly efficient, low-cost alkaline electrolyzers for a stable, flexible, efficient, and highly integrated future Danish energy system relying 100% on renewable energy. Although alkaline electrolysis is an established technology, many aspects of the existing technology need to be improved to promote especially their efficiency at high production rates and thereby reduce the overall levelized cost of hydrogen.

Active and stable HER and OER catalysts, based on low-cost abundant materials, are critical for this endeavour. $Ni_{1-x}Mo_xO_z$ has been identified as a good HER candidate, but more work is required to assess its stability upon discontinuous operation. Preliminary operando XRD and Raman measurements suggest that the catalyst suffers irreversible degradation upon deep depolarization. Repeated aggressive on/off cycles during the accelerated degradation testing also resulted in loss of the catalyst coating. This can be avoided at the system level by employing a protective voltage across the stack during shut down. An alternative solution at the materials level would be preferable though so as not to complicate the system design. Controlling the ratio of Ni to Mo, fine tuning the reduction temperature, and/or including potential buffering additives to the electrode may help overcome this limitation. GHS has also developed a well performing non-precious metal HER catalyst that appears to be tolerant to depolarization. A thorough examination of its properties and understanding of its response to electrode potential variations is required for further cathode development.

$Ni_{1-y}Fe_y$ LDH is indeed an excellent OER catalyst, but further R&D work is required to establish and potentially promote its long-term stability under technologically relevant operating conditions.

Recent literature suggests that the catalyst stability depends on multiple parameters, such as the Fe content, the thickness of the nanoplatelets, the KOH concentration in the electrolyte, the current density, the ability of the cell configuration to sustain a certain level of Fe in solution, etc. Efforts in tracing this multi-parametric landscape will be undertaken in a recently funded DFF project (FREESLI) and the findings will be taken up in future development and demonstration projects.

Porous matrix based electrodes were proven to be an excellent platform for zero-gap AEC. Within BEEST it was concluded that the Cathode is rather insensitive to the microstructure of the porous matrix, the main performance driver being the surface area and intrinsic activity of the electrocatalyst. Future efforts in cathode development will therefore focus on electrode designs and fabrication methods that can help achieve ultra high surface area cathodes with low-cost catalysts having as high intrinsic activity as possible and sufficient stability under depolarization.

The performance of the anode on the other hand depends critically on the ability of the porous electrode to promote mass transport of the electrolyte and of the generated O_2 gas. As this can also be influenced by the flow field characteristics and the catalyst coating properties, further anode development efforts will attempt to address the topic more holistically. The methodology developed in BEEST that enables to assess experimentally the impact of mass transport on the performance of the anode is an invaluable asset for future development efforts. As the anode constitutes by far the main efficiency loss component at this point, a lot can be gained by its optimization. A combined simulation and experimental approach is required to speed up this complex optimization. DTU and GHS will attempt to raise the necessary funding that can support this effort.

Besides catalyst and electrode development, AEC can also benefit by improved diaphragms/membranes and by making a leap to higher operating temperatures. Thinner diaphragms will help limit ohmic losses, which become significant at high

current densities for the commercial diaphragm available today. Reducing the thickness of the diaphragm is also critical in terms of minimizing electrolyte concentration polarization effects at high current densities, which impact negatively the performance of the anode. Efforts to raise funding for this development are ongoing. Development of dense anion transport membranes with low enough ohmic resistance will also be very beneficial for the same reasons, and offer promise for reduced cross-over (H_2 in O_2 stream and vice versa) and a higher dynamic range. Raising the operating temperature boosts both transport and charge transfer processes taking place in AEC, and thus has a pronounced effect on AEC efficiency and productivity. This concept is currently being explored within the ongoing IFD funded project EEEHy, and follow up projects will be pursued to support the demanding development efforts required in this very promising direction.

Annex

BEEST Work Package 1

Deliverable 1.1 – Report of the literature review on H_2 and O_2 evolution electrocatalysts in alkaline environment

1 SCOPE & INTRODUCTION

The purpose of this report is to provide an overview of the state-of-the-art electrocatalysts for alkaline water electrolysis by reviewing literature. The overview is to be used as a basis for the selection of materials and compositions to be investigated in more detail in a screening study and for further development.

For water electrolysis two reactions are considered, namely the hydrogen evolution reaction (HER) taking place at the cathode, discussed in Section 2, and the oxygen evolution reaction (OER) taking place at the anode, discussed in Section 3. Although the term *water splitting* catalyst is used widely in publications, it is wiser to distinguish clearly between the two half-cell reactions. The local environment is very different between the anode (oxidizing conditions) and cathode (reducing conditions), and hence the catalyst surface responsible for the electrocatalytic activity will be different between the two electrodes, even if employing otherwise identical materials. Secondly, since the processes are physically separated it is possible to optimize each electrode individually. Consequently, the HER and OER are treated individually.

1.1 ELECTROCATALYST REQUIREMENTS

A good electrocatalyst ideally fulfill all of the following criteria:

- High electrocatalytic activity
- Large electrochemically active surface area (ECSA)
- High electronic conductivity
- Good wettability
- High selectivity
- Sufficient stability, mechanical, chemical, and electrochemical
- Made from abundant and cheap materials
- Easy processing and fabrication

In practice, not all criteria can be satisfied to the desired extent, and compromises must be made. As an example, a higher surface area due to porosity will tend to weaken the mechanical stability of the material. Likewise is it possible, that the realization of large active surface areas can complicate the processing and fabrication by introducing additional preparation steps.

It is unfortunately common in the majority of recent publications, that stability aspects are only vaguely covered and often under conditions less harsh than in real systems. When addressed, it is often under relatively mild conditions (temperature, KOH concentration, polarization), for relatively short duration (10-48 h) and with lacking post-operando characterization. Consequently, most of the novel materials in research literature are still far away from any real applications.

1.2 EVALUATING ELECTROCATALYSTS

It is difficult to accurately compare published data between publications due to varying experimental conditions, as well as differences in the presented figures of merit. The three most widely used figures of merit are:

- Graphical representation by current-potential curves (I-V curves or polarization curves)
- The tafel slope, b [mV dec^{-1}]
- The overpotential η [V] at a given current density i [mA/cm^2], η_i, commonly at 10 mA/cm^2

Secondary to those, the following are occasionally used as well:

- The exchange current density, i_0 [mA cm^{-2}]
- The turn over frequency, TOF [s^{-1}], at a given overpotential
- The current density *i,* at a given overpotential η, i_η

The overpotential at 10 mA/cm^2 is commonly with respect to the projected geometrical electrode surface area, but are also occasionally presented with respect to the electrochemically active surface area (ECSA), which is a more interesting quantity towards the intrinsic activity.

1.2.1 Determining the electrochemically active surface area

It is a recurring challenge to estimate the intrinsic activity of the catalyst materials. To compare the intrinsic activity, data needs to be normalized with the active area. The common surface area estimates are based on the ECSA and can be estimated in different ways. This is commonly by assessing the capacitance of the electrochemical double layer, which is primarily done in two ways[1]:

- By performing cycling voltammetry (CV) at varying scan rates in a non-faradaic region, using that the double layer charging current i_c is a product of the scan rate v and the electrochemical double-layer capacitance C_{dl}.

$$i_c = v\, C_{dl}$$

- From electrochemical impedance spectroscopy (EIS) data by fitting an equivalent circuit using a resistor (R) and a Randles (RC) or modified Randles (RQ) circuit in series

The estimated capacitance is then converted to an area by estimating a surface specific capacitance, for which in alkaline electrolyte 40 µF/cm^2 is commonly used[2]. Alternatively, BET adsorption isotherms can be used, and it represent a physicochemical method applicable to some samples, though it is less commonly used.

In some fields of catalysis, the specific gravimetrical activity is an interesting parameter, in particular when the catalysts are noble materials such as Pt, Ru or Ir. This is rarely the case in alkaline media, and the gravimetrical activity is generally not considered for alkaline HER and OER catalysts.

1.2.2 Varying experimental conditions

In recent academic papers, the electrolyte used is commonly NaOH (aq) or KOH (aq) at concentrations of either 0.1 M or 1.0 M, with 1 M KOH (aq) being the most common. The experiments are generally conducted at room temperature. However, in older publications conditions are often closer to relevant conditions, such as temperatures in the range of 50-90°C, and concentrations of up to 6-10 M KOH (aq). Current technical conditions, i.e. operating conditions for commercial alkaline electrolysers, are in the range of 4-8 M KOH (aq) (~20-35 wt%), with operating temperatures in the range 60-90°C with a desire to elevate the working temperature further. Consequently, much published data are not necessarily representative of performance in real systems.

Due to the outlined variations in activity estimates and experimental conditions, literature data is best used to elucidate activity trends and as a starting point for further material development. Moreover, there is a strong need for validation of investigated and developed materials under technical conditions.

2 HYDROGEN EVOLUTION ELECTROCATALYSTS

The hydrogen evolution reaction in alkaline media is believed to proceed through a two-step reaction. It is initiated by a water dissociation step known as the Volmer step, here described with *M* representing a surface site.

(1) $\mathrm{M} + \mathrm{H_2O} + \mathrm{e^-} \rightarrow \mathrm{MH} + \mathrm{OH^-}$ (Volmer)

Followed by a chemical (Tafel) or electrochemical (Heyrovsky) hydrogen desorption step.

(2a) $\mathrm{MH} + \mathrm{MH} \rightarrow 2\mathrm{M} + \mathrm{H_2}\uparrow$ (Tafel)

(2b) $\mathrm{MH} + \mathrm{H_2O} + \mathrm{e^-} \rightarrow \mathrm{M} + \mathrm{OH} + \mathrm{H_2}\uparrow$ (Heyrovsky)

It is not unlikely that both hydrogen desorption processes can occur simultaneously, and that the limiting step may change with current density due to changes in surface coverage.

2.1 NOTABLE MATERIALS

2.1.1 Platinum

Platinum represent the state-of-the-art material in both acidic and alkaline media. While the activity of Pt under acidic conditions are orders of magnitude higher, it nonetheless display near-zero onset potential in alkaline media and is by all practical means as good as it gets. However, one key point of performing electrolysis under alkaline conditions is the option to avoid noble metals such as Pt. Consequently, Pt can be considered and excellent material to benchmark against, but is not feasible for scaled up electrodes.

2.1.2 Raney nickel – Ni-Al & Ni-Zn

Raney nickel represents a skeletal micro- and mesoporous nickel structured formed by leaching a sacrificial element from a nickel alloy. This is commonly achieved alloying with aluminium or zinc, with leaching being done in concentrated hot KOH solution, often with a complexing agent to prevent precipitation of hydroxide phases. Aluminium is common in thermal interdiffusion processes such as plasma spraying[3–6] or when powder-routes are used[7], whereas zinc is common from electroplating preparation methods[8]. It is unclear to what extent residual Zn or Al plays a role in the high activity demonstrated by Raney coatings, or if it is purely an effect of enlarged ECSA. Ternary elements have been employed to further improve the activity, such as Mo[4,9], or Sn[10]. The effective roughness factor of thick electrode layers can range from 1000 up to 60000[11,12].

2.1.3 Nickel molybdenum

Nickel-molybdenum alloys have in several publications shown extraordinary activity for HER, on par with that of platinum. Some of the earliest demonstrations of high activity is a British Petroleum patent from 1982[13], showing an <100 mV overpotential even at 1 A/cm^2, although at technical conditions. Most materials are prepared by preparing a mixed Ni-Mo-oxide, followed by a reduction step between at 400 and 600°C under hydrogen containing atmosphere. Common molybdenum-to-nickel content is in the range 15-40 at%, with several publications showing a degree of Mo-leaching under testing conditions[14] or when the electrode is not polarized[15,16]. Due to challenges with estimating the ECSA due to pseudo-capacitances[17] it is still an open question which Ni-Mo compositions that shows the highest intrinsic activity.

Notably, Ni-Mo often shows the highest performance in screening studies on transition-metal alloy materials[18,19], which perhaps offer a more fair comparison than when comparing across publications.

2.1.4 Nickel tin

Nickel-tin alloys have not garnered the same attention as e.g. the nickel-molybdenum alloys, however, a few publications have shown very good activity on electrodes prepared by electroplating. In fact, it appears that the cathode material of Chinese electrolyzer manufacturer PERIC is a nickel-tin alloy, consequence of them publishing two articles on the material[20,21]. Although there have been mixed reports in older publications with regards to stability[22], or lack thereof[23], recent reports show not only good activity but also good stability[21]. The highest activity is realized when the tin content falls in the range 33-50 at%. The highest activity appear to be at around 40 at% tin, corresponding to a Ni_3Sn_2 phase, but there is not complete correspondence between published data[22,24,25], and the observed and presented electrode performance likely strongly depend on the achieved morphology and ECSA. While small amounts of tin in nickel improves the activity, pure tin is a terrible HER catalyst[22].

2.1.5 Sulfides

Sulfide materials, and in particular nickel-sulfides represent an interesting class of materials, that have received significant attention in the literature. A large bundle of publications from before 2010 evaluate nickel-sulfur electrode materials prepared by electrodeposition. In fact, a Norsk Hydro patent from as early as 1978 is on a Ni-S material prepared by electroplating[26]. The bulk of the published work achieve amorphous-phase coatings[27–31], with some materials resulting in mixed amorphous-crystalline materials[27,32,33] depending on exact preparation conditions. Generally resulting sulfur contents range between 15 to 40 at% by EDX. Likewise, ternary elements have been investigated, e.g. Manganese[29], or Cobalt[34], or co-deposition with Iron-sulfide particles[33]. As is the case with other publications of older date, the electrodes are evaluating in conditions closer to those technically used, but without data at 1 M KOH and room temperature. It is generally observed that during long time test, the amorphous materials turn gradually more and more crystalline, and that the majority of the sulfur is lost from the surface part of the coating, although with varying degree of activation or deactivation. Higher activity from amorphous phases over crystalline phases have also been shown for MoS_x and CoS_x[35].

More recent work present work on crystalline materials commonly prepared by a sulfurization process, e.g. by gas-phase annealing with using upstream elemental sulfur[25,36], or by aqueous hydrothermal like processes, using e.g. Na_2S[37] or Thiourea[38]. These more recently developed materials are generally tested at 1 M KOH at room temperature.

Additionally, since MoS_2 has appeared interesting for HER in acidic conditions, a number of publication has emerged evaluated the performance of MoS_2 or similar materials under alkaline conditions. The plain MoS_2 is supposedly not stable in high pH[39], but Ni-doped MoS_2 have shown good activity[40].

2.1.6 Phosphides

Phosphides have received substantial attention recently, and in particular cobalt-phosphide or mixed nickel-cobalt-phosphide. CoP_x have been prepared by electrodeposition[41] showing very high activity, but recent transition-metal-phosphides are commonly realized by a phosphorization process. Either through direct phosphorization of a nickel material[42], or more commonly, by converting a previously grown structure such as transition-metal-layered double hydroxides grown hydrothermally into a phosphide. The phosphorization is normally done using annealing with upstream elemental phosphorous[42], or NaH_2PO_2[43,44].

2.1.7 Overview

A summary of the reviewed catalyst materials, by merit of electrode performance at ambient or near-ambient temperature, is presented in **Table 1**. Several publications are omitted as they are difficult to tabularize in a sensible way, as a consequence of the available data representation or experimental conditions.

Table 1 *Reviewed hydrogen evolution performance for electrode materials at ambient and near-ambient temperature. Data for several entries is associated with a large degree of uncertainty with regards to precise overpotentials, either due to data being represented by graphs, or by data referring to reference potentials other than the Reversible Hydrogen Evolution potential at non-standard conditions. Not all materials are labelled with accurate stoichiometry. The "a"-prefix denotes amorphous phase.*

** Is presented as a Cobalt, but clearly contains phosphorous.*

Material	η_{10}	Tafel slope	[KOH/NaOH]	Year	Ref.
	mV	mV dec^{-1}			
PGM					
Pt/C 20%	10	34	1 M	2016	[25]
Pt/C	13	35	1 M	2017	[45]
Pt/C	34	34	1 M	2016	[46]
Pt	90	32	1 M	2015	[42]
Ni/RuO_2	175	-	1 M	2010	[27]
Sulfides					
$Ni\text{-}Ni_3S_2$	50	-	1 M	1990	[32]
$a\text{-}NiS_x$	50	106.8	28 wt%	2003	[31]
$a\text{-}NiS_xCo_y$	50	94.3	28 wt%	2003	[34]
NiS/NiS_2	60	99	1 M	2016	[36]
$a\text{-}NiS_x$	85	-	1 M	1984	[30]
$Ni\text{-}MoS_2$	98	60	1 M	2016	[40]
Ni/Ni-FeS	110	62	6 M	1997	[33]
NiS	130	83	1 M	2016	[25]
Ni_3S_2	223	-	1 M	2015	[38]
Phosphides					
Co(P) *	20	42.6	1 M	2017	[41]
$NiCoP_2$	87	59	1 M	2017	[43]
Ni_5P_4	150	53	1 M	2015	[42]
CoP	158	58	1 M	2017	[43]
CoP	209	129	1 M	2014	[47]
FeP	218	146	1 M	2014	[44]
Nickel-molybdenum					
$MoNi_4/MoO_2$	15	30	1 M	2017	[48]
$MoNi_4/MoO_2$	17	36	1 M	2017	[45]
$MoNi_4/MoO_2$	28	36	1 M	2017	[49]
NiMo-NW	30	86	1 M	2016	[46]
Ni-Mo	34	-	1 M	2014	[50]
MoO_2	55	66	1 M	2015	[51]
Ni-Mo	70	-	2 M	2013	[14]
Raney Nickel					
Ni-Al	15	-	30 wt%	2013	[6]
Ni-Al-Mo	150	150	38 wt%	2011	[52]
Ni-Al-Mo	<60	99	1 M	2004	[9]
Ni-Al	<50	121	1 M	1993	[11]
Other					
Co-Mo-B	66	67	1 M	2017	[53]
Ni-Sn	80	86	30 wt%	2016	[21]
$NiFeO_x$	88	-	1 M	2015	[54]
NiSe	96	120	1 M	2015	[55]
MoC_x	151	59	1 M	2015	[56]
Mo_2C	190	54	1 M	2012	[39]
MoB	225	59	1 M	2012	[39]

2.2 LITERATURE REVIEWS

The literature contains vast amounts of information, more so than what can be included even in a thorough review. In fact, several review papers already exist, focusing on different aspects or material classes. Examples cover general alkaline HER[57], acidic and alkaline HER[58], nickel-based alkaline HER[59], transition metal-phosphides for both OER and HER[60], and Ni, Co, or Fe sulfides, selenides and phosphides for OER and HER[61].

Beyond review papers, one can turn to screening studies, or studies examining a wide range of materials under identical conditions. Such studies often more valuable towards providing a fair overview than compiling and comparing individual publications employing varying conditions and methodologies. Screening studies are however, due to the practical aspects of conducting experiments, often limited to a selection of materials. Unfortunately only a few screening studies exist for the hydrogen evolution reaction. As an example, Raj investigated a small range of binary Nickel coatings[19], whereas McCrory *et al.* have investigated a number of different primarily transition metal based materials[18]. Both found comparatively high activities for nickel-molybdenum compounds. A comparison of relevant candidate materials as summarized by McCrory can be seen in **Figure 1**.

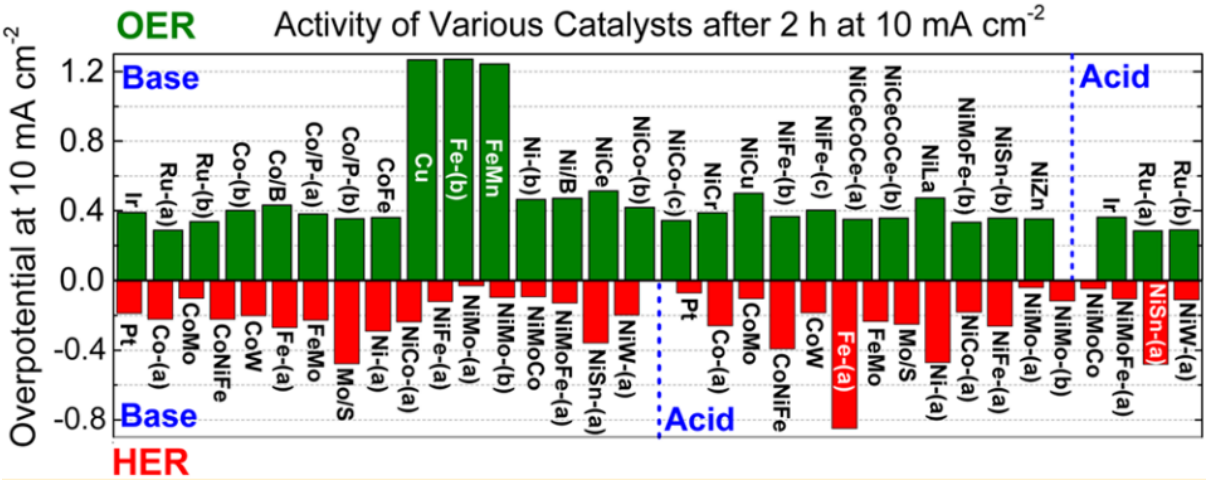

Figure 1 *Catalyst activity by overpotential at 10 mA cm^{-2} for various transition metal based compositions obtained by electrodeposition. Figure from [18].*

3 OXYGEN EVOLUTION ELECTROCATALYSTS

The oxygen evolution reaction in alkaline medium is a complex four electron reaction. It is not straightforward to outline all possible reaction pathways and reaction intermediates, due to the several possible electron and proton transfer steps, many of which can be coupled or decoupled. Nonetheless, a generalized OER mechanism, which reveal the commonly expected reaction intermediates, can be outlined with *M* denoting the reaction site.

(1) $\mathrm{M} + \mathrm{OH^-} \rightarrow \mathrm{MOH} + \mathrm{e^-}$

(2) $\mathrm{MOH} + \mathrm{OH^-} \rightarrow \mathrm{MO} + \mathrm{H_2O} + \mathrm{e^-}$

(3a) $\mathrm{MO} + \mathrm{OH^-} \rightarrow \mathrm{MOOH} + \mathrm{e^-}$

(4) $\mathrm{MOOH} + \mathrm{OH^-} \rightarrow \mathrm{M} + \mathrm{H_2O} + \mathrm{e^-} + \mathrm{O_2} \uparrow$

In analogue with the HER, a chemical desorption step is also occasionally suggested.

(3b) $\mathrm{MO} + \mathrm{MO} \rightarrow 2\mathrm{M} + \mathrm{O_2} \uparrow$

Other proposed reaction pathways can be found in the literature[62,63].

A recent notable theoretical prediction, seemingly valid for metal and metal oxide sites, suggest a universal scaling relation between the adsorption energies of MOH and MOOH intermediates, and in fact suggest a lower limit to the achievable overpotential for the OER on conventional catalytic sites[64].

OER catalysts are exposed to strongly oxidizing conditions. This means that, unlike the HER where catalysts tend to be metallic, the surface of OER catalysts are generally in an oxidized state. This can be either as an oxide, or as a hydroxide or oxyhydroxide or with a mixture of phases. As a consequence, several OER catalysts and candidate materials display relatively poor electronic conductivity, which in some cases can be inhibitive.

One approach researchers have attempted to circumvent this challenge is by preparing non-oxide compounds, such as transition metal pnictides (nitride, phosphide) or chalcogenides (sulfide, selenide), the latter being more common. Nonetheless, under the strong oxidizing conditions during the OER, most of the derived materials are expected to oxidize at the surface, and the various non-oxide compounds can perhaps be viewed as pre-catalysts, rather than the actual catalyst[65–67]. Even so, it may still represent a fruitful approach as it may improve the bulk conductivity and/or modify the surface oxide to improve the effect activity over bulk oxide catalyst, as well as in-situ transformations may result in a different surface morphologies as compared to alternative as-prepared materials. However, to compile a meaningful tabular overview, materials than can be considered pre-catalysts, whether addressed as such or not, will be referred to by their as-prepared compounds in the following.

3.1 NOTABLE MATERIALS

3.1.1 Oxides, perovskites & spinels

Several classes of as-prepared oxides have been investigated in the literature as OER catalyst. Notable early work by Bockris and Otagawa investigated a wide array of perovskite oxides in the 1980'ies[68,69]. Perovskites are an ABO_3 prototype structure, with alkaline or rare-earth cations on the A site and commonly first-row transition metal cations on the B site. They show a large degree of tunability due to the wide range of substitution elements and mixed stoichiometries possible, and have garnered significant interest as a result. Recent work showed high activity for $Ba_{0.5}Sr_{0.5}Co_{0.8}Fe_{0.2}O_{3-\delta}$[70], although

it was later shown to display dissolution of Ba and Sr and amorphization of the surface under OER conditions[71,72]. Likewise have lanthanide-barium-cobalt-based double perovskites showed promising activity[71], and work on tuning the strontium-cobalt perovskite[73], or the lanthanum-strontium-cobalt perovskite[74] systems have been carried out, although it is challenging to compare across publications. New work by suggest a multi-descriptor correlation for perovskite activity, and demonstrate the findings by comparing most of the promising perovskite compositions under identical conditions and thereby providing a good activity comparison on perovskite materials[75]. This is valuable, as the intrinsic activity is compared on a normalized oxide-surface-area basis, although it may not be directly comparable to other publications.

Similar to perovskites, transition metal oxides with the spinel host structure have received a lot of attention. The spinel structure is an AB_2O_4 structure, with A being a divalent cation, and B a trivalent cation. The spinel structure is easily prepared and is commonly realized by annealing precursor hydroxide structures in air at around 250-500°C. A lot of work by Singh *et al.* have investigated several transition metal compositions, with A-site atoms such as Mn, Cu, Co and Ni, and B-site atoms with Fe and various degree of substation with e.g. V, or Cr[76–80]. Several of these show very good OER activity, and find that the activity (by overpotential at 100 mA cm^{-2}) for selected compositions rank from best to worst: $NiFeCrO_4$ ~ $NiFe_{1.2}Cr_{0.8}O_4$ < $CoFe_{1.2}Cr_{0.8}O_4$ < $MnFe_{1.4}Cr_{0.6}O_4$ < $CuFe_{1.2}Cr_{0.8}O_4$ < Fe_3O_4. A focused review by Hamdani *et al.* compile a large amount of early published work on spinel structures for OER including Ni and Co-based compositions without Fe[81].

Noble metals

Besides the commonly sought cheaper transition metal oxide catalysts, iridium oxide and ruthenium oxide are often used for the oxygen evolution. IrO_2 and RuO_2 represent the state-of-the-art OER catalyst under acidic conditions, although only IrO_2 is sufficiently stable under real cell conditions in the long run. Although frequently used as a reference material, neither are stable under alkaline OER conditions as they suffer from dissolution, and they are anyway not relevant towards applications in the alkaline system due the high cost and very low elemental abundance[82].

3.1.2 Hydroxides, oxyhydroxides and layered double hydroxides

Several transition metals form hydroxide phases under OER conditions in alkaline medium. Even for non-oxide transition-metal compounds, the surface is believed to reorganize and oxidize to form hydroxides. Recently nickel-iron hydroxides have been shown to have excellent OER activity, and has become the state-of-the-art OER catalyst under alkaline conditions. The hydroxide phases are often labelled generically as M-O_xH_y, or simply M-O_x, since prepared materials often display mixed phases and change in-situ compared to the as-prepared materials.

One subclass which have received substantial attention is the layered double hydroxides (LDH). The LDH structure consists of alternating layers of transition-metals octahedrally coordinated to oxygen/hydroxyl and layers with intercalated water and anions. LDHs are commonly formed in the presence of both 2+ and 3+ cations, with anions intercalating to balance the excess positive charge from the 3+ cations. The prototype structure in the general form is written

$$\left[M^{II}_{1-x}M^{III}_{x}(OH)_2\right]^{z+}(A^{n-})_{z/n}\cdot yH_2O$$

With M representing either divalent cations, commonly Ni^{2+}, Co^{2+}, Fe^{2+}, Mg^{2+} or Zn^{2+}, or trivalent cations such as Fe^{3+}, Cr^{3+}, Al^{3+}, or Ga^{3+}. A represent intercalated cations such as OH^-, CO_3^{2-}, SO_4^{2-}, Cl^-, ClO_4^-, NO_3^- or CH_3COO^-. Larger organic molecules can also be substituted in, and e.g. formamide can be used to exfoliate the LDH structure to form mono-layers[83]. A particular notable LDH is the nickel-

iron LDH. It has been found that presence iron have a strong activating effect on nickel, and the Ni-Fe-LDH have even become the state-of-the-art alkaline OER catalyst in academic contexts[84,85].

3.1.3 Non-oxides

Several chalcogenides have shown promising OER activity, whether by intrinsic activity or as pre-catalysts. Several studies on primarily sulfides and more recently selenides have shown activity comparable or surpassing the most active demonstrated Ni-Fe hydroxides. A few publications on tellurides can also be found.

Phosphides for OER catalysis are less common, as they are mainly considered for the HER. Nonetheless, some studies can be found, often in relation to bifunctionality (HER and OER active) for a developed material, and not as a result of a targeted study. Nitrides and carbides are not commonly investigated.

3.1.4 Overview

A tabularized overview of reviewed OER catalysts are available in **Table 2**. The here reviewed perovskites were normalized to oxide-surface area, and assessed at 1 mA cm^{-2}. In contrast, most of the herein reviewed spinel catalysts were investigated by preparing an electrode by forming a paste with the prepared powder, and not normalized by area, however they are assessed at 100 mA cm^{-2} instead. Many hydroxide and chalcogenide materials were compared at the 10 mA cm^{-2} point, although with differences in support material. Foams represent naturally larger loadings and show correspondingly better performance as compared to powders investigated on glassy carbon electrodes (GC). A crude estimate based on reference [86] suggest about 30-50 mV in difference between foam and GC tests.

Table 2 *Reviewed oxygen evolution catalysts. GC = glassy carbon (electrode), + C = mixed with carbon, CFP = carbon fibre paper. Publications labelled their investigated materials differently, and the listed 'Material' is not always stoichiometrically accurate, but resemble what is used in the given publication.*

Material	Support	η_i	Tafel slope	[KOH/NaOH]	Year	Ref.
		mV	mV dec^{-1}			
Perovskites		***@ 1 mA cm^{-2}***				
$Ba_{0.5}Sr_{0.5}Co_{0.8}Fe_{0.2}O_3$	GC	330	-	0.1 M	2011	[70]
$Ho_{0.5}Ba_{0.5}CoO_3$	GC + C	330	-	0.1 M	2013	[71]
$Pr_{0.5}Ba_{0.5}CoO_3$	GC + C	330	-	0.1 M	2013	[71]
$Ba_{0.5}Sr_{0.5}Co_{0.8}Fe_{0.2}O_3$	GC + C	360	-	0.1 M	2013	[71]
$Sm_{0.5}Ba_{0.5}CoO_3$	GC + C	360	-	0.1 M	2013	[71]
$Gd_{0.5}Ba_{0.5}CoO_3$	GC + C	370	-	0.1 M	2013	[71]
$La_{0.5}Ca_{0.5}FeO_3$	GC	390	-	0.1 M	2011	[70]
$LaCoO_3$	GC + C	410	-	0.1 M	2013	[71]
$La_{0.5}Ca_{0.5}CoO_3$	GC	420	-	0.1 M	2011	[70]
$LaCoO_3$	GC	450	-	0.1 M	2011	[70]
$LaNiO_3$	GC	450	-	0.1 M	2011	[70]
Spinels		***@ 100 mA cm^{-2}***				
$NiCo_2O_4$	Graphite	184	-	1 M	2011	[87]
La-Co_3O_4	Ni support	230	55	1 M	2007	[78]
$NiFe_{1.2}Cr_{0.8}O_4$	Ni support	285	40	1 M	2006a	[77]
$CoFe_{1.2}Cr_{0.8}O_4$	Ni support	312	42	1 M	2002	[76]
$MnFe_{1.4}Cr_{0.6}O_4$	Ni support	330	35	1 M	2006	[88]
$NiFe_2O_4$	Ni support	352	40	1 M	2006a	[77]

$NiFe_{1.5}V_{0.5}O_4$	Ni support	380	40	1 M	2010	[79]
$NiFeVO_4$	Ni support	400	40	1 M	2010	[79]
$CuFe_{1.2}Cr_{0.8}O_4$	Ni support	428	50	1 M	2007	[80]
Hydroxides	***@ GC***	**@ 10 mA cm^{-2}**				
G-CoFeW	GC	223	37	1 M	2016	[86]
NiFeMn-LDH	GC	262	47	1 M	2016	[89]
Ni-Fe	GC + C	262	49.7	1 M	2017	[90]
NiFeCr-6:2:1	GC	280	131	1 M	2018	[91]
$Ni_{0.75}V_{0.25}$	GC	300	50	1 M	2016	[92]
NiFe-3:1	GC	322	144	1 M	2018	[91]
FeCo-LDH	GC	331	85	1 M	2016	[86]
$Ni_{0.75}Fe_{0.25}$	GC	335	64	1 M	2016	[92]
Hydroxides	***@ Foam***	**@ 10 mA cm^{-2}**				
G-CoFeW	Au/Ni foam	191	-	1 M	2016	[86]
NiFeV-LDH	Ni foam	192	42	1 M	2018	[93]
$Ni_{0.8}Co_{0.2}Fe_{0.1}$-LDH	Ni foam	220	42	1 M	2015	[94]
Ni-Fe	Ni foam	244	32	1 M	2016	[67]
FeCo-LDH	Au/Ni foam	279	-	1 M	2016	[86]
Ni-Fe/$NiCo_2S_4$	Ni foam	201 @ 60 mA cm^{-2}	46.3	1 M	2017	[37]
Ni-Fe	Ni foam	260 @ 60 mA cm^{-2}	57.7	1 M	2017	[37]
Sulfides		**@ 10 mA cm^{-2}**				
NiS_x	Ni foam	180	96	1 M	2016	[36]
$Fe_{17.5\%}$-Ni_3S_2	Ni foam	214	42	1 M	2018	[95]
Ni(Fe)S_2	GC + C	230	42	1 M	2017	[90]
Ni_3S_2	Ni foam	287	82	1 M	2018	[95]
$Fe_{0.1}$-NiS_2	Ti mesh	231 @ 100 mA cm^{-2}	43	1 M	2016	[96]
$NiCo_2S_4$	Ni foam	306 @ 60 mA cm^{-2}	56.8	1 M	2017	[37]
NiS_2	Ti mesh	420 @ 100 mA cm^{-2}	83	1 M	2016	[96]
Selenides		**@ 10 mA cm^{-2}**				
$CoNi_2Se_4$	CFP	160	72	1 M	2017	[97]
$Ni_xFe_{1-x}Se_2$	Ni foam	195	28	1 M	2016	[67]
$NiSe_2$	Ni foam	241	54	1 M	2016	[67]
NiSe	Ni foam	253	45	1 M	2016	[67]
$Ni_{0.85}Se$	Graphite	302	81	1 M	2016	[98]
NiSe	Ni foam	270 @ 20 mA cm^{-2}	64	1 M	2015	[55]
Other		**@ 10 mA cm^{-2}**				
NiTe	Ni foam	262	74	1 M	2018	[99]
$CoTe_2$	Ti mesh	340 @ 50 mA cm^{-2}	67	1 M	2018	[100]
Ni_2P	GC	290	47	1 M	2015	[101]
RuO_2	Ti mesh	278 @ 100 mA cm^{-2}	61	1 M	2016	[96]
IrO_x	Ni foam	347	107	1 M	2018	[95]

RuO_2	GC + C	350	90.3	1 M	2017	[90]

3.2 LIST OF LITERATURE REVIEW PAPERS

As evident from **Table 2** a direct comparison between materials is not straight forward. Consequently, screening studies employing a fixed methodology are valuable. Furthermore, due to the abundance of literature on all material classes, more focused and material-specific review studies provide a more in-depth view into the respectively addressed materials.

Some of the earliest work demonstrating a high activity of Ni-Fe materials was done by Corrigan. In line with that discovery, a screening study from 1989 investigate a range Ni-X co-precipitated hydroxide films achieved by electroplating[102]. Later and much more recently, a series of benchmarking studies by Jaramillo *et al.* investigated a number of mixed oxides for the OER, both by electrodeposition methods[1,18], and on particulate materials[2].

The by far largest and widest ranging screening study was done by Gerken *et al.* and covered more than 3400 unique ternary compositions[103]. Due to the large scale and automated nature of the study, the specific phases were not investigated, however, it does provide strong and clear trends in activity, and it is notable considering the current prevailing understanding that many surfaces restructure into hydroxide-type phases.

A few more limited compositions spaces have also been examined, e.g. Ni-Fe-Co-Al[104], and Ni-Fe-Co-Ce[105]. Likewise, recent work on understanding the correlating factors of perovskites effectively compare the commonly active compositions[75].

Complementary to screening studies a number of review papers also exist. These range from broad reaching and generic[63,72,106–109], to more specialized such as only focused on Ni-Fe hydroxide[85,110], cobalt-based[111], on phosphides[60], or phosphides, sulfides and selenides[61].

4 CONCLUDING REMARKS AND RECOMMENDATIONS

The alkaline hydrogen evolution and oxygen evolution reactions occurring during water electrolysis do not yet have standardized go-to catalysts. However, looking through the available literature, some trends present themselves for both the cathodic HER and the anodic OER.

In terms of HER, nickel-molybdenum systems generally come out on top. Although the Ni-Mo system have seen increasing interest, questions remain in terms of stability and active sites. The degree of Mo leaching or oxidatoin on depolarization is a possible concern. Furthermore, the active sites and optimal catalyst structure remain far from understood. Although alternative interesting catalysts exist besides Ni-Mo and platinum, such as amorphous nickel-sulfide, and perhaps cobalt-phosphide, it appears most promising to pursue the Ni-Mo system as it consistently show good activity across most published literature.

The OER is more complex, but the current prevailing trend in literature is to prepare nickel-iron-containing materials. Initially as pristine nickel-iron-hydroxides such as the Ni-Fe-LDH, and more recently in the form of e.g. sulfides or selenides, which generally present even higher activity. What is most critically lacking currently, is information on the behavior under technical conditions, and the possible adverse effects of improperly incorporated iron leaching. It seems prudent to pursue a plain oxide/hydroxide nickel-iron structure before looking into sulfurized versions of the material. Even among spinel structures, the mixed Ni-Fe-spinels display good activity. A further trend is the positive

effects of introducing chromium to the Ni-Fe catalysts. This appear to improve activity of Ni-Fe based catalysts, both when prepared as spinels[77], as LDH's[91], or in a less specified manner[103], even if it is a result of Cr-leaching and increased effective surface area[112].

5 REFERENCES

1. McCrory, C. C. L., Jung, S., Peters, J. C. & Jaramillo, T. F. Benchmarking Heterogeneous Electrocatalysts for the Oxygen Evolution Reaction. *J. Am. Chem. Soc.* **135**, 16977–16987 (2013).

2. Jung, S., McCrory, C. C. L., Ferrer, I. M., Peters, J. C. & Jaramillo, T. F. Benchmarking nanoparticulate metal oxide electrocatalysts for the alkaline water oxidation reaction. *J. Mater. Chem. A* **4**, 3068–3076 (2016).

3. Schiller, G. & Borck, V. Vacuum plasma sprayed electrodes for advanced alkaline water electrolysis. *Int. J. Hydrogen Energy* **17**, 261–273 (1992).

4. Schiller, G., Henne, R. & Borck, V. Vacuum plasma spraying of high-performance electrodes for alkaline water electrolysis. *J. Therm. Spray Technol.* **4**, 185–194 (1995).

5. Schiller, G., Henne, R., Mohr, P. & Peinecke, V. High performance electrodes for an advanced intermittently operated 10-kW alkaline water electrolyzer. *Int. J. Hydrogen Energy* **23**, 761–765 (1998).

6. Chade, D. *et al.* Evaluation of Raney nickel electrodes prepared by atmospheric plasma spraying for alkaline water electrolysers. *Int. J. Hydrogen Energy* **38**, 14380–14390 (2013).

7. Endoh, E., Otouma, H., Morimoto, T. & Oda, Y. New Raney nickel composite-coated electrode for hydrogen evolution. *Int. J. Hydrogen Energy* **12**, 473–479 (1987).

8. Balej, J., Divisek, J., Schmitz, H. & Mergel, J. Preparation and properties of Raney nickel electrodes on Ni-Zn base for H2 and O2 evolution from alkaline solutions Part I: electrodeposition of Ni-Zn alloys from chloride solutions. *J. Appl. Electrochem.* **22**, 705–710 (1992).

9. Birry, L. & Lasia, A. Studies of the Hydrogen Evolution Reaction on Raney Nickel–Molybdenum Electrodes. *J. Appl. Electrochem.* **34**, 735–749 (2004).

10. Huber, G. W., Shabaker, J. W. & Dumesic, J. A. Raney Ni-Sn Catalyst for H2 Production from Biomass-Derived Hydrocarbons. *Science (80-.).* **300**, 2075–2077 (2003).

11. Los, P., Rami, A. & Lasia, A. Hydrogen evolution reaction on Ni-Al electrodes. *J. Appl. Electrochem.* **23**, 135–140 (1993).

12. Miousse, D., Lasia, A. & Borck, V. Hydrogen evolution reaction on Ni-Al-Mo and Ni-Al electrodes prepared by low pressure plasma spraying. *J. Appl. Electrochem.* **25**, 592–602 (1995).

13. Brown, D. E. & Mahmood, M. N. Method of preparing active electrodes. (1982).

14. McKone, J. R., Sadtler, B. F., Werlang, C. a, Lewis, N. S. & Gray, H. B. Ni-Mo nanopowders for efficient electrochemical hydrogen evolution. *ACS Catal.* **3**, 166–169 (2013).

15. Divisek, J., Schmitz, H. & Balej, J. Ni and Mo coatings as hydrogen cathodes. *J. Appl. Electrochem.* **19**, 519–530 (1989).

16. Schalenbach, M. *et al.* Nickel-molybdenum alloy catalysts for the hydrogen evolution reaction: Activity and stability revised. *Electrochim. Acta* **259**, 1154–1161 (2018).

17. Csernica, P. M. *et al.* Electrochemical Hydrogen Evolution at Ordered Mo 7 Ni 7. *ACS Catal.* **7**, 3375–3383 (2017).

18. McCrory, C. C. L. *et al.* Benchmarking Hydrogen Evolving Reaction and Oxygen Evolving Reaction Electrocatalysts for Solar Water Splitting Devices. *J. Am. Chem. Soc.* **137**, 4347–4357 (2015).

19. Raj, I. A. Nickel-based, binary-composite electrocatalysts for the cathodes in the energy-efficient industrial production of hydrogen from alkaline-water electrolytic cells. *J. Mater. Sci.* **28**, 4375–4382 (1993).

20. Zhu, Y., Liu, T., Li, L., Song, S. & Ding, R. Nickel-based electrodes as catalysts for hydrogen evolution reaction in alkaline media. *Ionics (Kiel).* 1–7 (2017). doi:10.1007/s11581-017-2270-z

21. Zhu, Y. *et al.* Microstructure and hydrogen evolution catalytic properties of Ni-Sn alloys prepared by electrodeposition method. *Appl. Catal. A Gen.* **500**, 51–57 (2015).

22. Yamashita, H., Yamamura, T. & Yoshimoto, K. The Relation Between Catalytic Ability for Hydrogen Evolution Reaction and Characteristics of Nickel-Tin Alloys. *J. Electrochem. Soc.* **140**, 2238 (1993).

23. Santos, M. B. F., da Silva, E. P., Andrade, R. & Dias, J. A. F. NiSn and porous NiZn coatings for water electrolysis. *Electrochim. Acta* **37**, 29–32 (1992).

24. Jović, V. D., Lačnjevac, U., Jović, B. M., Karanović, L. & Krstajić, N. V. Ni-Sn coatings as cathodes for hydrogen evolution in alkaline solution. Chemical composition, phase composition and morphology effects. *Int. J. Hydrogen Energy* **37**, 17882–17891 (2012).

25. Zhu, W. *et al.* Nickel sulfide microsphere film on Ni foam as an efficient bifunctional electrocatalyst for overall water splitting. *Chem. Commun.* **52**, 1486–1489 (2016).

26. Holte, J. B., Andreassen, K. A., Widding, K. & Harang, H. Fremgangsmåte for framstilling av aktive katoder for kloralkali- og vannspaltnings-celler. (1978).

27. Cao, Y. *et al.* Electrodeposited Ni–S intermetallic compound film electrodes for hydrogen evolution reaction in alkaline solutions. *Mater. Lett.* **64**, 261–263 (2010).

28. He, H., Liu, H., Liu, F. & Zhou, K. Distribution of sulphur and electrochemical properties of nickel sulphur coatings electrodeposited on the nickel foam as hydrogen evolution reaction cathodes. *Mater. Lett.* **59**, 3968–3972 (2005).

29. Shan, Z., Liu, Y., Chen, Z., Warrender, G. & Tian, J. Amorphous Ni–S–Mn alloy as hydrogen evolution reaction cathode in alkaline medium. *Int. J. Hydrogen Energy* **33**, 28–33 (2008).

30. Vandenborre, H., Vermeiren, P. & Leysen, R. Hydrogen evolution at nickel sulphide cathodes in alkaline medium. *Electrochim. Acta* **29**, 297–301 (1984).

31. Han, Q., Liu, K., Chen, J. & Wei, X. A study on the electrodeposited Ni–S alloys as hydrogen evolution reaction cathodes. *Int. J. Hydrogen Energy* **28**, 1207–1212 (2003).

32. Sabela, R. & Paseka, I. Properties of Ni-S x electrodes for hydrogen evolution from alkaline medium. *J. Appl. Electrochem.* **20**, 500–505 (1990).

33. Assunção, N. A., de Giz, M. J., Tremiliosi-Filho, G. & Gonzalez, E. R. A Study of the Hydrogen Evolution Reaction on a Ni/NiFeS Electrodeposited Coating. *J. Electrochem. Soc.* **144**, 2794

(1997).

34. Han, Q., Liu, K., Chen, J. & Wei, X. Hydrogen evolution reaction on amorphous Ni–S–Co alloy in alkaline medium. *Int. J. Hydrogen Energy* **28**, 1345–1352 (2003).

35. Staszak-Jirkovský, J. *et al.* Design of active and stable Co–Mo–Sx chalcogels as pH-universal catalysts for the hydrogen evolution reaction. *Nat. Mater.* **15**, 197–203 (2015).

36. You, B. & Sun, Y. Hierarchically Porous Nickel Sulfide Multifunctional Superstructures. *Adv. Energy Mater.* **6**, 1502333 (2016).

37. Liu, J. *et al.* Hierarchical NiCo2S4@NiFe LDH Heterostructures Supported on Nickel Foam for Enhanced Overall-Water-Splitting Activity. *ACS Appl. Mater. Interfaces* **9**, 15364–15372 (2017).

38. Feng, L.-L. *et al.* High-Index Faceted Ni 3 S 2 Nanosheet Arrays as Highly Active and Ultrastable Electrocatalysts for Water Splitting. *J. Am. Chem. Soc.* **137**, 14023–14026 (2015).

39. Vrubel, H. & Hu, X. Molybdenum Boride and Carbide Catalyze Hydrogen Evolution in both Acidic and Basic Solutions. *Angew. Chemie Int. Ed.* **51**, 12703–12706 (2012).

40. Zhang, J. *et al.* Engineering water dissociation sites in MoS 2 nanosheets for accelerated electrocatalytic hydrogen production. *Energy Environ. Sci.* **9**, 2789–2793 (2016).

41. Liu, B., Zhang, N. & Ma, M. Cobalt-based nanosheet arrays as efficient electrocatalysts for overall water splitting. *J. Mater. Chem. A* **5**, 17640–17646 (2017).

42. Ledendecker, M. *et al.* The Synthesis of Nanostructured Ni 5 P 4 Films and their Use as a Non-Noble Bifunctional Electrocatalyst for Full Water Splitting. *Angew. Chemie Int. Ed.* **54**, 12361–12365 (2015).

43. Li, Y., Jiang, Z., Huang, J., Zhang, X. & Chen, J. Template-synthesis and electrochemical properties of urchin-like NiCoP electrocatalyst for hydrogen evolution reaction. *Electrochim. Acta* **249**, 301–307 (2017).

44. Liang, Y., Liu, Q., Asiri, A. M., Sun, X. & Luo, Y. Self-Supported FeP Nanorod Arrays: A Cost-Effective 3D Hydrogen Evolution Cathode with High Catalytic Activity. *ACS Catal.* **4**, 4065–4069 (2014).

45. Chen, Y.-Y. *et al.* Self-Templated Fabrication of MoNi 4 /MoO 3- x Nanorod Arrays with Dual Active Components for Highly Efficient Hydrogen Evolution. *Adv. Mater.* **29**, 1703311 (2017).

46. Fang, M. *et al.* Hierarchical NiMo-based 3D electrocatalysts for highly-efficient hydrogen evolution in alkaline conditions. *Nano Energy* **27**, 247–254 (2016).

47. Tian, J., Liu, Q., Asiri, A. M. & Sun, X. Self-Supported Nanoporous Cobalt Phosphide Nanowire Arrays: An Efficient 3D Hydrogen-Evolving Cathode over the Wide Range of pH 0–14. *J. Am. Chem. Soc.* **136**, 7587–7590 (2014).

48. Zhang, J. *et al.* Efficient hydrogen production on MoNi4 electrocatalysts with fast water dissociation kinetics. *Nat. Commun.* **8**, 15437 (2017).

49. Jin, Y., Yue, X., Shu, C., Huang, S. & Shen, P. K. Three-dimensional porous MoNi4 networks constructed by nanosheets as bifunctional electrocatalysts for overall water splitting. *J. Mater. Chem. A* **5**, 2508–2513 (2017).

50. Wang, Y. *et al.* A 3D Nanoporous Ni-Mo Electrocatalyst with Negligible Overpotential for Alkaline Hydrogen Evolution. *ChemElectroChem* **1**, 1138–1144 (2014).

51. Jin, Y. & Shen, P. K. Nanoflower-like metallic conductive MoO 2 as a high-performance non-precious metal electrocatalyst for the hydrogen evolution reaction. *J. Mater. Chem. A* **3**, 20080–20085 (2015).

52. Salvi, P. *et al.* Hydrogen evolution reaction in PTFE bonded Raney-Ni electrodes. *Int. J. Hydrogen Energy* **36**, 7816–7821 (2011).

53. Gupta, S. *et al.* Co-Mo-B Nanoparticles as a non-precious and efficient Bifunctional Electrocatalyst for Hydrogen and Oxygen Evolution. *Electrochim. Acta* **232**, 64–71 (2017).

54. Wang, H. *et al.* Bifunctional non-noble metal oxide nanoparticle electrocatalysts through lithium-induced conversion for overall water splitting. *Nat. Commun.* **6**, 7261 (2015).

55. Tang, C., Cheng, N., Pu, Z., Xing, W. & Sun, X. NiSe Nanowire Film Supported on Nickel Foam: An Efficient and Stable 3D Bifunctional Electrode for Full Water Splitting. *Angew. Chemie Int. Ed.* **54**, 9351–9355 (2015).

56. Wu, H. Bin, Xia, B. Y., Yu, L., Yu, X.-Y. & Lou, X. W. Porous molybdenum carbide nano-octahedrons synthesized via confined carburization in metal-organic frameworks for efficient hydrogen production. *Nat. Commun.* **6**, 6512 (2015).

57. Safizadeh, F., Ghali, E. & Houlachi, G. Electrocatalysis developments for hydrogen evolution reaction in alkaline solutions – A Review. *Int. J. Hydrogen Energy* **40**, 256–274 (2015).

58. Zeng, M. & Li, Y. Recent advances in heterogeneous electrocatalysts for the hydrogen evolution reaction. *J. Mater. Chem. A* **3**, 14942–14962 (2015).

59. Gong, M., Wang, D.-Y., Chen, C.-C., Hwang, B.-J. & Dai, H. A mini review on nickel-based electrocatalysts for alkaline hydrogen evolution reaction. *Nano Res.* **9**, 28–46 (2016).

60. Wang, Y., Kong, B., Zhao, D., Wang, H. & Selomulya, C. Strategies for developing transition metal phosphides as heterogeneous electrocatalysts for water splitting. *Nano Today* **15**, 26–55 (2017).

61. Anantharaj, S. *et al.* Recent Trends and Perspectives in Electrochemical Water Splitting with an Emphasis on Sulfide, Selenide, and Phosphide Catalysts of Fe, Co, and Ni: A Review. *ACS Catal.* **6**, 8069–8097 (2016).

62. Matsumoto, Y. & Sato, E. Electrocatalytic properties of transition metal oxides for oxygen evolution reaction. *Mater. Chem. Phys.* **14**, 397–426 (1986).

63. Fabbri, E., Habereder, A., Waltar, K., Kotz, R. & Schmidt, T. J. Developments and perspectives of oxide-based catalysts for the oxygen evolution reaction. *Catal. Sci. Technol.* (2014). doi:10.1039/C4CY00669K

64. Man, I. C. *et al.* Universality in Oxygen Evolution Electrocatalysis on Oxide Surfaces. *ChemCatChem* **3**, 1159–1165 (2011).

65. Wygant, B. R., Kawashima, K. & Mullins, C. B. Catalyst or Precatalyst? The Effect of Oxidation on Transition Metal Carbide, Pnictide, and Chalcogenide Oxygen Evolution Catalysts. *ACS Energy Lett.* **3**, 2956–2966 (2018).

66. Wu, Z., Gan, Q., Li, X., Zhong, Y. & Wang, H. Elucidating Surface Restructuring-Induced Catalytic Reactivity of Cobalt Phosphide Nanoparticles under Electrochemical Conditions. *J. Phys. Chem. C* **122**, 2848–2853 (2018).

67. Xu, X., Song, F. & Hu, X. A nickel iron diselenide-derived efficient oxygen-evolution catalyst. *Nat. Commun.* **7**, 12324 (2016).

68. Bockris, J. O. & Otagawa, T. Mechanism of oxygen evolution on perovskites. *J. Phys. Chem.* **87**, 2960–2971 (1983).

69. Bockris, J. O. & Otagawa, T. The Electrocatalysis of Oxygen Evolution on Perovskites. *J. Electrochem. Soc.* **131**, 290 (1984).

70. Suntivich, J., May, K. J., Gasteiger, H. A., Goodenough, J. B. & Shao-Horn, Y. A Perovskite Oxide Optimized for Oxygen Evolution Catalysis from Molecular Orbital Principles. *Science (80-.).* **334**, 1383–1385 (2011).

71. Grimaud, A. *et al.* Double perovskites as a family of highly active catalysts for oxygen evolution in alkaline solution. *Nat. Commun.* **4**, 2439 (2013).

72. Trotochaud, L. & Boettcher, S. W. Precise oxygen evolution catalysts: Status and opportunities. *Scr. Mater.* **74**, 25–32 (2014).

73. Zhou, W., Zhao, M., Liang, F., Smith, S. C. & Zhu, Z. High activity and durability of novel perovskite electrocatalysts for water oxidation. *Mater. Horizons* **2**, 495–501 (2015).

74. Elumeeva, K. *et al.* A Simple Approach towards High-Performance Perovskite-Based Bifunctional Oxygen Electrocatalysts. *ChemElectroChem* **3**, 138–143 (2016).

75. Cheng, X. *et al.* Oxygen Evolution Reaction on Perovskites: A Multieffect Descriptor Study Combining Experimental and Theoretical Methods. *ACS Catal.* **8**, 9567–9578 (2018).

76. Singh, R. N., Singh, N. K. & Singh, J. P. Electrocatalytic properties of new active ternary ferrite film anodes for O2 evolution in alkaline medium. *Electrochim. Acta* **47**, 3873–3879 (2002).

77. Singh, R. N., Singh, J. P., Lal, B., Thomas, M. J. K. & Bera, S. New NiFe2-xCrxO4 spinel films for O2 evolution in alkaline solutions. *Electrochim. Acta* **51**, 5515–5523 (2006).

78. Singh, R. N., Mishra, D., Anindita, Sinha, A. S. K. & Singh, A. Novel electrocatalysts for generating oxygen from alkaline water electrolysis. *Electrochem. commun.* **9**, 1369–1373 (2007).

79. Anindita, Singh, A. & Singh, R. N. Effect of V substitution at B-site on the physicochemical and electrocatalytic properties of spinel-type NiFe2O4 towards O2 evolution in alkaline solutions. *Int. J. Hydrogen Energy* **35**, 3243–3248 (2010).

80. Singh, R. N., Singh, J. P., Lal, B. & Singh, A. Preparation and characterization of CuFe2-xCrxO4(0⩽x⩽1.0) nano spinels for electrocatalysis of oxygen evolution in alkaline solutions. *Int. J. Hydrogen Energy* **32**, 11–16 (2007).

81. Hamdani, M., Singh, R. N. & Chartier, P. Co3O4 and co-based spinel oxides bifunctional oxygen electrodes. *Int. J. Electrochem. Sci.* **5**, 556–577 (2010).

82. Vesborg, P. C. K. & Jaramillo, T. F. Addressing the terawatt challenge: scalability in the supply of chemical elements for renewable energy. *RSC Adv.* **2**, 7933 (2012).

83. Song, F. & Hu, X. Exfoliation of layered double hydroxides for enhanced oxygen evolution catalysis. *Nat. Commun.* **5**, 1–9 (2014).

84. Trotochaud, L., Young, S. L., Ranney, J. K. & Boettcher, S. W. Nickel-iron oxyhydroxide oxygen-evolution electrocatalysts: the role of intentional and incidental iron incorporation. *J. Am. Chem. Soc.* **136**, 6744–53 (2014).

85. Dionigi, F. & Strasser, P. NiFe-Based (Oxy)hydroxide Catalysts for Oxygen Evolution Reaction in Non-Acidic Electrolytes. *Adv. Energy Mater.* **6**, 1600621 (2016).

86. Zhang, B. *et al.* Homogeneously dispersed, multimetal oxygen-evolving catalysts. *Science (80-.).* **1525**, 1–11 (2016).

87. Chien, H.-C., Cheng, W.-Y., Wang, Y.-H., Wei, T.-Y. & Lu, S.-Y. Ultralow overpotentials for oxygen evolution reactions achieved by nickel cobaltite aerogels. *J. Mater. Chem.* **21**, 18180 (2011).

88. Singh, R. N., Singh, J. P., Nguyen Cong, H. & Chartier, P. Effect of partial substitution of Cr on electrocatalytic properties of MnFe2O4 towards O2O2-evolution in alkaline medium. *Int. J. Hydrogen Energy* **31**, 1372–1378 (2006).

89. Lu, Z. *et al.* Ternary NiFeMn layered double hydroxides as highly-efficient oxygen evolution catalysts. *Chem. Commun.* **52**, 908–911 (2016).

90. Zhou, M. *et al.* In situ electrochemical formation of core–shell nickel–iron disulfide and oxyhydroxide heterostructured catalysts for a stable oxygen evolution reaction and the associated mechanisms. *J. Mater. Chem. A* **5**, 4335–4342 (2017).

91. Yang, Y. *et al.* Highly Active Trimetallic NiFeCr Layered Double Hydroxide Electrocatalysts for Oxygen Evolution Reaction. *Adv. Energy Mater.* **8**, 1703189 (2018).

92. Fan, K. *et al.* Nickel–vanadium monolayer double hydroxide for efficient electrochemical water oxidation. *Nat. Commun.* **7**, 11981 (2016).

93. Li, P. *et al.* Tuning Electronic Structure of NiFe Layered Double Hydroxides with Vanadium Doping toward High Efficient Electrocatalytic Water Oxidation. *Adv. Energy Mater.* **8**, 1703341 (2018).

94. Long, X., Xiao, S., Wang, Z., Zheng, X. & Yang, S. Co intake mediated formation of ultrathin nanosheets of transition metal LDH—an advanced electrocatalyst for oxygen evolution reaction. *Chem. Commun.* **51**, 1120–1123 (2015).

95. Zhang, G. *et al.* Enhanced Catalysis of Electrochemical Overall Water Splitting in Alkaline Media by Fe Doping in Ni3S2 Nanosheet Arrays. *ACS Catal.* **8**, 5431–5441 (2018).

96. Yang, N. *et al.* Iron-doped nickel disulfide nanoarray: A highly efficient and stable electrocatalyst for water splitting. *Nano Res.* **9**, 3346–3354 (2016).

97. Amin, B. G., Swesi, A. T., Masud, J. & Nath, M. CoNi 2 Se 4 as an efficient bifunctional electrocatalyst for overall water splitting. *Chem. Commun.* **53**, 5412–5415 (2017).

98. Wu, X. *et al.* Ni0.85Se as an efficient non-noble bifunctional electrocatalyst for full water splitting. *Int. J. Hydrogen Energy* **41**, 10688–10694 (2016).

99. Wang, Z. & Zhang, L. In situ growth of NiTe nanosheet film on nickel foam as electrocatalyst for oxygen evolution reaction. *Electrochem. commun.* **88**, 29–33 (2018).

100. Ji, L. *et al.* Hierarchical CoTe 2 Nanowire Array: An Effective Oxygen Evolution Catalyst in Alkaline Media. *ACS Sustain. Chem. Eng.* **6**, 4481–4485 (2018).

101. Stern, L.-A., Feng, L., Song, F. & Hu, X. Ni 2 P as a Janus catalyst for water splitting: the oxygen evolution activity of Ni 2 P nanoparticles. *Energy Environ. Sci.* **8**, 2347–2351 (2015).

102. Corrigan, D. A. & Bendert, M. R. Effect of Coprecipitated Metal Ions on the Electrochemistry of Nickel Hydroxide Thin Films: Cyclic Voltammetry in 1M KOH. *J. Electrochem. Soc.* **136**, 723 (1989).

103. Gerken, J. B., Shaner, S. E., Massé, R. C., Porubsky, N. J. & Stahl, S. S. A survey of diverse earth

abundant oxygen evolution electrocatalysts showing enhanced activity from Ni–Fe oxides containing a third metal. *Energy Environ. Sci.* **7**, 2376 (2014).

104. Zhang, C. *et al.* Mapping the performance of amorphous ternary metal oxide water oxidation catalysts containing aluminium. *J. Mater. Chem. A* **3**, 756–761 (2015).

105. Haber, J. A. *et al.* High-Throughput Mapping of the Electrochemical Properties of (Ni-Fe-Co-Ce)O x Oxygen-Evolution Catalysts. *ChemElectroChem* **1**, 524–528 (2014).

106. Song, F. *et al.* Transition Metal Oxides as Electrocatalysts for the Oxygen Evolution Reaction in Alkaline Solutions: An Application-Inspired Renaissance. *J. Am. Chem. Soc.* **140**, 7748–7759 (2018).

107. Lu, F., Zhou, M., Zhou, Y. & Zeng, X. First-Row Transition Metal Based Catalysts for the Oxygen Evolution Reaction under Alkaline Conditions: Basic Principles and Recent Advances. *Small* 1701931 (2017). doi:10.1002/smll.201701931

108. Suen, N.-T. *et al.* Electrocatalysis for the oxygen evolution reaction: recent development and future perspectives. *Chem. Soc. Rev.* **46**, 337–365 (2017).

109. Mohammed-Ibrahim, J. & Xiaoming, S. Recent progress on earth abundant electrocatalysts for hydrogen evolution reaction (HER) in alkaline medium to achieve efficient water splitting – A review. *J. Energy Chem.* **34**, 111–160 (2019).

110. Gong, M. & Dai, H. A mini review of NiFe-based materials as highly active oxygen evolution reaction electrocatalysts. *Nano Res.* **8**, 23–39 (2015).

111. Zhong, H. *et al.* Recent Advances of Cobalt-Based Electrocatalysts for Oxygen Electrode Reactions and Hydrogen Evolution Reaction. *Catalysts* **8**, 559 (2018).

112. Xu, D. *et al.* The role of Cr doping in Ni Fe oxide/(oxy)hydroxide electrocatalysts for oxygen evolution. *Electrochim. Acta* **265**, 10–18 (2018).

Catalyst screening report

BEEST project

Florian Gellrich

December 2019

Abstract

The literature on electrocatalysts for the alkaline water electrolysis is broad. Among the published electrocatalysts, Nickelmolybdenum (NiMo) and Nickel-Iron layered double hydroxide (NiFe LDH) electrocatalysts for the hydrogen and oxygen evolution reaction, respectively, come out on top of others in terms of performance. However, a direct comparison between different NiMo and NiFe LDH electrocatalysts from literature is challenging, as a standardized testing procedure is missing. Furthermore, most of the recent literature focuses on low electrolyte concentrations up to 1 M KOH only, while technical electrolyzers utilize electrolyte concentrations of up to 11.6 M KOH.

DTU Energy has therefore evaluated a diverse range of synthesis methods for NiMo and NiFe LDH electrocatalysts published in literature. The synthesis methods were chosen to be easily scaleable to the technical size, in order to ensure that the synthesis methods are technically feasible with low economical impact. The as-synthesized electrocatalysts were tested in the same way as thin-film electrodes. This way ensures that a fair comparison baseline between the different synthesis methods is given. The tested electrocatalysts were evaluated with respect to their intrinsic electrochemical performance and their electrochemical active surface area in comparison to state-of-the-art Nickel.

We find that NiMo HER electrocatalysts are well-performing in 11.6 M KOH. NiMo electrocatalysts show an exceptional high electrochemical active surface area. Nevertheless, the intrinsic electrocatalytic performance of NiMo is similar to the performance of a fresh Nickel electrocatalyst for the HER. However, the performance of a fresh Nickel electrocatalyst does not last showing performance degradation in the first minutes of electrolysis, which is in agreement with the literature. This degrading behavior, in contrast, was not observed for NiMo electrocatalysts. This discovery suggests that Nickel is the active site in a NiMo electrocatalyst, which is stabilized by the presence of Molybdenum.

Furthermore, we have seen a notable intrinsic performance gain from NiFe LDH in comparison to Nickel for the OER, along with a high electrochemical active surface area. These measurements were conducted in 1 M KOH at first, as the literature does not present measurements on NiFe LDH above this concentration. The two most promising synthesis methods were then repeated. Along with these, the incorporation of a third element, either Chromium and Aluminium, into the NiFe LDH was evaluated. This decision was guided by literature where an even higher activity for such three-element LDHs in comparison to NiFe LDH is reported. These tests were then conducted in a technical relevant electrolyte concentration of 11.6 M KOH. Surprisingly, the intrinsic performances of the electrocatalysts were lower than in 1 M KOH and the electrolyte showed discoloration. The

findings suggest that the NiFe (and NiFeAl, NiFeCr) LDH electrocatalysts degrade in the higher electrolyte concentration case. These tests were conducted on LDHs with high Iron-content. DTU Energy has observed Iron-rich side-phases on these electrocatalysts, which are presumably causing degradation and falsifying the surface area estimation, which accounts for the decreased intrinsic performance. However, the stability of a NiFe LDH electrocatalyst in a technical electrode remains elusive at this point.

As the chosen electrocatalysts have to ensure decade-long stability in a technical electrolyzer, it is crucial to understand them on a fundamental level. Firstly, the degrading performance of Nickel for the HER, which has not been observed in NiMo, has to be understood. The fundamental understanding of this difference will lead to a more detailed understanding of the high-performing NiMo electrocatalyst and, thus, will help improving its performance and reliability. Secondly, the observed degradation of NiFe LDH thin-film electrodes in a technical electrolyte raises the question, if these electrocatalysts can provide the necessary decade-long stability in technical electrodes. Accordingly, it is necessary to evaluate the stability and performance of these high performing OER electrocatalysts in technical electrodes.

DTU Energy has therefore built a setup, which allows for spectroscopic investigations of porous electrodes under operating conditions in alkaline electrolytes. The setup can, for example, be utilized with Raman spectroscopy, X-ray diffraction and Ambient Pressure X-ray photoelectron spectroscopy. The ongoing work on the stability of the well-performing NiMo and NiFe LDH electrocatalysts under technical conditions will be decisive in ensuring a reliable technology.

Contents

1 Introduction

As one of the most crucial parts in alkaline water electrolysis, electrocatalysts are in the focus of several studies. The efficiencies of the water splitting reactions, namely the hydrogen evolution and the oxygen evolution reactions, are determined by the performance of the electrocatalysts.

Overall, the losses in an electrolyzer are of multiple nature, as shown in eq. (1.1). The contributions consist of the electrodes ($\eta_{Cathode}$ and η_{Anode}), the separator ($\eta_{Separator}$), the electrolyte ($\eta_{Electrolyte}$), the interconnects ($\eta_{Interconnects}$), and the electrocatalysts (η_{HER} and η_{OER}), which are the most important part. Electrocatalysts have the biggest share in the contribution to the total losses. Therefore, it is important to study the single electrocatalyst.

$$\sum \eta = \eta_{HER} + \eta_{Cathode} + \eta_{OER} + \eta_{Anode} + \eta_{Separator} + \eta_{Electrolyte} + \eta_{Interconnects} \tag{1.1}$$

This report will show which electrocatalysts have been considered to study for the alkaline water electrolysis. After an introduction on how the measurements are made and which requirements have to be met, a literature background to the studied materials is given and taken for comparison to the measured data.

1.1 The choice of electrocatalysts for the alkaline water electrolysis

The literature consists of a vast variety of highly active electrocatalysts for the alkaline water electrolysis. Most of the work on electrocatalysts for the hydrogen evolution reaction, which do not fall in the Platin-group-metals, has been conducted on Nickel-based electrocatalysts. Besides Raney-Nickel, Nickelmolybdenum electrocatalysts appear on top of all other reported electrocatalysts in terms of activity for the hydrogen evolution reaction.

The work on electrocatalysts for the oxygen evolution reaction consists mostly of comparatively low active perovskites, as well as spinels and hydroxides. Precious metal free electrocatalysts for the oxygen evolution reaction show the most promising activity for Nickel-based spinels and hydroxides, when the electrocatalyst contains Iron.

McCrory et al [1] conducted a screening study in 1 M NaOH (and 1 M H_2SO_4) for a great collection of electrocatalysts. The authors compared the overpotential at a geometric current density of 10 mA/cm^2 after 2 hours of polarization for the different electrocatalysts. The results of this study are represented in fig. 1 and are well in agreement with the aforementioned observations in the literature; Nickel-Molybdenum electrocatalysts for the hydrogen evolution reaction and Nickel-Iron electrocatalysts for the oxygen evolution reaction stick out on top of the reported electrocatalysts.

Therefore, this work will focus on the investigation of Nickel-Molybdenum and Nickel-Iron electrocatalysts for the alkaline water electrolysis.

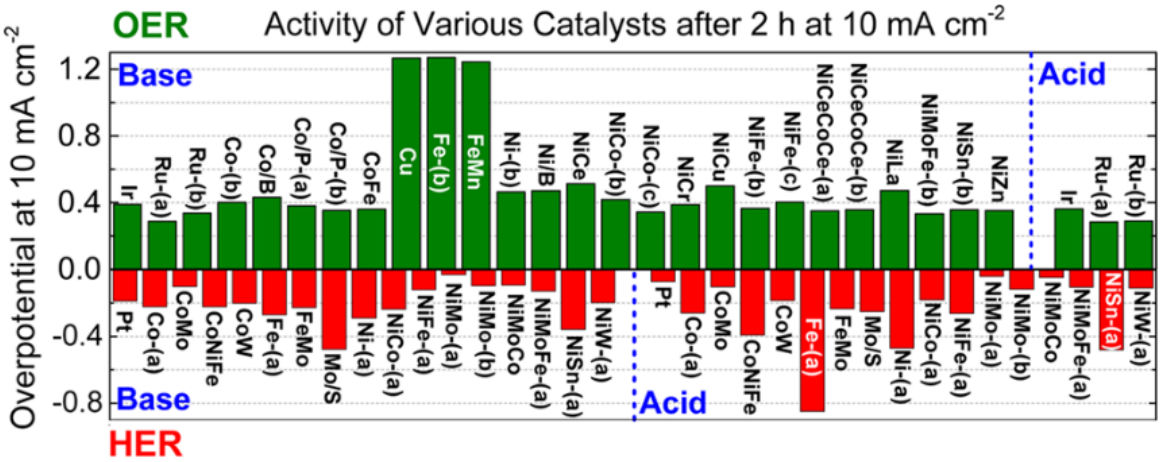

fig. 1: The overpotential of various electrocatalysts at a geometric current density of 10 mA/cm^2 after a polarization time of 2 hours. The given values for the oxygen evolution reaction (OER - top of the figure) and the hydrogen evolution reaction (HER - bottom of the figure) are measured in 1 M H_2SO_4 (denoted as Acid) or 1 M NaOH (denoted as Base). Reproduced from [1].

1.2 Requirements for electrocatalysts

Alkaline water electrolyzers consist of low-cost materials and are operational for several years. In order to ensure the low-cost and decade-long operation, the electrocatalysts have to fulfill three main, general requirements.

Firstly, the electrocatalyst need to perform well. This requirement can be met with a high intrinsic activity and a high active surface area. Secondly, the electrocatalysts must be robust in the operational range of an industrial electrolyzer. Alkaline water electrolyzers are objected to run dynamically from shut-down up to 2 A/cm^2. The electrocatalysts do not have to be phase-stable, but their response on the dynamic operation should not decrease the electrocatalytic activity. Further, any degradation products should not contaminate the electrolyzer, which could result in a decreased runtime or overall electrolyzer efficiency. Thirdly, the electrocatalysts have to be low in costs. This requires an economical synthesis with green chemicals. An overview of this correlation is shown in fig. 2.

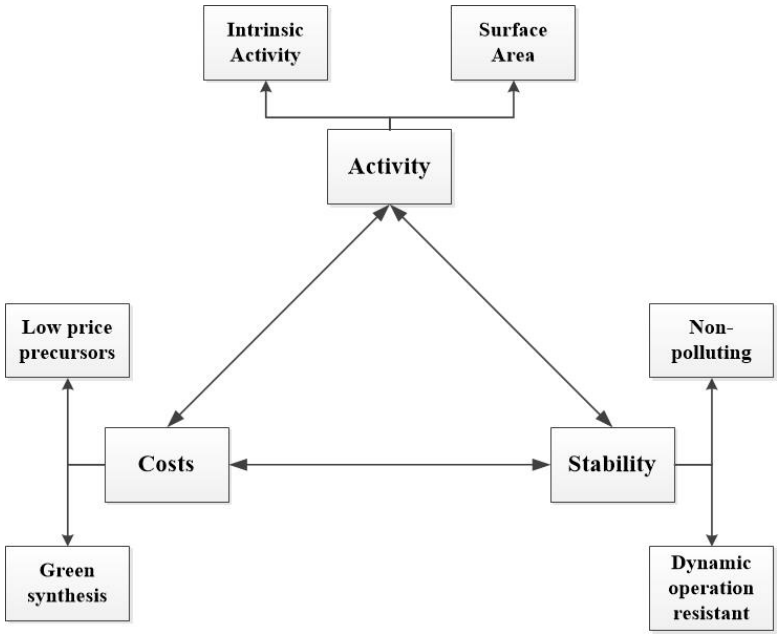

fig. 2: The triangle of requirements for electrocatalysts and the respective sub-divisions.

The choice of electrocatalysts in chap. 1.1 has been conducted with focus on low-cost materials, which show promising high activity. However, these electrocatalysts haven't been studied sufficiently. The reason for their high activity, due to either intrinsic activity or high surface area, has not been addressed adequately. In addition, most of the literature does not address the stability requirement and focuses on 1 M KOH (or NaOH) at room temperature, while industrial electrolyzers operate with 20-45 wt % KOH[1] and up to 100 °C.

[1] 45 wt % KOH is equal to 11.6 M KOH

1.3 The determination of intrinsic electrocatalytic properties

In order to increase the overall kinetic activity of an electrocatalyst, it is crucial to determine its intrinsic activity. Therefore, thin-film model electrodes are utilized. Such electrodes subsist of a thin electrocatalyst layer on a smooth surface, which ensures that the roughness factor is as low as possible. In that context, the influence of the surface area is almoste negligeable and can be excluded by assessing the electrochemical active surface area (ECSA).

In addition, the thin electrocatalyst layer assures a well-defined electrochemical potential, as the potential is uniform over the electrocatalytic layer. Porous electrodes, on the other hand, experience a potential-distribution over the thickness of the electrode, as shown in fig. 3.

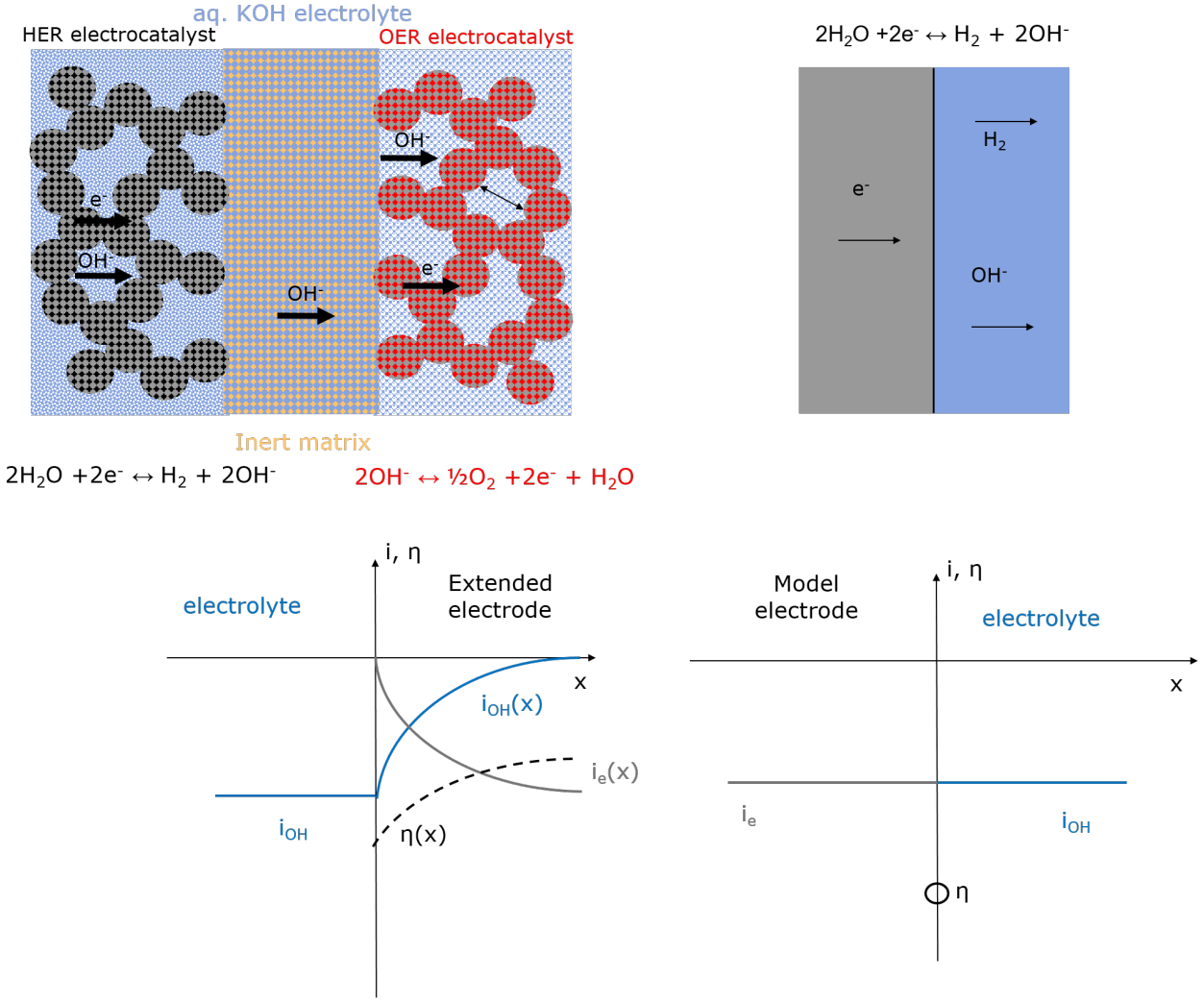

fig. 3: The overpotential distribution over a porous electrode (left) and the uniform overpotential in a thin-film electrode (right) during the hydrogen evolution reaction in alkaline electrolyte.

This effect originates from the mass-transport through the porous structure; the concentration of ions is not uniform in the porous structure and therefore results in a different local conductivity of the electrolyte and, further, in a distribution of the electrons in the eletrode. The latter causes an overpotential increase over the electrode's thickness. The effect, on the other hand, is negligeable for highly conducting electrolytes. Nonetheless, the effect is not present in thin-film electrodes, which allows for measurements of intrinsic properties on these.

1.4 The testing setup

The screening of the electrocatalysts was conducted in a three-electrode configuration made of Polytetrafluorethylen (PTFE) and a Gamry Reference 3000[2] potentiostat. PTFE is a well-known corrosion resistant fluoropolymer, which, in contrast to glass, is not affected by alkaline solutions [2]. The cell house, which was purchased from Gaskatel[3], is constructed in a three-compartment filterpress-configuration. The working electrode compartment has been replaced by a homemade PTFE-compartment, which allows to heat up the compartment with six resistors connected to a PID-controller. All three compartments are sealed with EPDM-sealings to another. The working electrode compartment and counter electrode compartment have been further seperated by a Zirfon separator, similar to technical electrolyzers, to avoid gass-crossover.

The working electrode (A = 3.14 cm^2) consisted of an as aforementioned thin-film electrode. A Nickel-foil (200 μm thick) was used as substrate for these electrodes. Nickel was chosen, as the final technical electrodes will be of a Nickel kind. In this way, the influence from the substrate-catalyst interaction is similar to the technical electrodes, which allows for the direct compareability between the electrocatalyst testing and the technical electrodes. The determination of the Nickel kinetics were conducted on uncoated Nickel-foils. For NiMo and NiFe LDH, thin layers of the respective catalysts have been deposited on the Nickel-foil, either with an in situ synthesis method or by drop-casting.

The counter electrode was a coiled Nickel-wire. Platinum, as often used in the literature as counter electrode, has been excluded as counter electrode material. It is known that Platinum can pollute alkaline electrolytes and thus falsify (overestimate) kinetic measurements [2]. Nickel, on the other hand, is known to be an alkaline stable material. Furthermore, any Nickel-type ions in the electrolyte are not expected to influence the kinetic measurements, as the tested electrocatalysts are a Nickel-type themselves.

The reference electrode was a commercial reversible hydrogen electrode (RHE), which has been

[2]https://www.gamry.com/potentiostats/reference-3000/
[3]https://www.testcell.info/

purchased from Gaskatel[4]. The advantage of an RHE lies in the pH relaxation of the reference potential. The potential of an RHE is, by definition, the equilibrium potential of the HER at any pH-value. The equilibrium potential of the OER is 1.23 V, respectively.

The cell house, as shown in fig. 4, was placed in a protective housing and flushed with nitrogen.

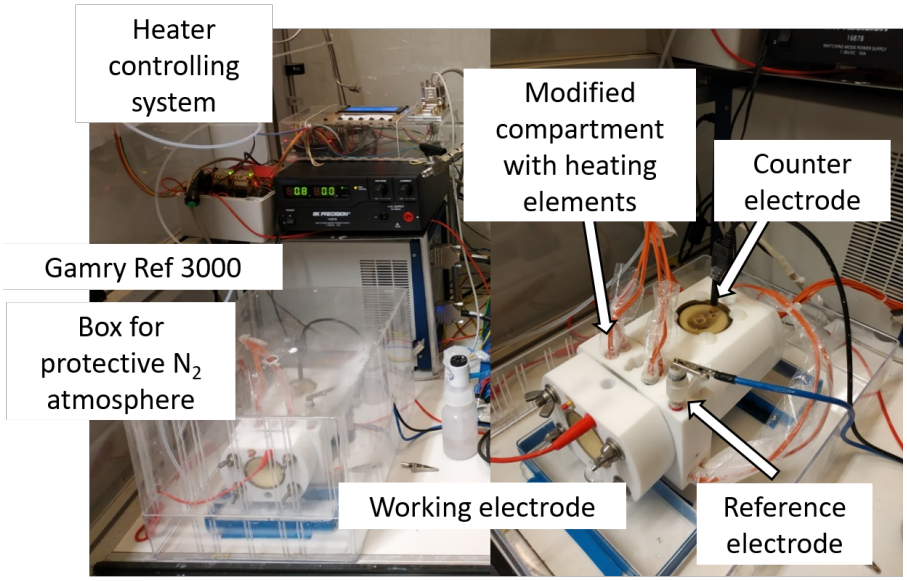

fig. 4: The electrocatalyst testing setup at DTU Energy. The cellhouse, made of PTFE, is placed in a nitrogen-flushed protective housing.

The testing setup has been verified by measuring a Platinum-foil. Platinum is a well-studied noble-metal electrocatalyst, which is often used to benchmark HER electrocatalysts. The Platinum-measurements have been conducted to evaluate the total measurement and analysis error. Platinum is known to be a reliable and stable electrocatalyst. Therefore, any variation between measurements must occur through artifacts in the system, such as e.g. pollutants or the testing protocol, or through the accuracy of the analysis method. fig. 5 shows the Tafel-curves obtained for 10 consecutive measurements in 1 M KOH at room temperature. The electrochemical active surface area has been determined for each measurement by the underpotential deposition of hydrogen [3, 4].

The consecutive measurements did not show a trend between the measurements. The slight scatter between the measurements resulted in a total error (measurement and analysis) of $\pm$ 10 mV. The error of the Tafel-slope, as shown in fig. 6 (left), is $\pm$ 8 mV/Dec. The intrinsic overpotential at a current density of 10 mA/cm^2 with 143 $\pm$ 10 mV, as seen in fig. 6 (right), is well in agreement with values, which can be drawn from literature values [4, 5]. These measurements show that mesurements in this testing setup, including the corresponding analysis, are reliable within the aforementioned errors.

[4]https://www.referenceelectrode.info/

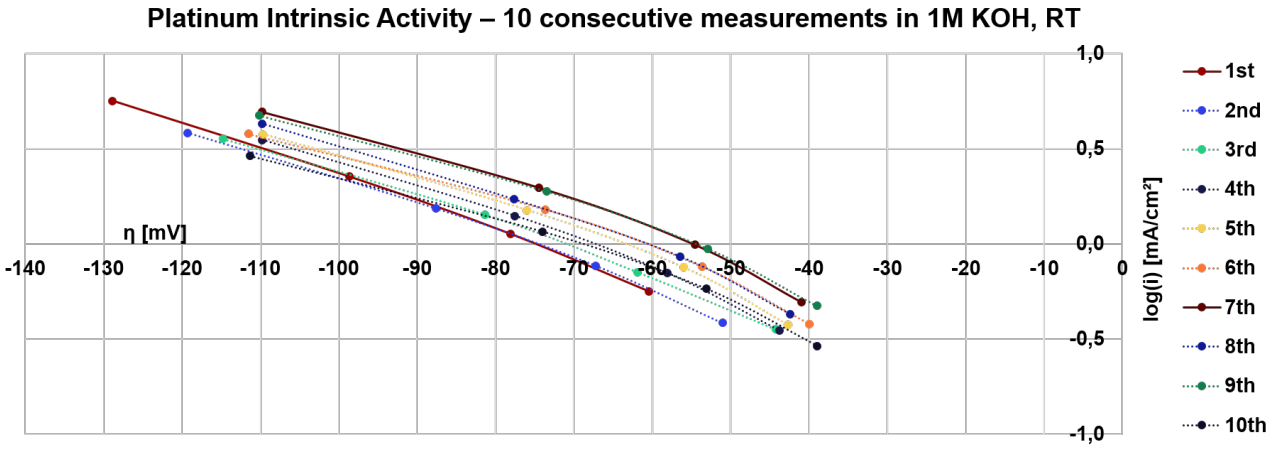

fig. 5: 10 consecutive measurements of a Platinum-foil in 1 M KOH at room temperature. The ECSA has been determined by the H_{upd}-method. The deviation between the measurements is $\pm$ 10 mV.

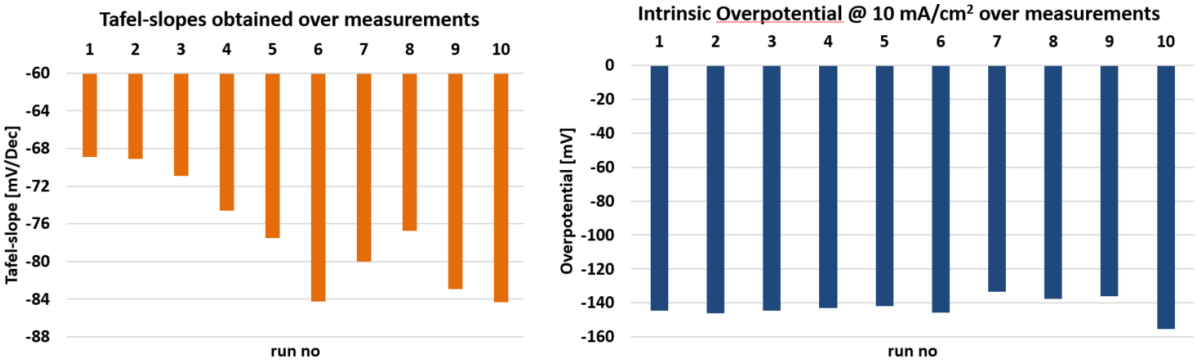

fig. 6: Tafel-slopes (left) and overpotentials at an intrinsic current density of 10 mA/cm^2 (η_{10}, right) of the 10 consecutive measurements on a Platinum-foil in 1 M KOH at room temperature. The deviation between the Tafel-slopes is $\pm$ 8 mV/Dec and $\pm$ 10 mV between the η_{10}-values.

2 Nickel

Nickel is the state-of-the-art electrocatalyst for the alkaline water electrolysis. In order to increase the performance of the system, the chosen electrocatalysts should outperform Nickel. Hence, the understanding of the Nickel kinetics is crucial in the knowledge-building process for well-performing alkaline water electrocatalysts.

2.1 The surface states of Nickel in alkaline media

The first description of the different oxidation states of Nickel in alkaline media were made by Bode [6]. The correlation between the two different hydroxides and the two different oxihydroxides are visualized in the Bode-diagram, as given in fig. 7. The turbostatic $\alpha - Ni(OH)_2$ has intercalated water molecules in between its layers. This form can reversibly convert to the $\gamma - NiOOH$ oxihydroxide. The more crystalline form of the Nickelhydroxides is $\beta - Ni(OH)_2$. It forms irreversibly through aging out of the α-form, by the loss of the intercalated water molecule. The corresponding $\beta - NiOOH$ oxihydroxide can, through an overcharging process, intercalate water molecules and thus transform to the γ-form.

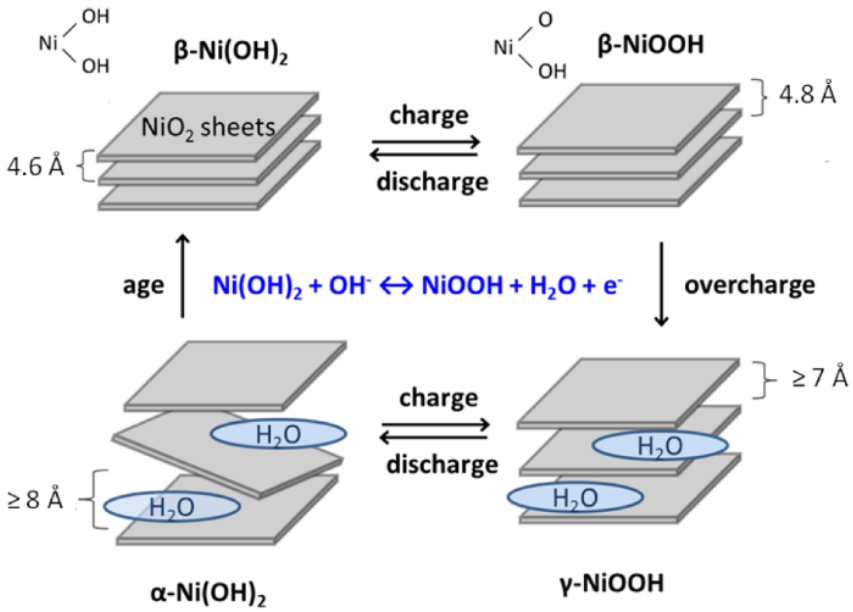

fig. 7: The hydroxides and oxihydroxides of Nickel according to the Bode-scheme [6]. Reproduced from [7].

The Bode-scheme has been applied as general descriptor for the redox-transitions of Nickel in the past decades. However, recent literature questions if the surface states of Nickel only consist of the α/γ and the β/β-transitions [8]. It is possible that further Nickel-species exist, especially a Ni^{4+} under oxygen evolution conditions in $\gamma - NiOOH$. A more detailed description of these transitions will be spared at this point, but could be followed in recent publications [8, 9].

2.2 The literature background of the hydrogen evolution reaction on Nickel

The obtainable kinetic values in the literature for smooth Nickel electrodes are reported for NaOH and KOH in different electrolyte concentrations. The values that have been taken in this work reach from 0.01 M up to 34 w% (8 M). To accomodate the different electrolyte concentrations, fig. 8, 9 and 10 represent the reported values for Tafel-slopes, exchange current densities and the overpotential at 10 mA/cm^2, respectively, for polycrystalline Nickel at room temperature with regards to the measurement pH. The presented values have been taken for smooth Nickel surfaces to get an overview of intrinsic kinetic properties. Some values are specially marked, when the authors made an effort to assess intrinsic properties by correctiong for the electrochemical active surface area (ECSA).

The figures reveal a great variety over several orders of magnitude in reported literature values. If only the ECSA corrected intrinsic values are considered, the Tafel-slope can reach from 95 - 145 mV/Dec, the exchange current density from 7 - 344 $\cdot 10^{-5}$ mA/cm^2 and the overpotential at 10 mA/cm^2 from 409 - 563 mV.

This scatter raises the question why polycrystalline Nickel behaves differently for the authors. Summing up the available literature knowledge on this artifact, it can be concluded that the surface state of Nickel and its kinetic response is depending on the electrode preparation and pretreatment, as well as the electrode's history [23].

Oschchepkov et al [24, 26] show that a partially oxidized Nickel surface enhances the HER performance drastically. Through kinetic modelling, the authors claim that the HER on pure Nickel proceeds with the Heyrovsky-Volmer mechanism, which is indicative for a strong adsorption of the hydrogen intermediate and thus a low reaction rate. The partial oxidation of the surface with a Nickeloxide species reduces the strength of the hydrogen adsorption. Accordingly, the rate of the Volmer step and, overall, the reaction rate increases significantly. A comparison of the exchange current densities with respect to the temperature for a pure and partially oxidized Nickel electrode is given in fig. 11.

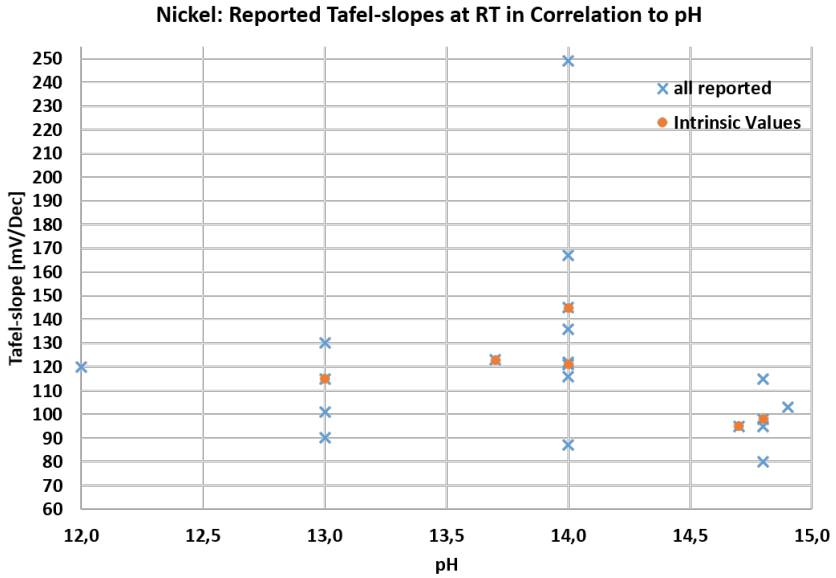

fig. 8: Reported Tafel-slopes for the HER on polycrystalline Nickel in alkaline electrolyte at room temperature with respect to the measurement pH [10–25]. Values summarized in chap. A, page xxi.

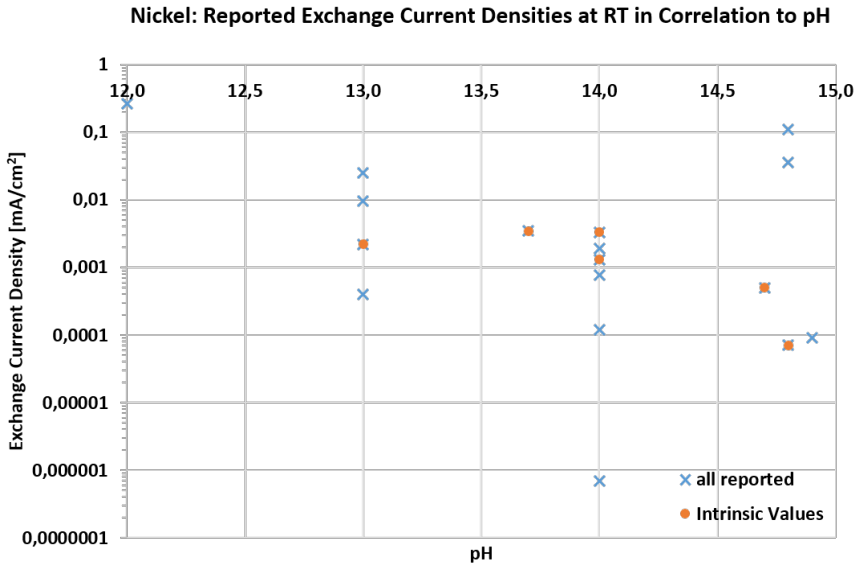

fig. 9: Reported exchange current densities for the HER on polycrystalline Nickel in alkaline electrolyte at room temperature with respect to the measurement pH [10–25]. Values summarized in chap. A, page xxi.

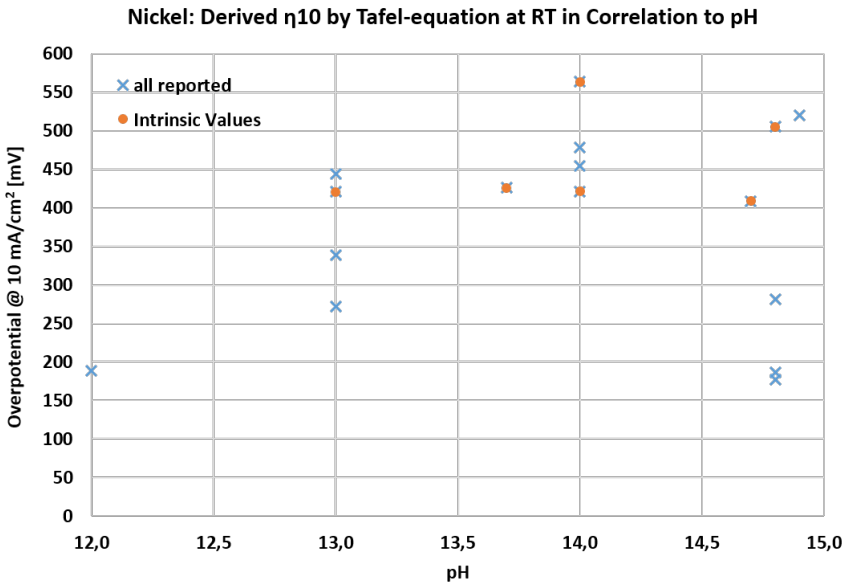

fig. 10: Overpotential at 10 mA/cm^2 for the HER on polycrystalline Nickel in alkaline electrolyte at room temperature with respect to the measurement pH [10–25]. Values summarized in chap. A, page xxi.

The findings of Oschchepkov et al are well in agreement with the ones made by Liang et al [21]. Liang et al applied the Scanning Electrochemical Microscopy technique to unambigiously determine the amount of hydrogen produced during the HER on partially oxidized Nickel electrodes. Through a combination of eletrochemical measurements with surface titration, the authors could divide the electrochemically measured reduction current into Nickelhydroxide/oxide reduction and hydrogen evolution. It was found that a partially oxidized surface, when the electrode potential was scanned up to 1 V vs RHE[1], could enhance the performance of the HER on Nickel. When scanned at higher potentials than 1 V vs RHE, the HER performance drastically decreased (see fig. 12). The authors also expressed a warning, as great amounts of the electrochemically measured reduction current had to be correlated to Nickelhydroxide/oxide reduction. Therefore, some reported values for partially oxidized Nickel electrodes can be considered erroneous.

The impact of the partial oxidation of Nickel is further potential depending. As it can be seen in fig. 13, the influence of the partial oxidation is visible when the potential of the partial oxidation is above + 500 mV vs RHE (- 438 mV vs Ag/AgCl). This referrs to the potential window of α-Nickelhydroxide, which is reported to be a reversible electrochemical reaction [22, 27, 28]. It further indicates that potential cycling in the α-Nickelhydroxide region does not influence the performance of the HER on Nickel, confirming that this transition is electrochemically reversible.

[1]The authors report the potentials vs Ag/AgCl and 0.01 M KOH. The values have been recalculated to the RHE scale to allow for comparison

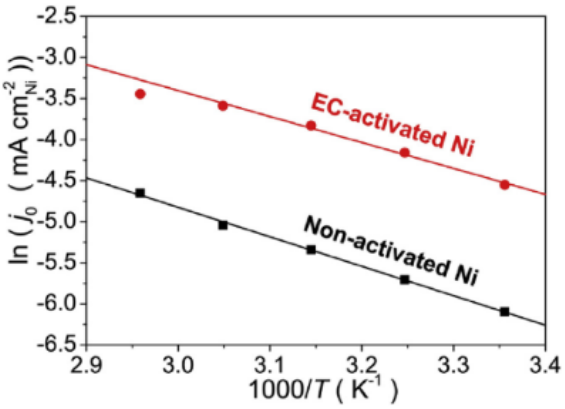

fig. 11: Calculated exchange current densities over reciprocal temperature for bare and partially oxidized Nickel. The potential of the partial oxidation is identical to $0.062\ V$ in fig. 12. Reproduced from [24].

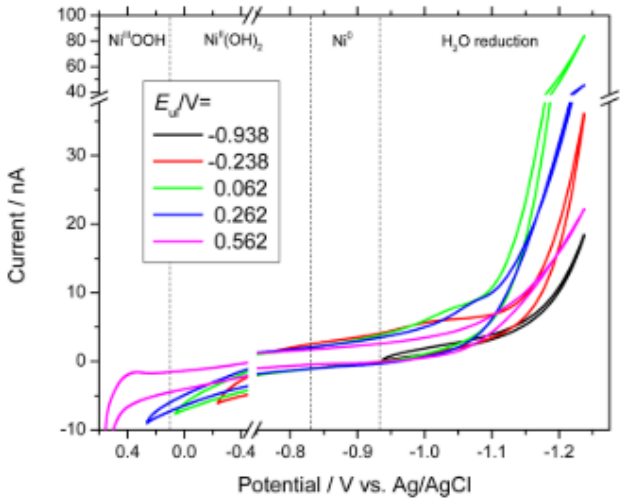

fig. 12: Cyclic Voltammograms of a Nickel electrode with increasing upper potential limit, reported vs Ag/AgCl (1 M KCl) in 0.01 M KOH. Reproduced from [21].

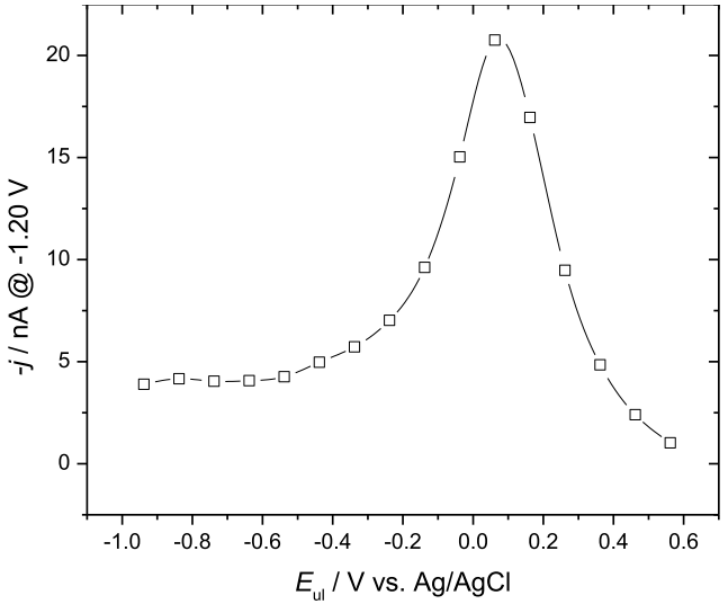

fig. 13: The measured current of the hydrogen evolution reaction at -1.20 V by Surface Interrogation Scanning Electrochemical Microscopy in relation to the upper potential limit from fig. 12. Results from Voltammetry at 50 mV/s in 0.01 M KOH. The Equilibrium potential for the HER is -938 mV vs the Ag/AgCl reference. Reproduced from [29].

The influence of Nickeloxide on Nickel, as seen above, is of great importance. Medway et al [30] show that Nickeloxide is formed in air on Nickel(111) single-crystal surfaces. Upon immersion into 1 M KOH, additional Nickelhydroxide is formed on top of the Nickeloxide. The Nickeloxide cannot be reduced electrochemically, as hydrogen is only absorped into the Nickeloxide layer. This finding is in well-agreement with a previous study by Visscher and Barendrecht [31].

Another finding for the history dependence of Nickel was made by Pătru et al [32]. Pătru et al claim that the intrinsic performance of Nickel is depending on the morphology and the internal stress by comparing different Nickel nanoparticle catalysts. The highest activity was found in small particles with high internal stress and a monotone correlation between high material strain and high performance could be drawn.

A further mechanical effect on Nickel at HER potentials has been seen in the initiation of cracks, which is changing the mechanical nature of Nickel [33]. Evaluating Nickel single-crystals, the authors find that a Nickel α-phase transforms into a hydride, which initiates cracks and influences the performance. These findings are in-line with the findings of Soares et al and Hall et al [34, 35].

Both groups, Soares et al and Hall et al, applied X-ray diffraction on previously highly negatively polarized Nickel electrodes, with roughly 1000 mV of overpotential. For both, Nickelhydrides are found to be produced during the HER, as visible in the XRD patterns in fig. 14 and 15. It is a matter of debate, if this hydride phase is present in the surface and subsurface, or if it can be present in the bulk or in the grain boundaries [36]. Only surface or subsurface hydrides would influence the kinetic response of Nickel. The results from X-ray diffraction, which are greatly influenced by the bulk, cannot address this point.

Finally, a time-depending altering effect of Nickel can be found in literature [12, 34], as seen in fig. 16 and 17. This altering effect has been ascribed to the formation of Nickelhydride [12, 34, 38], but remains elusive due to the unresolved question about the presence of surface and subsurface hydrides.

In summary, the unambigious correlation between the kinetics on Nickel and the surface state is yet been resolved sufficiently. It is, however, known that the pretreatment of a Nickel electrode greatly influences its kinetic performance.

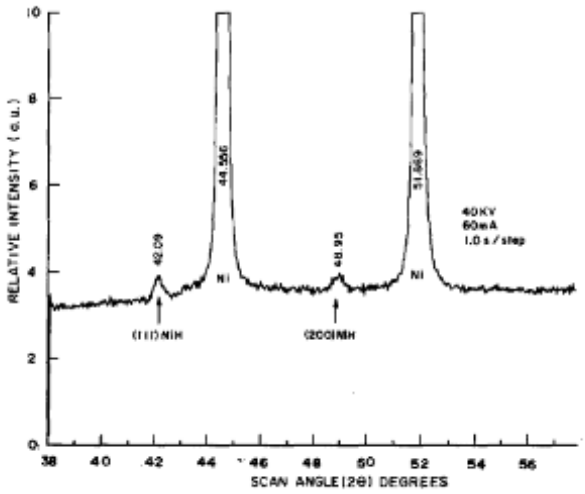

fig. 14: XRD pattern of a Nickel electrode, 20 minutes after being polarized at 300 mA/cm^2 for 2 h. Reproduced from [37].

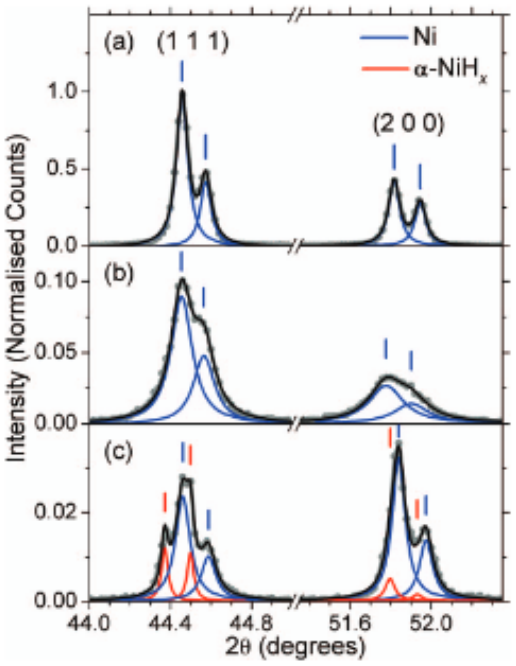

fig. 15: XRD pattern of a) fresh Nickel electrode, b) after 141 h at 500 mA/cm^2 in 1 M NaOH, c) after 66.5 h at 500 mA/cm^2 in 30% KOH. Reproduced from [34].

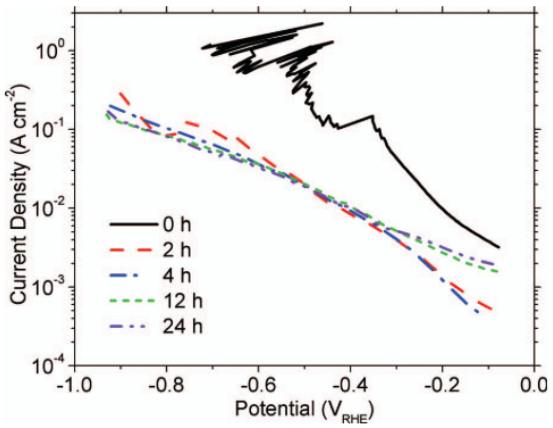

fig. 16: iR-corrected Tafel-slopes in 30% KOH of a freshly polished Nickel electrode (0 h) and after polarization at 500 mA/cm^2 (- 1 V vs RHE, iR-uncorrected) for various times. Reproduced from [34].

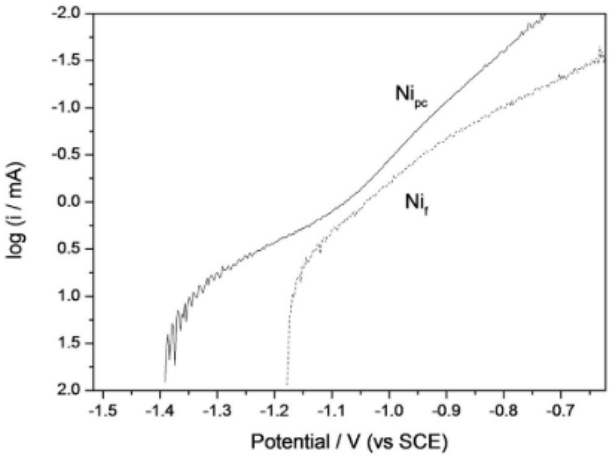

fig. 17: Tafel-slopes in 1 M KOH of a freshly polished Nickel electrode (Ni$_f$) and after 4 h polarization at - 1.5 V vs SCE (Ni$_{pc}$). The Equilibrium Potential of the HER is - 583 mV vs SCE. Reproduced from [12].

2.3 Testing results of the hydrogen evolution reaction on Nickel

The kinetics of Nickel have been studied at various pH values, with focus on the technically relevant high pH (pH > 14) measurements. All test results are surface area corrected by the obtained double layer capacitance from a.c. impedence spectroscopy at overpotentials of 200-300 mV [1, 39, 40], with a correction factor of $40\ \mu F/cm^2$ [1]. This procedure has been questioned in the literature [41, 42]. It is generally accepted that the reversible transition of a monolayer of $\alpha - Ni(OH)_2$ gives the best surface area estimation for the hydrogen evolution potential range [22, 24, 25, 39]. It was therefore decided to verify the in situ impedance approach, as it is a benifitial approach.

Conway and Bai [43] have modelled the influence of an overpotential dependant pseudocapacitance on the obtained capacitance from a.c. impedance spectroscopy. The pseudocapacitance, as shown in fig. 18 as a function of the three different HER rate determining steps, becomes negligeable for overpotentials greater than 200 mV.

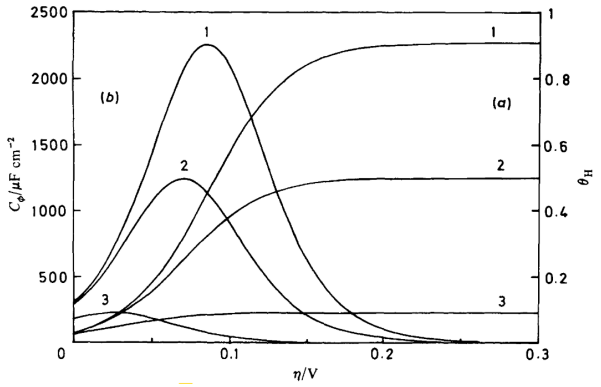

fig. 18: The pseudocapacitive influence (left axis) and the hydrogen absorbtion rate (right axis) from overpotentially deposited hydrogen on Nickel electrodes. Results based on kinetic modelling. Reproduced from [43].

To proof the feasability of the in situ method, the surface area of various Nickel electrodes were first estimated with the $\alpha - Ni(OH)_2$ method. Then, a.c. impedance spectroscopy was conducted at several overpotentials. The correlation of the ECSA determined in situ versus the $\alpha - Ni(OH)_2$ method is represented in fig. 19. Supported by the findings of Conway and Bai, the in situ method is applicable, when the overpotential exceeds 200 mV. Furthermore, a fair estimate at lower overpotentials could be drawn, as fig. 19 allows to conclude on an overpotential based correction factor.

fig. 20 represents the Tafel-slopes and the overpotentials at an intrinsic current density of 10 mA/cm^2 for three tests, and their average, on Nickel-foils in 11.6 M KOH at room temperature.

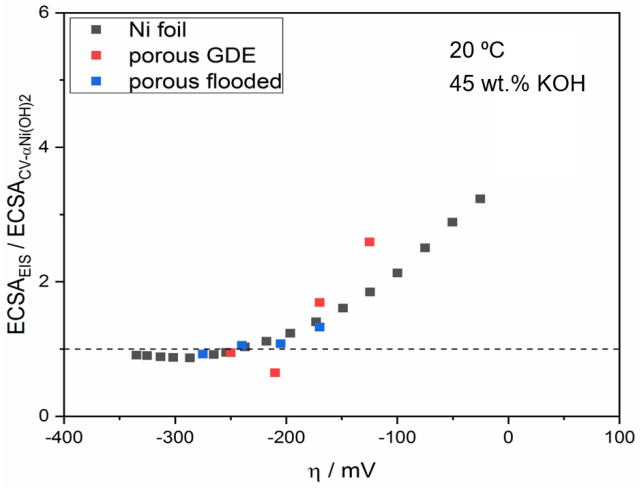

fig. 19: Experimentally obtained correlation between the in situ obtained electrochemical surface area by a.c. impedance spectroscopy to the formation of a monolayer of $\alpha - Ni(OH)_2$. Measurements on different Nickel electrodes in 11.6 M KOH at room temperature.

All foils have been mechanically polished with sandpaper and cleaned with ethanol and deionized water prior to testing.

Although prepared and tested in the same way, and, although the foils were of the same batch, the kinetic values vary more than within the experimentally deduced measurement error (see chap. 1.4). This scatter is to be dedicated to the history effect of Nickel.

In order to adress the history effect, a thorough cleaning protocol for the Nickel electrodes has been established. This protocol is based on the gathered literature knowledge and summarized in tab. 1.

The electrode is cleaned mechanically and chemically to remove surface oxides, hydroxides and possible impurities [39, 44]. Directly after, the Nickel electrode is stored in water. It is known that Nickel can form a thin Nickeloxide layer when exposed to air [30]. Nickeloxide is furhter reported to be electrochemically inreducible [30, 45] and, thus, its formation has to be avoided. The immersion into an aqueous electrolyte, however, is known to form $\alpha - Ni(OH)_2$ [46], or even $\beta - Ni(OH)_2$ [30], depending on the literature source. This process can be limited by mounting the electrode in the testing station as fast as possible. The transition is preferably done within less than one hour, as the hydroxide surface state is known to age with time, even in water [47]. The published knowledge on the Nickelhydroxides shows that both can be reduced within the hydrogen evolution region, when the overpotential exceeds 200 mV [27, 48]. Thus, electrochemical reduction for one hour is conducted at a current density, which exceeds 200 mV of overpotential, after iR-correction. To ultimately remove the evolved hydrogen, and any possibly formed Nickelhydrides [22, 34, 35], the electrode is swept in the reversible $\alpha - Ni(OH)_2$ region between -100 and +500 mV vs RHE [21, 22]. As this process is reported as reversible, a fresh Nickel surface is obtained after the cyclic voltammograms.

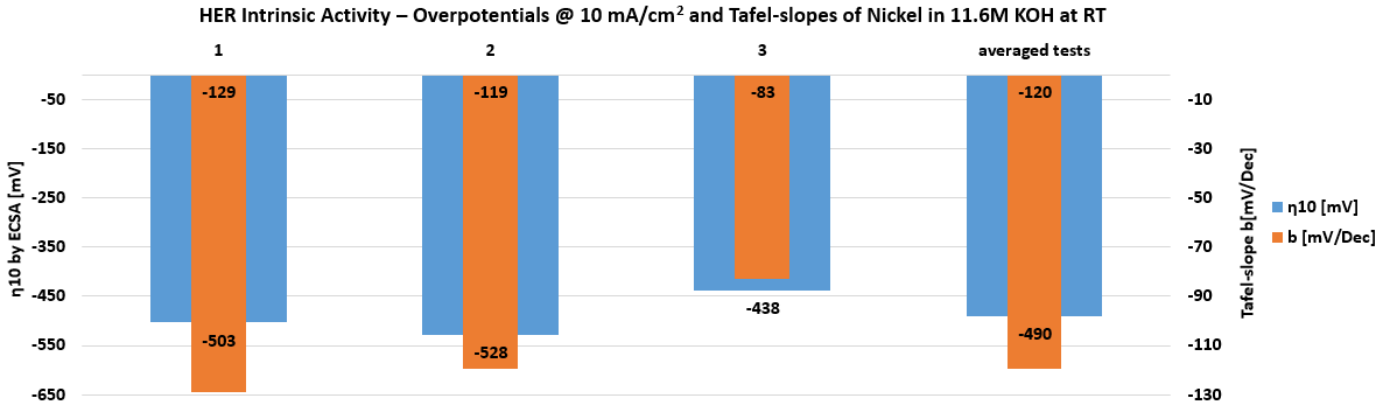

fig. 20: The overpotential at an intrinsic current density of 10 mA/cm^2 and the correlated Tafel-slopes of three Nickel-foils, and their average, for the hydrogen evolution reaction in 11.6 M KOH at room temperature.

tab. 1: The cleaning protocol for Nickel electrodes

step	procedure	description
1	mechanical polishing	sandpaper polishing to remove surface oxides/hydroxides
2	chemical etching	sonication in 5 M HCl and in Ethanol to remove impurities, surface oxides/hydroxides
3	water storage	protection from formation of surface oxides in air
4	hydroxide reduction	electrochemical reduction of surface hydroxides formed in water
5	electrochemical oxidation	oxidation of hydrogen and possible hydrides in the reversible $\alpha - Ni(OH)_2$ region

The above described cleaning protocol was applied to study the Nickel kinetics in the technical relevant electrolyte of 11.6 M KOH. The electrode was swept in the $\alpha - Ni(OH)_2$ region prior to each Chronopotentiometry scan, in order to regenerate a fresh Nickel surface in each measurement step. As it is shown in fig. 21, the overpotential of the hydrogen evolution increases with time at all of the Chronopotentiometry steps. This effect is well in agreement with the literature, which ascribes this effect to the formation of surface hydrides altering the performance. This finding, however, requires further understanding.

The initial Nickel performance was gathered with a tangential method, to accomodate the effect of the double layer charging. The approach was chosen, as the onset potential of any hydrogen-induced degradation of the Nickel performance has to occur on the initial hydrogen evolution potential of a fresh Nickel surface. Therefore, the intercept between the double layer charging tangente and the degradation tangente, assuming that the degradation is of a first order kinetics, must be the initial HER performance of a fresh Nickel electrode.

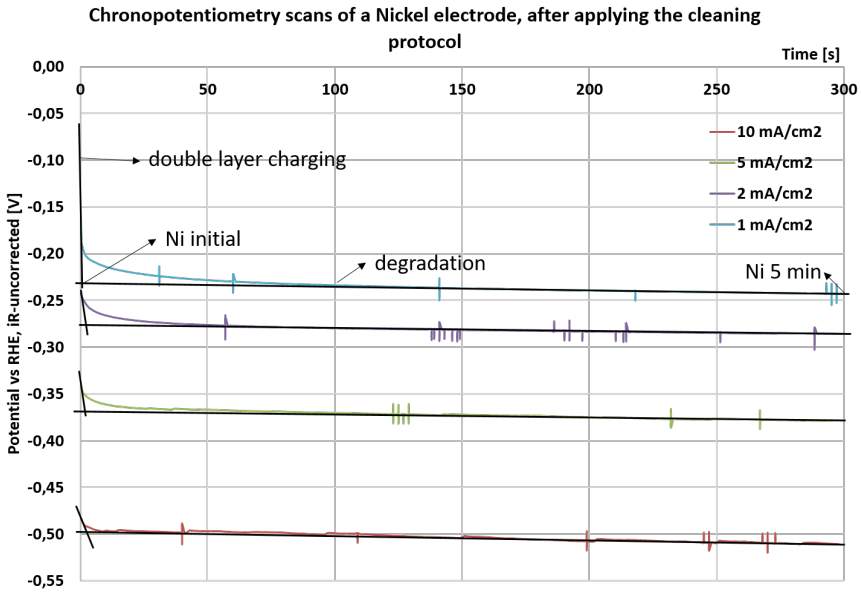

fig. 21: The Chronopotentiometry scans at different current densities of a fresh Nickel electrode in 11.6 M KOH at room temperature during hydrogen evolution. The black lines indicate the tangential approach to obtain the initial Nickel performance, when considering the double layer charging.

The evaluation of the HER kinetics on a fresh Nickel surface at pH 15 shows an initially high performance of $b = 97\ mV/Dec$, $i_0 = 0.001295\ mA/cm^2$ and $\eta_{10} = 378\ mV$. In comparison to the literature values, as shown in fig. 22, 23, and 24, fresh Nickel displays a promisingly high performance initially, which then gradually decreases within only five minutes. The comparison further shows the obtained kinetic values at various pH-values, when the cleaning protocol was not

applied. All these values are withing the scatter of the literature values, which further reveals the importance of a thorough cleaning and testing procedure of Nickel electrodes.

It is remarkable that, in the test with the applied cleaning protocol, the exchange current density appears to be unaffected, while the Tafel-slope is worsening and causing the performance loss within only a few minutes of electrolysis. The increase of the Tafel-slope is directly to be associated with a change in the reaction mechanism. The amount of active surface sites remains the same, as seen by the unaffected exchange current density. Therefore, the active sites must experience a modification that causes a change in the absorption behaviour of the intermediate species. This can be a matter of the formation of Nickelhydrides, which result in a change of the absorbtion energy of the water molecule and thus ending in a decrease of the water-splitting Volmer-step.

A similar explanation for the change of the reaction mechanism can be a high coverage of physisorbed hydrogen on the surface. Shingawa et al [49] show by microkinetic modelling, that the generally accepted conclusion with the Volmer-step as rate limiting step, when the Tafel-slope is as high as 120 mV/Dec, can be misleading. Such a high Tafel-slope, which is almost approached in the latest test on a fresh Nickel surface after five minutes, can be obtained with a rate limiting Heyrovsky-step, when the hydrogen coverage of the surface exceeds 0.6. In summary, further proof, e.g. by spectroelectrochemical tests, is needed for an unambigious conclusion of the altering effect.

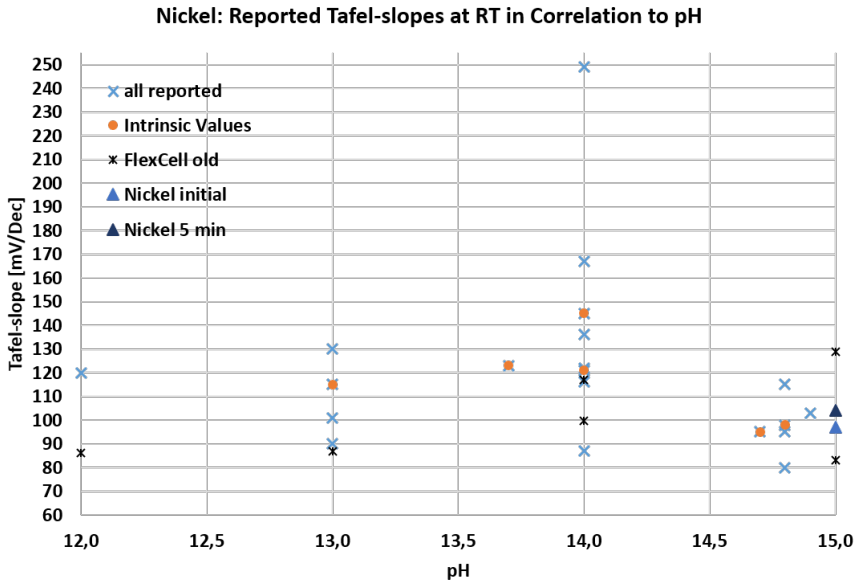

fig. 22: Reported Tafel-slopes for the HER on polycrystalline Nickel in alkaline electrolyte at room temperature with respect to the measurement pH. Comparison of literature values [10–25] to measured values. Values denoted as "FlexCell old" are self-measured values without the cleaning protocol. "Nickel initial" and "Nickel 5 min" indicate the measured values with the applied cleaning protocol for the initial and the value after 5 min, respectively.

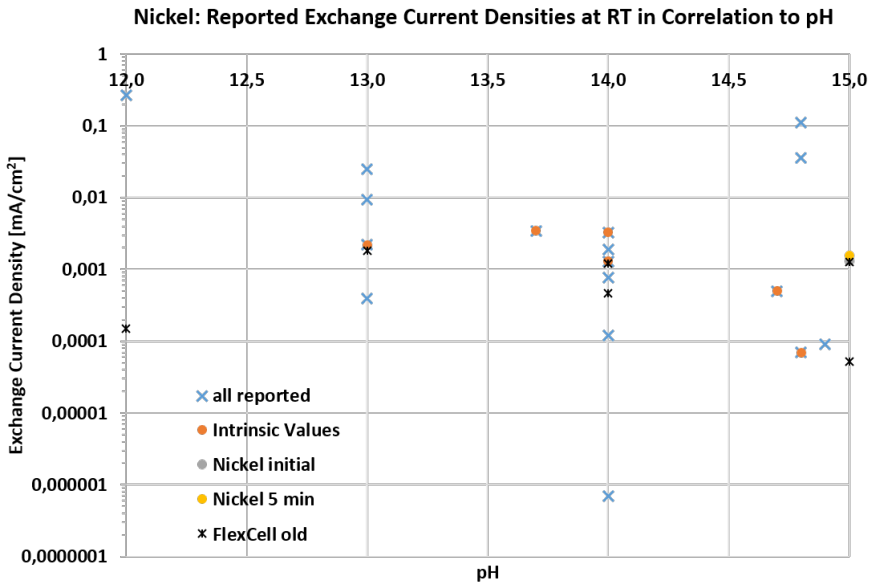

fig. 23: Reported exchange current densities for the HER on polycrystalline Nickel in alkaline electrolyte at room temperature with respect to the measurement pH. Comparison of literature values [10–25] to measured values. Values denoted as "FlexCell old" are self-measured values without the cleaning protocol. "Nickel initial" and "Nickel 5 min" indicate the measured values with the applied cleaning protocol for the initial and the value after 5 min, respectively.

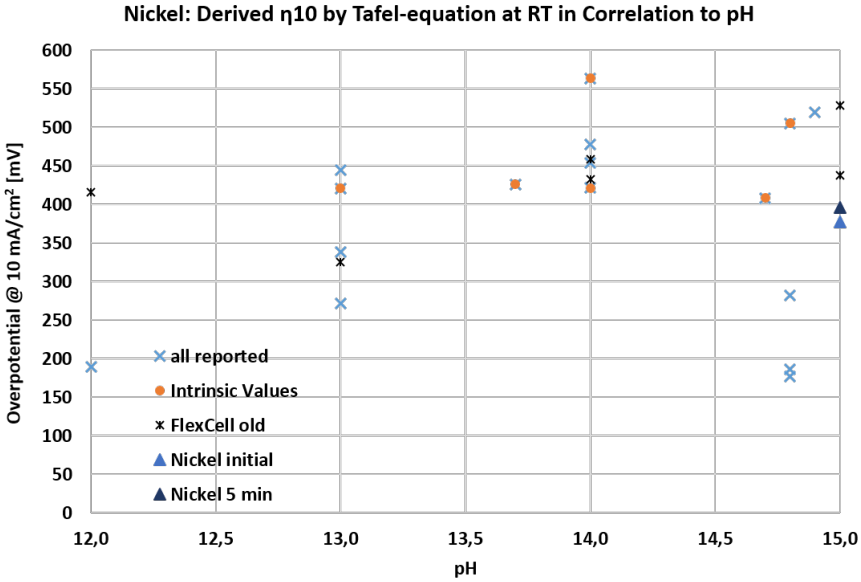

fig. 24: Overpotential at 10 mA/cm^2 for the HER on polycrystalline Nickel in alkaline electrolyte at room temperature with respect to the measurement pH. Comparison of literature values [10–25] to measured values. Values denoted as "FlexCell old" are self-measured values without the cleaning protocol. "Nickel initial" and "Nickel 5 min" indicate the measured values with the applied cleaning protocol for the initial and the value after 5 min, respectively.

The current understanding, on the other hand, indubitably reveals the degrading behaviour of a Nickel electrode under hydrogen evolution conditions. The degradation is to be correlated to a hydrogen-influenced change of the surface state and further to a change in the reaction mechanism, but not to a loss of active surface sites. This knowledge is of importance when studying Nickel-based binary/ternary hydrogen evolution electrocatalysts. The absence of this effect can be a descriptor for the reported high performance of Nickel-based electrocatalysts in literature, especially when Nickel is the active site in such electrocatalysts. The literature often only focuses on the performance values, instead of the reason for the high performance.

2.4 The literature background of the oxygen evolution reaction on Nickel

The history dependence of Nickel on the performance of the hydrogen evolution has been extensively described in chap. 2.2. Expectedly, the history of Nickel and its correlated surface states of the Nickelhydroxides and Nickeloxihydroxides plays a major role in the oxygen evolution kinetics as well.

A detailed study of the history effect on the OER has been conducted by Lyons and Brandon [50]. In brief, Lyons and Brandon conducted different pretreatment procedures on Nickel electrodes for the OER, concluding that the β/β-cycle performs superior to the α/γ-cycle. This has been referred to the avoidance of inactive Ni^{4+}-species, which can be partly present in $\gamma - NiOOH$. A schematic of the aging process of Ni^{3+} to Ni^{4+} in a Nickeloxide-layer is shown in fig. 25.

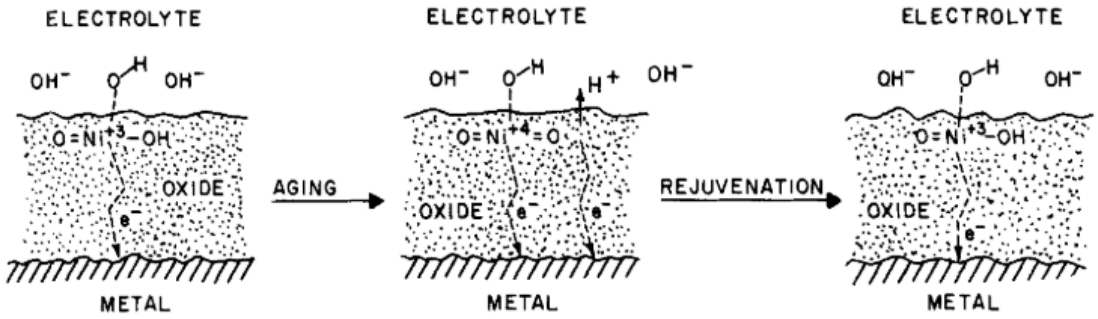

fig. 25: Schematic process of the OER overpotential aging of Ni^{3+} to Ni^{4+} for $\eta > 330\,mV$ and its rejuvenation by lower overpotentials of $\eta < 270\,mV$. Reproduced from [51].

As the influence of the different hydroxides and oxihydroxides of Nickel has been elaborated earlier in this report, a more detailed explanation for the OER is omitted and the reader is referred to the literature [8, 50–53].

The OER kinetics of Nickel are highly influenced from the presence of Iron in the electrode or the electrolyte. It is well-known that a pure Nickel electrode has a low performance for the OER, while even trace amounts of Iron greatly enhance the performance [7, 54–56]. Hence, it is not straightforward to deduce the OER kinetics of Nickel from literature alone, as many sources do not specifically adress this crucial detail. For this reason, comparative plots of the respective Tafel-slopes, exchange current densities and overpotentials at 10 mA/cm^2, as given in the hydrogen evolution chapter, have not been made.

The importance of the Iron-effect is clearly illustrated in fig. 26. It is of importance to note that Iron-free electrolytes require overpotentials far greater than 400 mV to activate a Nickel electrocatalyst for the OER [56]. Therefore, a pure Nickel electrocatalysts is not favorable for the OER in alkaline electrolytes. It requires an incorporated second element to be an active electrocatalyst. Especially Iron appears to activate a Nickel electrocatalyst for the OER, as trace impurities of it already decrease the onset-potential from about 450 mV to 300 mV of overpotential in the given example.

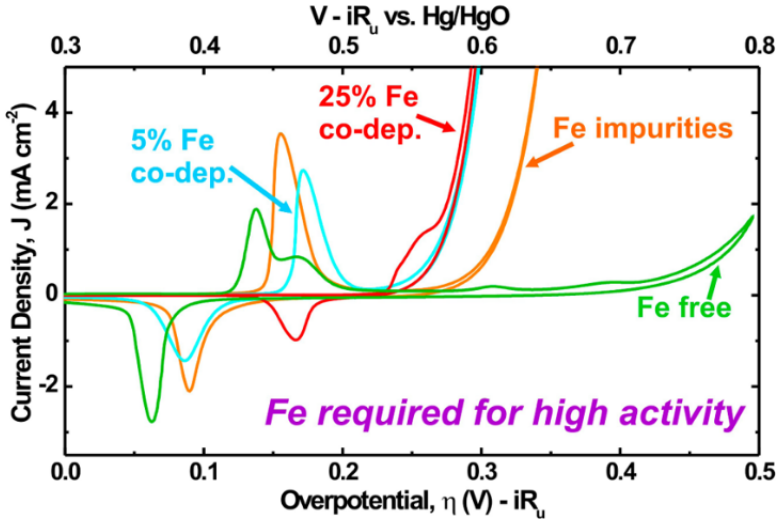

fig. 26: The influence of intentionally incorporated Iron and Iron-impurities on the oxygen evolution performance of a Nickel electrode. Iron-free electrolytes result in a low OER performance of Nickel electrodes. Cyclic Voltammograms in 1 M KOH, reproduced from [56].

2.5 Testing results of the oxygen evolution reaction on Nickel

In order to assess intrinsic properties, the estimation of the ECSA is a crucial part. As the literature discusses several approaches without a convincing consensus [1, 41, 50, 57], it was decided to apply the a.c. impedance in situ method as well for the OER. The in situ method is more favorable than other methods. In the first place, it does not require the addition of further chemicals, which could in principle influence the further kinetic response. Secondly, it is of benefit to estimate the surface area during electrolysis, as the gas-evolution could block parts of the surface, which is accounted for only by the impedance method. The correction factor for the obtained double layer capacitance was 60 $\mu F/cm^2$ [41, 57].

The tests were conducted in Fe-free KOH electrolyte, as confirmed by ICP-OES. An overview of four different tests in 11.6 M KOH, and their average, is given in fig. 27. All electrodes were Nickel-foils of the same batch, which have been polished with sandpaper and further cleaned with ethanol and deionized water. As clearly visible, the tests vary more than within the established errors (chap. 1.4). Since the value for η_{10} is below 450 mV in two tests, it is considerable that trace impurities of Iron are present. This value is closer to the Iron-impurity test than to the Iron-free test in fig. 26.

The Iron could be, for instance, already be present in the tested foil, as the testing electrolyte has proved to be Iron-free in ICP-OES. However, since the tested OER electrocatalysts outperform Nickel intrinsically, as shown later in this report, and the history as well as the Iron-effect have already been addressed extensively in the literature [50, 56], it was decided to not further investigate on the effect. A pure Nickel OER electrocatalyst would be unfavorable for the alkaline water electrolysis and thus doesn't demand further testing.

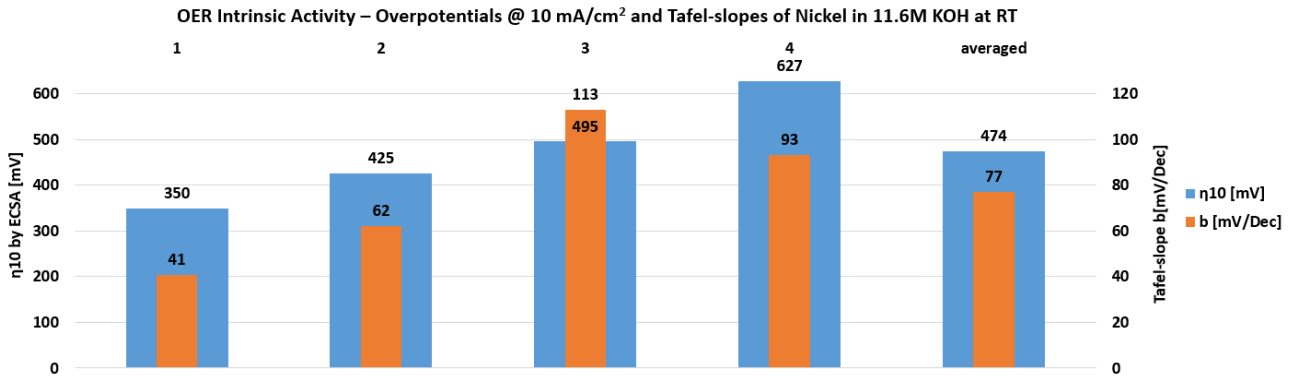

fig. 27: The overpotential at an intrinsic current density of 10 mA/cm^2 and the correlated Tafel-slopes of four Nickel-foils, and their average, in 11.6 M KOH at room temperature.

3 NiMo electrocatalysts for the hydrogen evolution reaction

3.1 The choice of the NiMo synthesis methods

The recent published literature offers several different synthesis methods for an abundance of Nickelmolybdenum electrocatalysts. While the majority promises to deliver outstanding performance, only a few sources actually address the reason for the high activity, as well as the behavior under technical conditions.

However, some publications address the influence of the composition of Nickelmolybdenum electrodes on the electrochemical kinetics. One study [17], as illustrated in fig. 28, addresses the performance of different Ni-Mo-ratios by comparing different metallurgically prepared foils. The study shows that a 1:1 ratio is favorable for the hydrogen evolution reaction. This is in-line with the findings by another study, which found 40% to be a favorable amount of Mo for the geometric activity [13]. Although the same publication claims that 20% of Molybdenum has the highest intrinsic activity, it seems most suitable to aim for a Mo-content of 40-50% in a Nickelmolybdenum electrocatalyst.

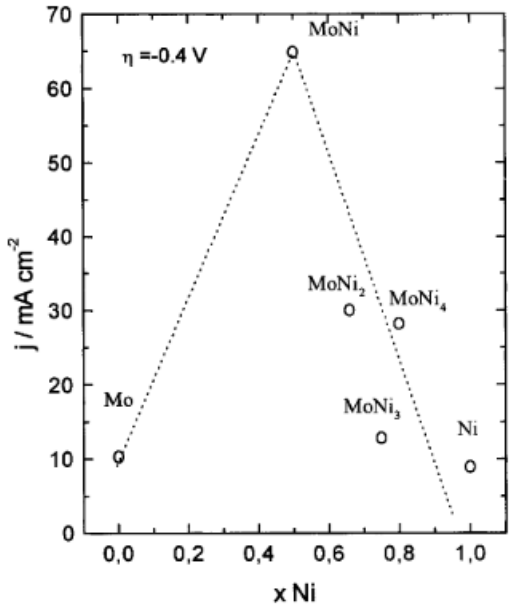

fig. 28: Vulcano-plot of different $MoNi_x$-compositions. Current density at an overpotential of 400 mV in 1 M NaOH. Reproduced from [17].

In order to ensure a robust, cost-effective, and green synthesis, three different synthesis methods for Nickelmolybdenumoxide precursors have been chosen from the literature: A hydrothermal synthesis [58], a solgel synthesis [59], and a coprecipitation synthesis [60]. The synthesis methods are denoted as Cuboids, Solgel, and Coprecip, respectively. The Cuboids and the Solgel electrocatalysts contain 50% Mo, while the Coprecip method has 40% Mo. All three methods give a Nickelmolybdenumoxide precursor, which can be loaded on different substrates by either drop-casting, spray-coating, dip-coating, screen-printing, robo-casting, or painting. The hydrothermal (Cuboids) method has an advantage over the other methods, as the precursor production can be combined with an in situ catalyst loading by adding the substrate to the catalyst-synthesis. The Nickelmolybdenumoxides have to be reduced in a hydrogen-atmosphere in a further step.

The production of the Nickelmolybdenumoxide-precursors is described in the appendices under chap. C. The three Nickelmolybdenumoxides are dropcasted with Isopropanol as solvent on cleaned Nickel-foils of 25 by 25 mm (see chap. B for the cleaning procedure). The precursor-covered substrates are reduced at five different temperatures (400 to 800 $^{\circ}C$, 100 $^{\circ}C$ interval), which resulted in a total of 15 different electrocatalysts. The different temperatures are chosen, as the literature shows that the presence of an oxide could increase the HER performance compared to fully reduced electrocatalysts [61]. DTU Energy decided to investigate the influence of the reduction process, focussing on the performance and the reliability of the obtained electrocatalysts.

3.2 Screening results of various NiMo electrocatalysts in 11.6 M KOH

The screening of the 15 different electrocatalysts required a method to correct for the ECSA. Several methods are proposed in the literature, while none of those has so far proven to be the state-of-the-art. As an example, obtaining the double layer capacitance from cyclic voltammetry in the potential region slightly above the hydrogen evolution equilibrium potential [62, 63] is in contrast to the findings, which show that Molybdenum is leaching out in this potential window [64, 65].

To compare the NiMo screening results to the Nickel results, it was decided to apply the in situ a.c. impedance method to obtain the ECSA. As shown in fig. 29, Nickelmolybdenum electrocatalysts show a pseudocapacitance around the equilibrium potential of the hydrogen evolution reaction. This pseudocapacitance is to be correlated to the redox-activity of Molybdenum, which becomes negligeable for overpotentials greater than 150 mV [65, 66]. Hence, the a.c. impedance method estimates

the ECSA of Nickelmolybdenum electrocatalysts accordingly to Nickel electrocatalysts, with fitted spectra at overpotentials greater than 200 mV and a correction factor of $40\ \mu F/cm^2$ [1].

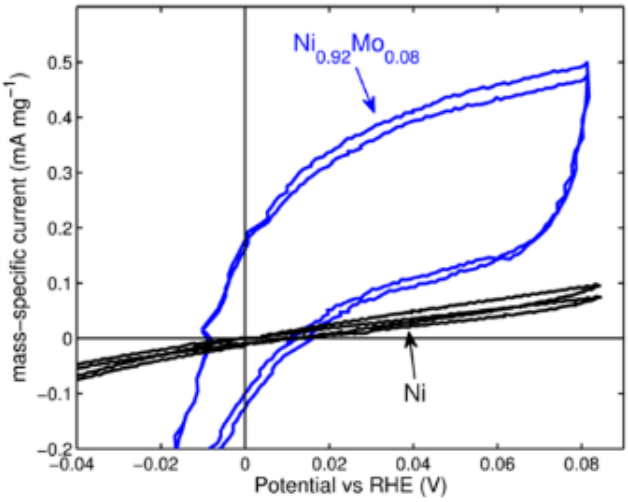

fig. 29: A cyclic voltammogramm of a Nickelmolybdenum electrode in comparison to a Nickel electrode. The CV of the Nickelmolybdenum electrode shows an influence of a pseudocapacitance in the potential region of the equilibrium potential of the HER. Reproduced from [66].

The results of the NiMo electrocatalyst screening are summarized in fig. 30, 31, and 32 for the Cuboid, the Solgel, and the Coprecip electrocatalysts, respectively. Each figure shows the overpotential at an intrinsic current density of 10 mA/cm^2 and the Tafel-slope of the electrocatalysts reduced at different temperatures. For comparison, the best achieved Nickel test from chap. 2.3, which is the performance of a fresh Nickel electrocatalyst, is always given as the first value.

It is remarkable that, after correcting for the ECSA, Nickelmolybdenum electrocatalysts appear to not outperform a fresh Nickel electrocatalyst, when comparing the different η_{10} values. Looking further at the Tafel-slopes, as to compare the reaction mechanisms, it is clearly visible that Nickelmolybdenum electrocatalysts perform better than pure Nickel, irrespectively of the reduction temperature. Further, a performance degradation with time, as seen on fresh Nickel (chap. 2.3), has not been observed for the Nickelmolybdenum electrocatalysts.

Interestingly, the Tafel-slope decreases with the reduction temperature for the Cuboids electrocatalysts. The reason for the slight better performance of NiMo electrocatalysts can be of two reasons. Firstly, it is possible that the presence of Molybdenum in the reduction process influences the morphology and availability of active Nickel sites. While Molybdenum does not contribute to the intrinsic properties of the electrocatalyst, it aids in the production of highly active and degradation resistant Nickel sites during the thermochemical reduction. Secondly, the presence of Molybdenum or Molybdenumoxide can influence the adsorbtion processes and hence the reaction mechanism, which would describe an intrinsic effect of Molybdenum.

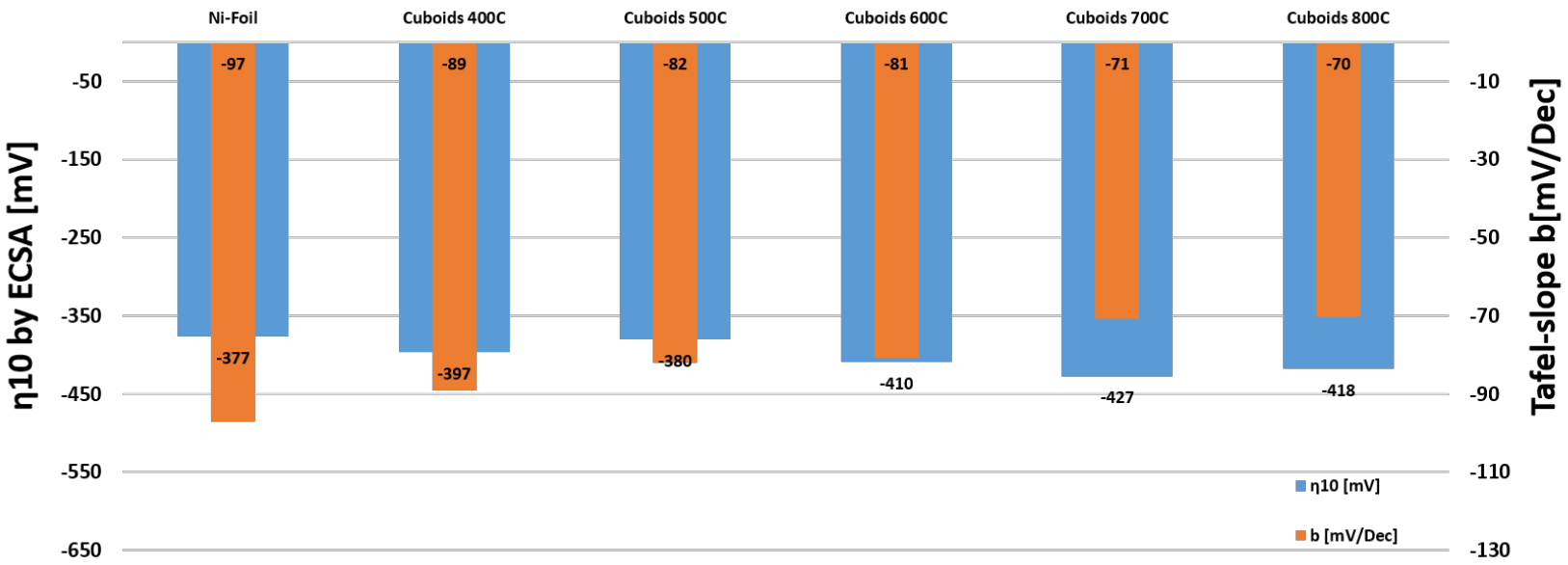

fig. 30: The overpotential at an intrinsic current density of 10 mA/cm^2 and the correlated Tafel-slopes of NiMo electrocatalysts made by hydrothermal synthesis and reduced at five different temperatures in comparison to the best achieved Nickel-foil test. The tests were conducted in 11.6 M KOH at room temperature.

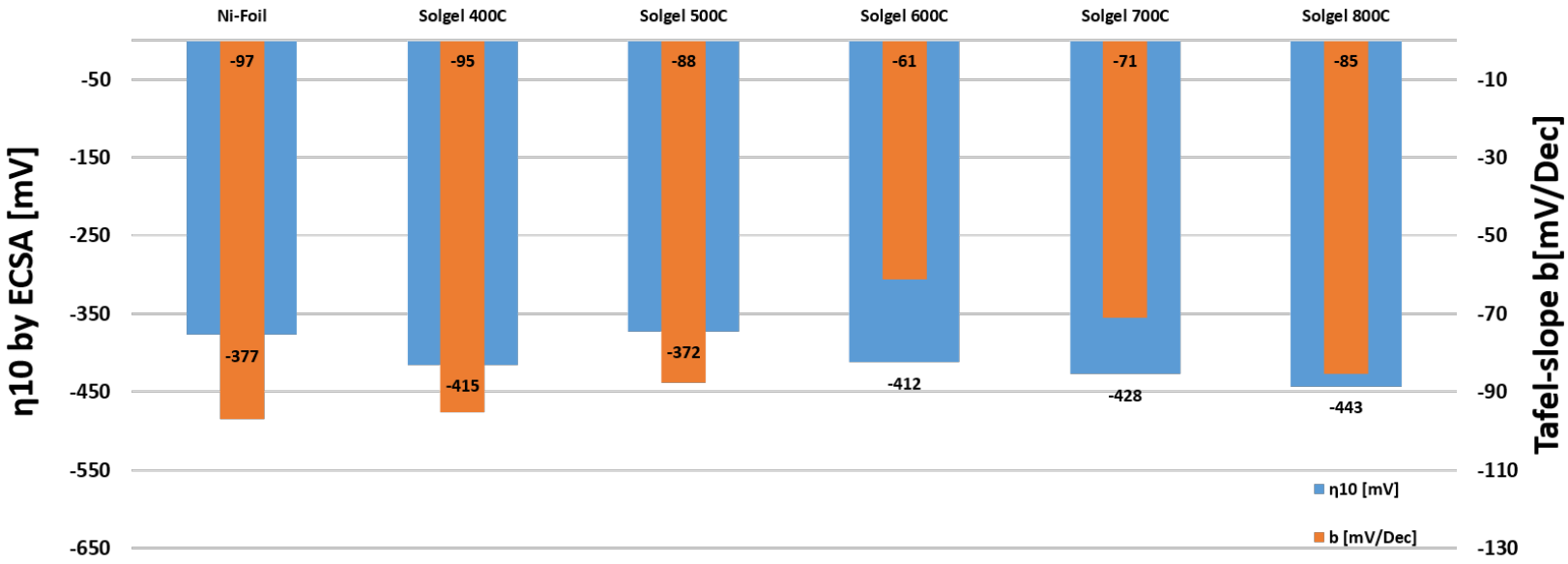

fig. 31: The overpotential at an intrinsic current density of 10 mA/cm^2 and the correlated Tafel-slopes of NiMo electrocatalysts made by solgel synthesis and reduced at five different temperatures in comparison to the best achieved Nickel-foil test. The tests were conducted in 11.6 M KOH at room temperature.

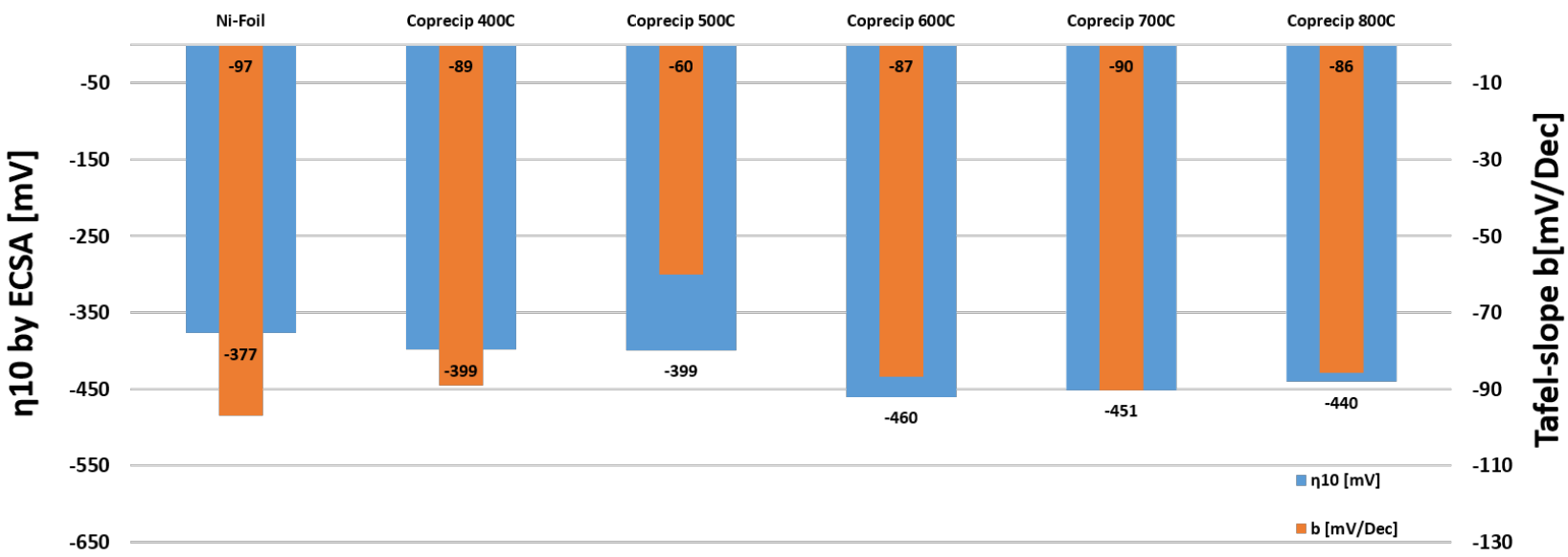

fig. 32: The overpotential at an intrinsic current density of 10 mA/cm^2 and the correlated Tafel-slopes of NiMo electrocatalysts made by co-precipitation synthesis and reduced at five different temperatures in comparison to the best achieved Nickel-foil test. The tests were conducted in 11.6 M KOH at room temperature.

To understand these possible explanations further, fig. 33 represents the obtained electrochemically active surface area per mass of electrocatalyst as a function of the reduction temperature. The ECSA is a tool in the determination of the intrinsic properties. As clearly visible, the ECSA monotoneously decreases with the reduction temperature for the three different electrocatalyst synthesis methods, with one outliner at 600 $°C$ for the Solgel electrocatalyst. This finding would rather suggest that the presence of Molybdenum results in the formation of active Nickel sites during the thermochemical reduction process, rather than an intrinsic activity of Molybdenum.

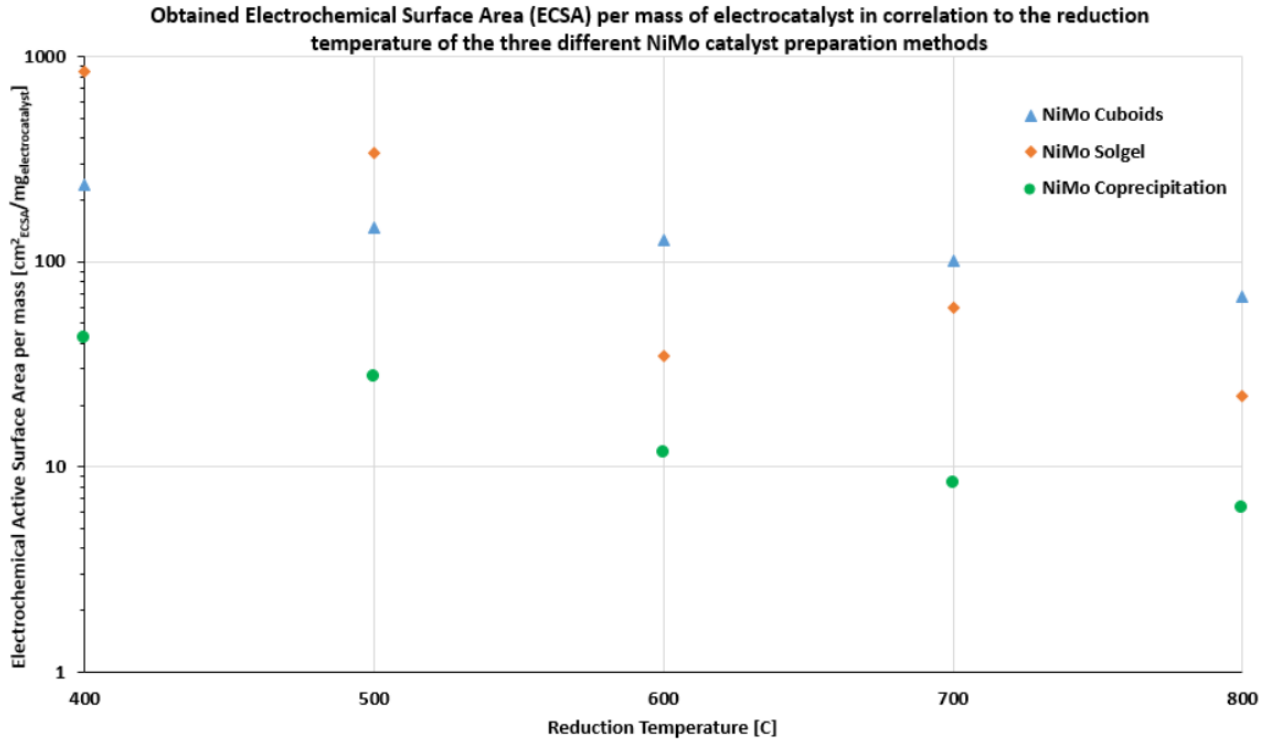

fig. 33: The obtained electrochemical active surface area (ECSA) per mass of electrocatalyst in correlation to the reduction temperature of the three different NiMoOx precursor production (Cuboids, Solgel, Coprecip) methods. Vertical axis in logarithmic scaling.

For a more detailed analysis, fig. 34 illustrates the overpotential at a geometric current density of 10 mA/cm^2 with respect to the surface enhancement factor, which is calculated as ECSA per geometric surface area. In case that Molybdenum is solely responsible for the amount of highly active Nickel sites, the plotted correlation must represent a monotoneous trend. A direct scaling between the surface area and the geometric performance would show an absence of intrinsic differences.

In a broader view, a semi-logarithmic monotoneous correlation can be found. In this correlation, low surface area Nickelmolybdenum electrocatalysts perform as good as aged or (partially) oxidized Nickel. With increasing surface area, the performance of the Nickelmolybdenum electrocatalysts trend to perform as well as a fresh Nickel surface, and further outperforming it.

On the other hand, a more focussed view on the different reduction temperatures shows a change in the trend behavior. For all three different synthesis-methods, the change is clearly visible between the low and medium reduction temperatures (500 and 600 $°C$). The change is further not directly correlated to the surface enhancement factor; it occurs in the range of 15-50. DTU Energy has performed in situ X-ray Diffraction on the reduction process of the different Nickelmolybdenumoxides (chap. 3.3). It is known that, at 600 $°C$, the electrocatalysts are almost fully reduced to Nickelmolybdenum alloys. As shown above, the Tafel-slope decreases with increasing reduction temperature for the Cuboids, while the Solgel electrocatalyst tend to increase the Tafel-slope above 600 $°C$. Due to these findings, a single scaling between the geometric performance and the surface area cannot be determined, albeit the deviation of this trend appears to have a lower impact on the performance than the scaling with the surface area.

In conclusion, the primary descriptor for the high performance of Nickelmolybdenum electrocatalysts is the high active surface area. However, a secondary descriptor lays in the gain of an intrinsic effect by the presence of Molybdenum. It is unequivocally evident that the different forms of Molybdenum, either as Nickelmolybdenum/Molybdenumoxide mixture (reduction temperature 400-600$°C$) or as fully reduced alloy (reduction temperature 700-800$°C$), influence the intrinsic properties of the Nickelmolybdenum electrocatalyst. On the other hand, it cannot be deduced if the gain of intrinsic properties is due to the electrochemical activity of Molybdenum/Molybdenumoxide, or if the thermochemical reduction process forms different active forms of Nickel. The current testing results cannot address this question alone. Further tests, especially spectroscopic analyses under operating conditions, are necessary to answer this question unambigiously. In general, it can be deduced that the presence of Molybdenum in Nickelmolybdenum is of high benefit, for the geometric performance by the production of high surface areas, as well as for the intrinsic properties, while the gain of intrinsic properties is more pronounced for low-temperature reduced Nickelmolybdenum electrocatalysts.

The Cuboids and the Solgel electrocatalysts show the most promising results. Both electrocatalyst synthesis methods result in high surface area electrocatalysts and high intrinsic activities. In an economical perspective, both methods are superior to the Coprecip synthesis in terms of the electrocatalyst amount, the needed chemicals for the precursor-synthesis, and the electrochemical performance. Depending on the finally chosen reduction temperature and the catalyst loading procedure, the Solgel and the Cuboids electrocatalysts have to be evaluated against another in an economical analysis.

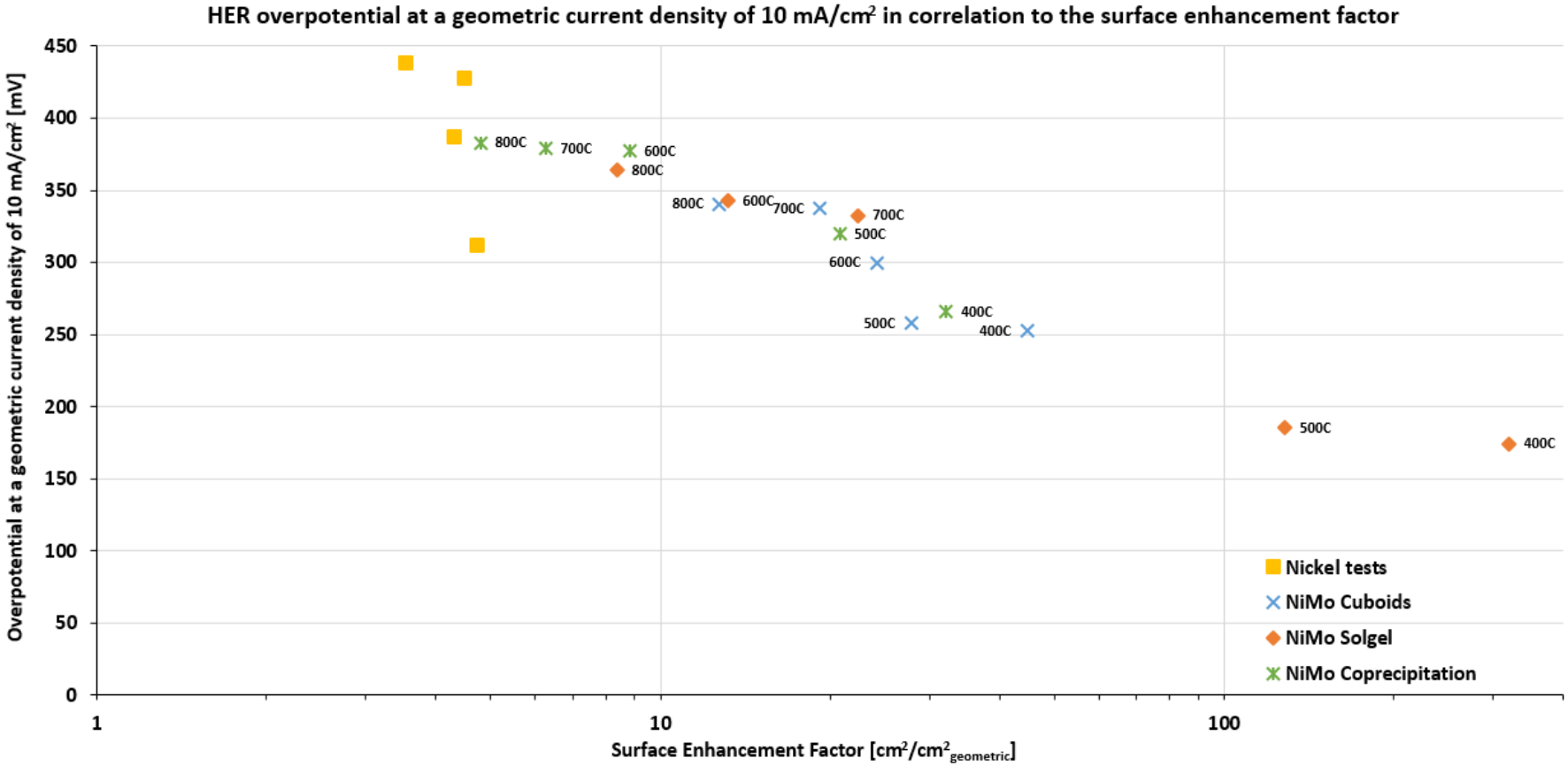

fig. 34: The HER overpotential at a geometric current density of 10 mA/cm^2 of the 15 different NiMo electrocatalysts and of the Nickel tests from chap. 2.3 in comparison to the surface enhancement factor (electrochemical active surface area divided by geometric surface area). The reduction temperature of the Cuboids is given to the left of the respective data point, the reduction temperature of the Solgel and Coprecip electrocatalysts is given to the right of the respective data point. The tests were conducted in 11.6 M KOH at room temperature. Horizontal axis in logarithmic scaling.

3.3 Characterization of the NiMo electrocatalysts

The surface coverage of the thin-film electrodes was controlled with a light microscope. In addition, Scanning Electron Microscope was conducted on carbon-coated electrodes to understand the different electrochemical results from chap. 3.2. A collection of images at low and high magnification can be seen in fig. 35. Cuboids show a scaffolding of Molybdenumoxides, at a length of 10 - 15 μm and a width of 400 - 600 nm of the single particle. The unreduced Solgel electrocatalyst displays a well-distributed array of nanosized (100 - 700 nm) particles, while Coprecip appears to be more aggregated than the Solgel electrocatalyst. Furthermore, the Coprecip particle size is greather than the nanosized Solgel particles, in the order of about 1 μm.

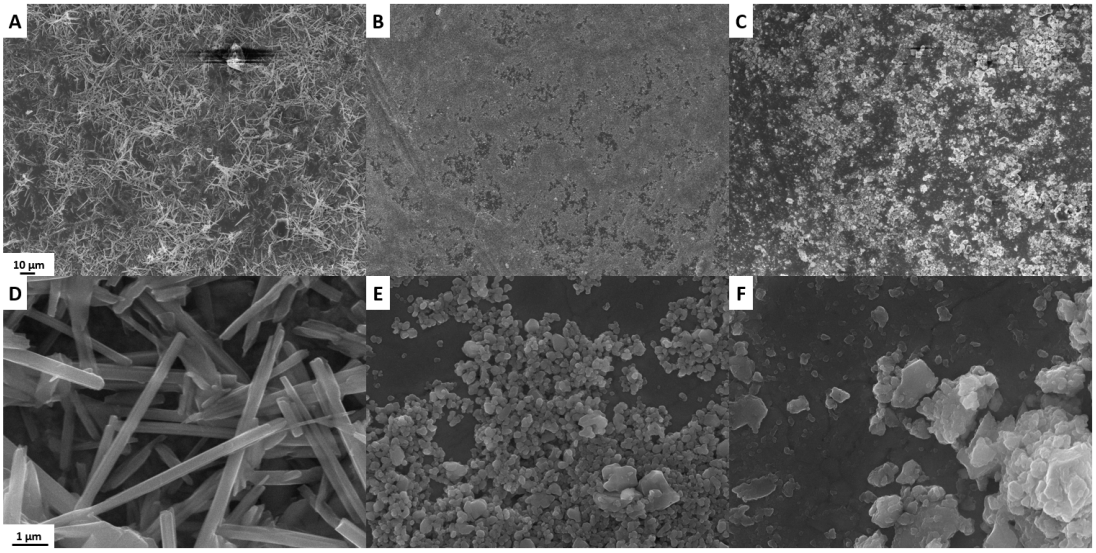

fig. 35: Scanning Electron Microscope images of unreduced Nickelmolybdenum electrocatalysts. A/D: Cuboids. B/E: Solgel. C/F: Coprecip. A, B, C are at the same low magnification. D, E, F are at the same high magnification. The images show a good surface coverage with electrocatalyst and differences in the morphology of the three different synthesis methods.

For a deeper understanding of the reduction temperature depending electrochemical performance and electrochemical active surface area of the NiMo electrocatalysts, as represented in fig. 34, DTU Energy performed X-ray diffraction during the reduction process. The in-situ measurements are conducted under water-wetted safety gas (5% H_2 in Ar) with a Rigaku Smartlab X-ray diffractometer (Copper anode), at a temperature of 25 $°C$ and 200-800 $°C$ (intermediate steps of 100 $°C$), and 2Θ angles of 20-140°. The obtained diffraction patterns are illustrated in fig. 36.

For the Cuboids, the diffraction patterns show no change from room temperature to 300 $°C$. At 400 $°C$, the main peak at around 30° disappears, while two new main peaks arise at 45°. These two new main peaks increase in intensity by increasing the reduction temperature to 500 $°C$. At this reduction temperature, a new peak arises at 26°, which becomes the main peak at the reduction temperatures

of 600-800 $°C$. The changes of these patterns are due to the formation of $NiMoO_4$ at 400 $°C$, while different Molybdenumoxides are present at lower temperatures. At 500 $°C$, Nickelmolybdenum-alloys, with Ni_4Mo as primary alloy, are produced in co-existence to $NiMoO_4$ and Ni. The increasing temperature results in a further reduction of the Nickelmolybdenumoxides, which are partly present at a reduction temperature of 600 $°C$. At higher temperatures, the oxides are well-reduced to Nickelmolybdenumalloys and Nickel.

A similar procedure occurs in the reduction process of the Solgel electrocatalysts. At 400 $°C$, the Solgel electrocatalyst consists of several Nickelmolybdenumoxides, while the Cuboids are primarily consisting of $NiMoO_4$. At 500 $°C$, the Solgel electrocatalyst is similar to the Cuboids, consisting of a mixture of Nickelmolybdenumalloys, with Ni_4Mo as primary alloy, and $NiMoO_4$. At higher reduction temperatures, the Nickelmolybdenumoxides gradually reduce, until only well reduced alloys are present at reduction temperatures higher than 600 $°C$. At 800 $°C$, the amount of Ni_4Mo is higher than at lower reduction temperatures.

The Coprecip electrocatalysts behave differently. Until 300 $°C$, the peak intensities are low. This indicates that the electrocatalyst is amorphous and only partly crystalline. At 400 $°C$, the electrocatalyst forms crystalline $NiMoO_4$. At 500 and 600 $°C$, different Nickelmolybdenum-alloys and Nickel are co-present to $NiMoO_4$. Increasing the reduction temperature results in the full reduction to Ni_4Mo.

The results from X-ray diffraction are further supported by an SEM-analysis of the reduced electrocatalysts, which is illustrated in fig. 37 for the Cuboids thin-film electrodes. The scaffolding of the unreduced Cuboids is still present at 400 $°C$. At 600 $°C$, nano-sized particles are formed on the surface of the Nickelmolybdenumoxide cuboidal beams. The image taken for the 800 $°C$ reduced electrode shows a coral-like networking of the fully reduced Nickelmolybdenum-alloy. A similar picture (fig. 38) could be drawn for the Solgel electrocatalysts, with the difference that the Nickelmolybdenumoxides aren't cuboidal beams. A deeper analysis of the Coprecip electrocatalysts is left-out at this point, as they clearly underperform the other electrocatalysts.

It is of importance to note that the full reduction and interconnection of the electrocatalyst decreases the surface area and the electrochemical performance. However, this processes grants a stronger mechanical interconnection, which therefore increases the stability of the electrocatalysts. Hence, a trade-off between high performing electrodes, reduced at lower temperature, and high stability, for electrodes reduced at high temperature, has to be made. In this perspective, further tests at a later stage have shown that low reduction temperatures might not be sufficient enough to ensure a robust, decade-long high performing electrode. This work is on-going and spared at this point.

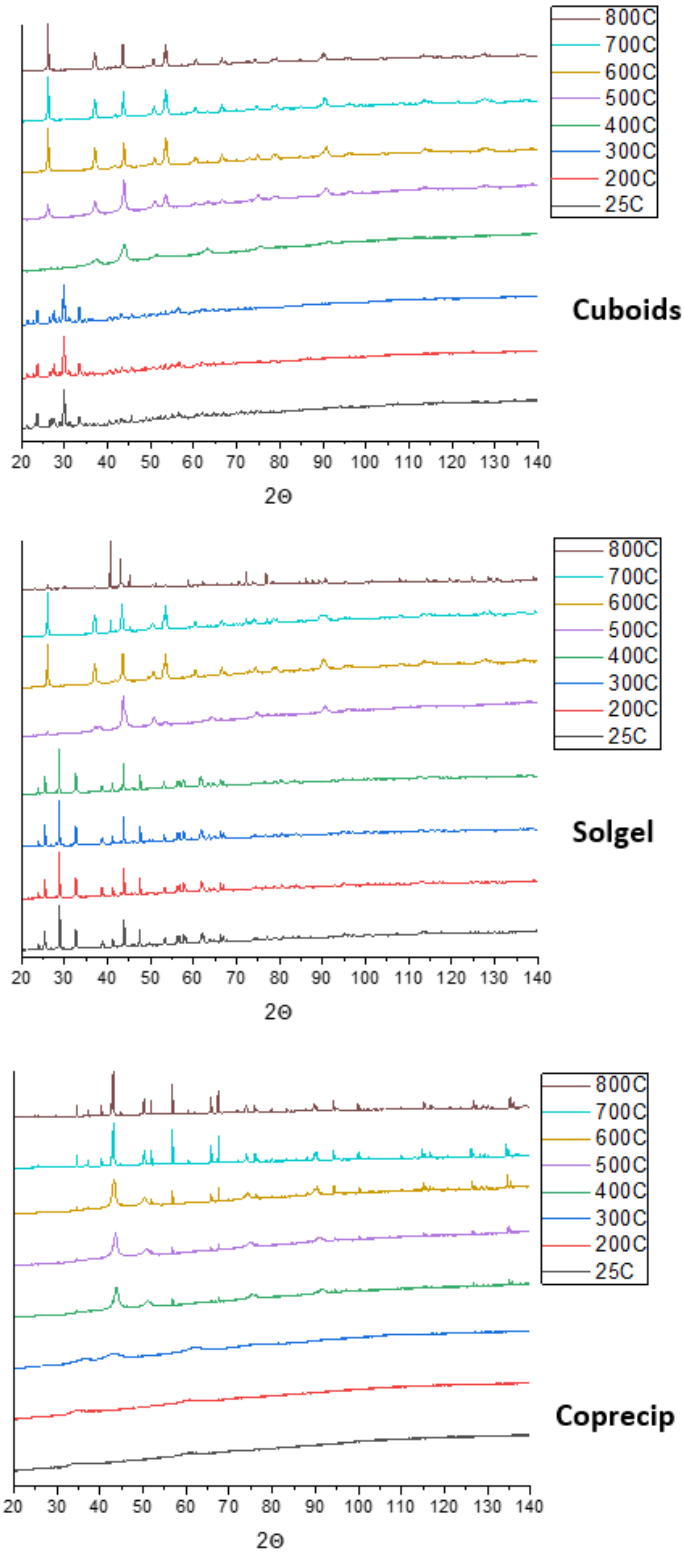

fig. 36: In situ X-ray diffraction patterns of the three different NiMo synthesis methods during the reduction process in safety gas (water-wetted 5% H_2 in Ar). Top: Cuboids, mid: Solgel, bottom: Coprecip. Increasing reduction temperature from bottom to top in the respective patterns. All patterns are corrected to the peak maximum.

fig. 37: SEM images of reduced Cuboids thin-film electrodes. The reduction temperatures are A: 400 $°C$, B: 600 $°C$, C: 800 $°C$. All three images are taken at the same magnification.

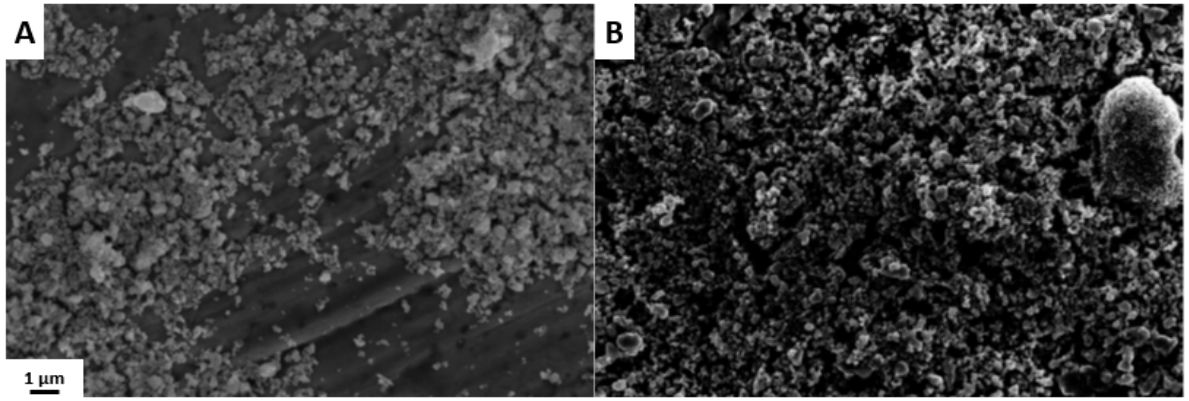

fig. 38: SEM images of reduced Solgel thin-film electrodes. The reduction temperatures are A: 400 $°C$, B: 600 $°C$. The images are taken at the same magnification.

4 NiFe LDH electrocatalysts for the oxygen evolution reaction

4.1 The choice of the NiFe LDH synthesis methods

NiFe layered double hydroxide electrocatalysts are in the focus of several recent studies. The abundance of different studies ends in a broad diversity of published synthesis-methods. Besides nanomaterials and different distinctive morphologies, the stochiometry of Nickel to Iron varies between the different studies. This vast variety, and the different testing methods, leads different working groups to different results on the origin of the high activity of NiFe LDH for the OER. For instance, it is postulated that the active site in NiFe LDH is Fe^{3+} [67], $NiOOH$ or $NiOOH$ stabilized Fe^{4+} [68], while the local morphology, irrespectively of the form of Iron, is taken as the descriptor for the high OER activity elsewhere [69].

In brief, it is unmanageable to determine the best synthesis method for NiFe LDH by literature alone. In addition, the different electrocatalyst structures and stochiometries are presumably different from the as-synthesized uncharged state to the charged state under oxygen evolving conditions, which doesn't allow to draw conclusions from ex situ measurements alone [70].

However, the already existing knowledge on the performance of NiFe LDH electrocatalysts can be taken as a starting point to screen several promising synthesis methods. In the first place, the stochiometric ratio of Nickel to Iron is of importance in the screening study. Louie et al [71] investigated the effect of the Iron content in electrodeposited NiFe LDH on the OER activity. The findings, as illustrated in fig. 39, show the highest activity for Iron-contents of about 10-50%, with the most promising results between 20-40%. Although the shown results reflect the geometric, not surface area corrected, performance of NiFe LDH, it can be taken as a qualitative descriptor, as the authors used electrodeposited thin-film electrodes. A great deviation to intrinsic properties is unexpected in thin-film electrodes. The findings of Louie et al are further supported by a collection made by Diongi and Strasser [70] shown in fig. 40. The authors collected several reported overpotentials for different Iron-contens and plotted the relativ correlation to the best achieved value of each source. Albeit the measurement conditions, and the synthesis conditions, and the current densities, at which the overpotentials are taken, vary between the sources, the overall picture is similar to Louie et al; NiFe LDH electrocatalysts display the highest activity for an Iron-content of 10-50%.

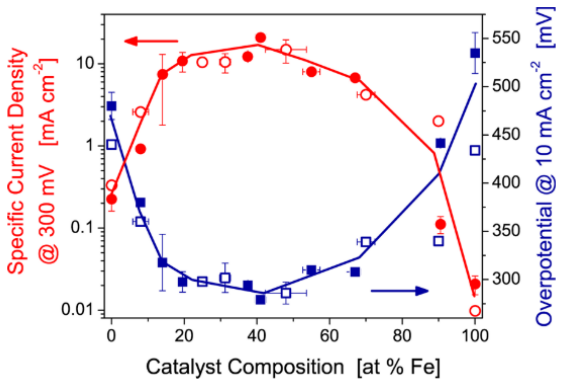

fig. 39: The OER activity of electrodeposited NiFe LDH with respect to the amount of Iron. Left axis: Current density at an overpotential of 300 mV. Right axis: Overpotential at a current density of 10 mA/cm^2. Test results from 0.1 M KOH at room temperature. Reproduced from [71].

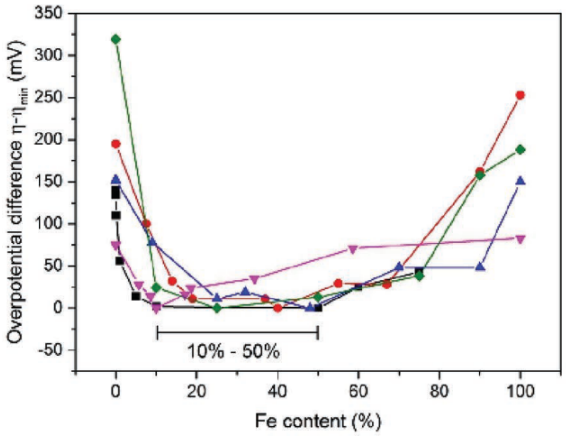

fig. 40: Collection of reported OER overpotentials in correlation to the Fe-content of NiFe layered double hydroxide electrocatalysts. The testing conditions, and current densities, and the electrocatalyst production methods vary between the measurements. The highest reported activities can be found for Fe-contents of 10-50%. Reproduced from [70].

In this light, DTU Energy decided to investigate a choice of synthesis-methods, which are reported for Ni to Iron ratios in the most promising span of 33-50%. Since it is published that the morphology is crucial for the performance of NiFe LDH [69], DTU Energy decided to take the Nickel to Iron ratio as published for the respective synthesis method, instead of normalizing the ratio to one nominal composition. The change of the composition would result in a different morphology from the published methods and therefore not allow for a comparison between different synthesis methods. Such a deviation would therefore build up the uncertainty of the reproducibility and the robustness of the synthesis method, which is contraindicated with a view on an upscaled electrocatalyst development and quality management. Furthermore, a huge performance gap due to the amount of Iron in the span of 33-50% is not expected according to the literature.

The choice of synthesis-methods was guided by two main requirements. Firstly, the synthesis should require as less steps and chemicals as possible. Especially green chemicals are preferred, as the benefit of a high performing electrocatalyst would underscore the need of an expensive and environmentally challenging synthesis route, or the disposal of heavily regulated chemicals (e.g. organic solvents). Secondly, it is well-known that the conductivity of NiFe LDH electrocatalysts is low compared to metals [72]. Hence, the loading of the electrocatalyst on the electrode has to be considered. Since NiFe LDH electrocatalysts are not thermochemically reduced, as in the case of the HER electrocatalysts, the catalyst loading procedure must happen during the synthesis method. In this way,

the low electrocatalyst conductivity is compensated by the in situ gained interconnection to a highly conducting metal substrate. This further results in the best achievable interconnection between electrocatalyst and electrode in terms of mechanical and chemical stability, as a stable and reliable ex situ loading procedure is lacking to date. Such methods usually apply binder-materials to attach electrocatalysts to conducting surfaces (e.g. in RDE measurements on glassy carbon electrodes), but a high temperature and high alkaline resistant binder has not been found yet.

Due to these requirements, four different synthesis methods have been chosen, which allow a direct growth of the electrocatalyst on Nickel-substrates. The chosen methods are a hydrothermal synthesis at 120 $°C$ [73] (Ni:Fe - 1:1), another hydrothermal synthesis at 150 $°C$ [74] (Ni:Fe - 1:1), a precipitation synthesis at 90 $°C$ [75], conducted either on a hot plate (Ni:Fe - 1:1) or in an oven (Ni:Fe - 2:1), and another precipitation synthesis at 55 $°C$ [76] (Ni:Fe - 6:4). The exact procedures are describe in the appendix in chap. D.

4.2 Screening results of various NiFe LDH electrocatalysts

One of the greatest disadvantages in the literature, besides the above described inconsistency, are the chosen testing conditions. The literature on NiFe LDH electrocatalysts for the OER does not reflect technologically relevant conditions. The electrolyte never exceeds a concentration of 1 M KOH (pH 14) and room temperature. To ensure a reliable technological alkaline water electrolysis, it is of major significance to understand these electrocatalysts in highly concentrated alkaline solutions above 1 M and, in a further step, at elevated temperatures up to 100 $°C$.

As a first step, the comparability to the published knowledge has to be given. Therefore, DTU Energy screened the previously described thin-film NiFe LDH electrodes in 1 M KOH at room temperature first, which is described in chap. 4.2.1. In a second step, as described in chap. 4.2.2, the studies were narrowed to the two best performing synthesis methods and conducted in 11.6 M KOH. This study further contained three-element LDH electrocatalysts, in which Chromium and Aluminium have been incorporated into the NiFe LDH electrocatalysts. These elements are very promising candidates to even further increase the performance of NiFe LDH OER electrocatalysts. Different studies have shown that three-element NiFeX LDH electrocatalysts are outperforming NiFe LDH, especially the extensive screening study from Gerken et al [77].

4.2.1 Screening of NiFe LDH in 1 M KOH

The electrochemical active surface area of layered double hydroxides have been determined similar to the OER on Nickel, with the in situ a.c. impedance method and a correction factor of $60\ \mu F/cm^2$. This approach was chosen for two different reasons. In the first place, the same approach for NiFe LDH electrocatalysts and the Nickel tests (chap. 2.5) allows to draw conclusions on the performance-impact of Iron, as the Nickel tests have shown to be influenced by Iron. Hence, a direct comparison to the NiFe LDH electrocatalysts is necessary. In the second place, the in situ a.c. impedance method allows to correct for surface blocking, e.g. due to bubbles.

Another possible approach to correct for the ECSA of NiFe LDH electrocatalysts is a potentiostatic impedance at a potential, at which the LDH is charged, but not yet evolving oxygen. The correction factor for this method is given with $81\ \mu F/cm^2$ [72]. However, since this approach is only validated for LDH electrocatalysts, and it does not accomodate surface blocking under operating conditions, and a comparability to the Nickel-tests is required, the first described method to estimate the ECSA has been chosen.

The results of this screening study are shown in fig. 41. It can easily be seen that all five different approaches to produce NiFe LDH electrocatalysts, as expected, outperform a Nickel electrocatalyst intrinsically. The best-performing electrocatalysts have been made by the hydrothermal synthesis method at 120 $°C$ and by the precipitation method at 90 $°C$ (hot plate and oven). The low Tafel-slopes of 26-32 mV/Dec reflect a well-performing electrocatalyst with optimal water splitting characteristics.

Interestingly, the precipitation synthesis in the oven, with a nominal composition of 2:1, outperforms the electrocatalyst produced on a hot plate (nominal composition of 1:1) slightly. This correlation, which is oppositional to the literature, is rather owned to the experimental and analysis error of $\pm\ 10\ mV$ and shows that both approaches have been similarly succesful.

The hydrothermal synthesis at 120 $°C$ outperforms all other synthesis methods. This method is further the most preferrable synthesis route due to its simplicity and the lowest amount of required chemicals. Furthermore, the precipitation synthesis at 90 $°C$ requires ethylene glycol. The use of this organic solvent is a disadvantage of the synthesis method, which makes it a secondary choice in comparison to the hydrothermal approach. This approach only requires urea in addition to Nickel-nitrate and Iron-nitrate. Urea is a naturally occuring substance in the human metabolism and thus harmless. Furthermore, the well-controlled synthesis conditions in an autoclave, which is placed in a furnace, ensures a robust and reproducable synthesis route. This aspect is crucial for the quality management of technical electrodes.

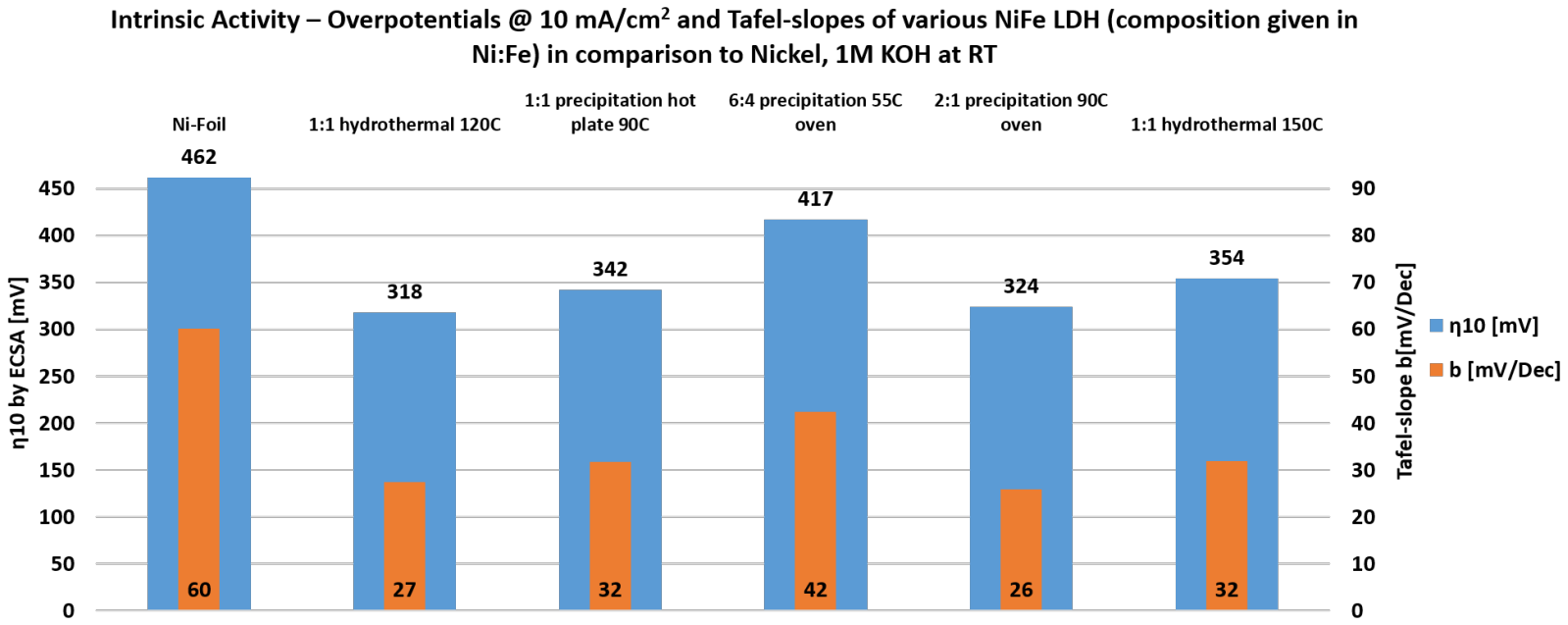

fig. 41: The OER overpotential at an intrinsic current density of 10 mA/cm^2 and the correlated Tafel-slopes of a variety of NiFe layered double hydroxide electrocatalysts in comparison to the best achieved Nickel-foil test. The tests were conducted in 1 M KOH at room temperature.

4.2.2 Screening of NiFeX LDH in 11.6 M KOH

The hydrothermal synthesis at 120 $°C$ and the hot plate synthesis have been repeated, with additional Aluminium and Chromium as third-element LDHs. The tests conducted in 11.6 M KOH are compared to the best achieved Nickel-Test (see chap. 2.5), where signs of unintentionally Iron-incorporation have been observed. The overpotentials at 10 mA/cm^2, with respect to the intrinsic overpotential and the geometric surface area, as well as the Tafel-slopes of the aforementioned samples, are illustrated in fig. 42.

The tests of the electrocatalysts in 11.6 M KOH showed a dark discoloration of the electrolyte in all six cases, with a visible blackening of the thin-film electrode. In comparison to the bare Nickel-foil, all six electrocatalysts perform intrinsically as well as the potentially Iron-influenced Nickel-foil, or worse in case of NiFeAl. The low Tafel-slope of 35-45 mV/Dec, for the NiFe and NiFeCr electrocatalysts, show that the catalysts are well-performing. As the Nickel electrocatalyst performs similar, with an overpotential at an intrinsic current density of 10 mA/cm^2 of 350 mV compared to 332-383 mV for NiFe and NiFeCr, the geometric current densities are compared as well. The geometric current densities show that the best-performing electrocatalysts are NiFe, outperforming the Nickel electrocatalyst.

The difference between the intrinsic and geometric performance, as well as the comparison to potentially Iron-influenced Nickel and the visible electrolyte-discoloration, demonstrates that the layered double hydroxide electrocatalysts suffer severe degradation. Complementarily, the degradation of the electrocatalysts can further influence the measured capacitance from a.c. impedance spectroscopy, which can contain a pseudocapacitance from the degradation species. Another source for a pseudocapacitance can result from inactive side-phases. Hence, the surface area correction does not account solely for the surface area proportional double layer, which results in an overestimation of the ECSA. This artifact is responsible for the similar intrinsic performance seen in fig. 42 (top), as an overestimation of the ECSA underestimates the intrinsic properties.

The comparison of the geometric performance alone discloses that NiFe and NiFeCr LDH electrocatalysts are very well-performing electrocatalysts. Compared to the literature [67, 70, 71], see also fig. 39, an overpotential below 300 mV (at a current density of 10 mA/cm^2) for thin-film electrodes is benchmarking. This value is only outperformed by high surface area electrodes.

The results further show a major problem for layered double hydroxide electrocatalysts, which is only rarely described in the literature: The stability of these electrocatalysts under technologically relevant conditions. The discoloration of the electrolyte reveals the catalyst-decomposition, which is a major problem for technical electrolyzers. It has been recently understood that the morphology of

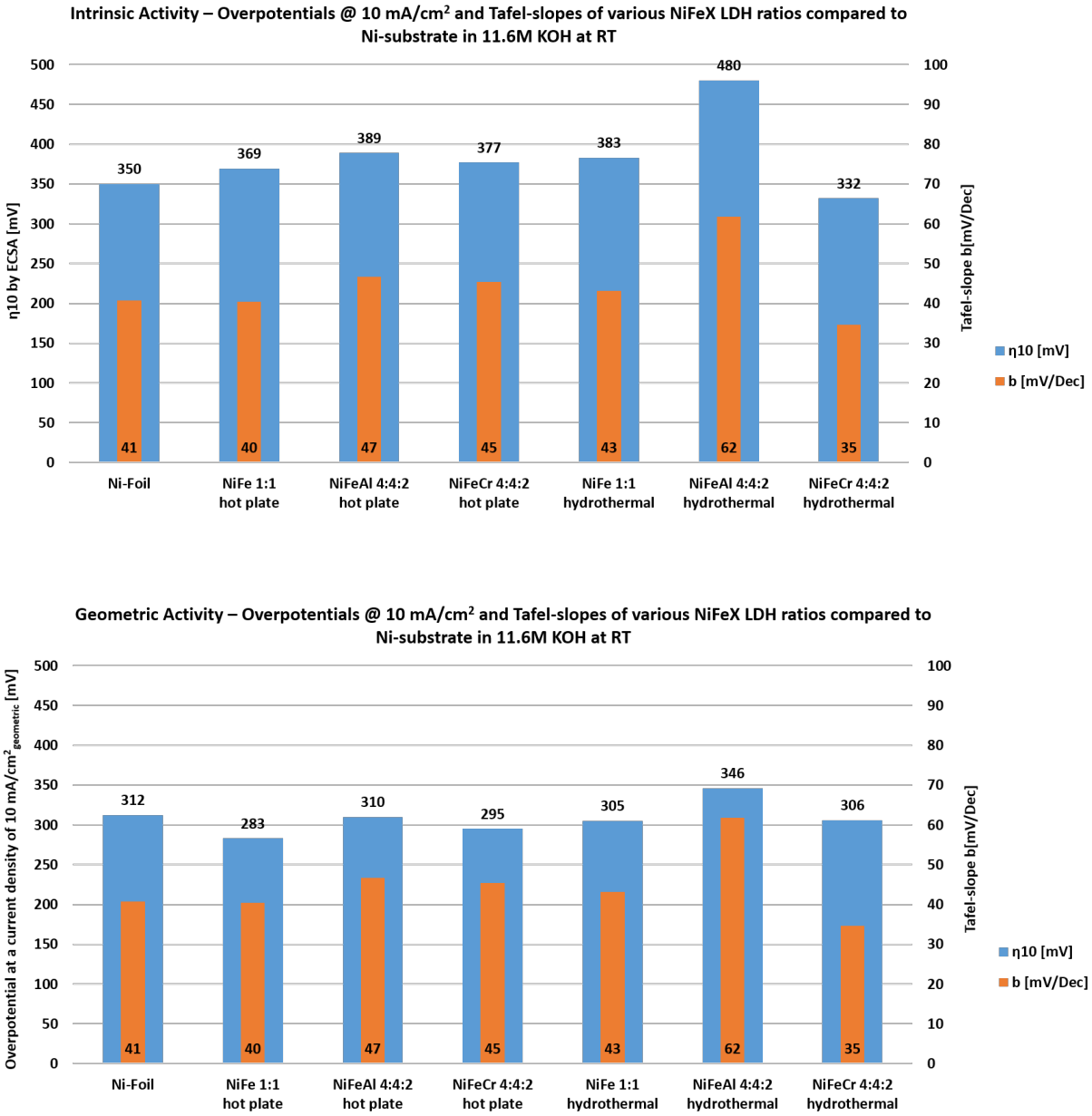

fig. 42: The OER overpotential at top: the intrinsic and bottom: the geometric current density of 10 mA/cm^2 and the correlated Tafel-slopes. Six different NiFeX layered double hydroxide electrocatalysts are shown in comparison to the best achieved Nickel-foil test. The hot plate synthesis took place at 90 $°C$, the hydrothermal synthesis at 120 $°C$. The electrochemical tests were conducted in 11.6 M KOH at room temperature.

LDH electrocatalysts, in particular the availability of proton acceptors in the double layer structure, is crucial for their stability [78].

However, the tested thin-film electrodes were a 1:1 composition, with regards to the Nickel to Iron ratio. As shown in chap. 4.3, DTU Energy investigated the as-synthesized thin-film electrodes with Scanning Electron Microscope, coupled with Energy-Dispersive X-ray spectroscopy. The results showed that the electrodes contained Iron-rich side phases. These observations are in agreement with the literature. As illustrated by Friebel et al, see fig. 43, the synthesis of electrodeposited NiFe LDH produces highly inactive $\gamma - FeOOH$ side phases, for a nominal Iron-content above 20%.

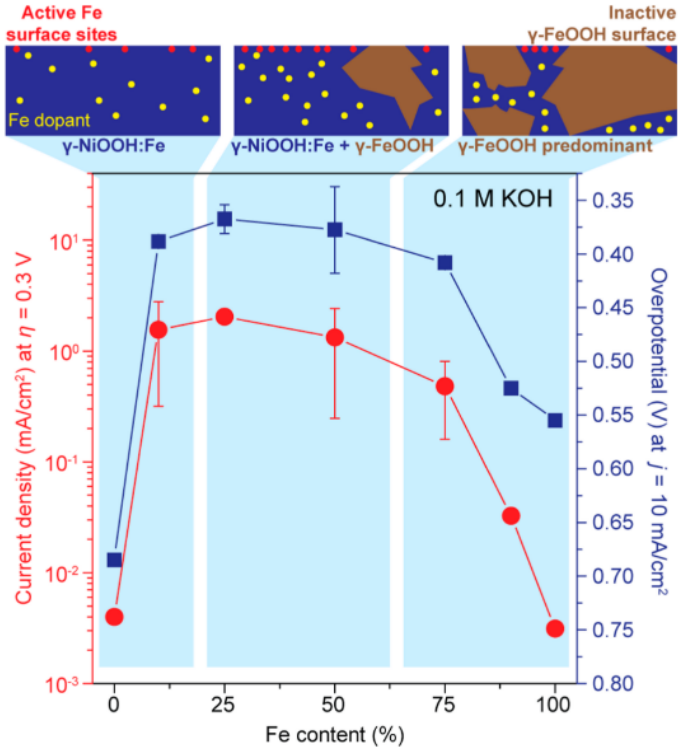

fig. 43: The OER activity of electrodeposited NiFe LDH with respect to the amount of Iron, corresponding to fig. 39. The top of the figure illustrates the influence of increasing Iron-content on the formation of highly active Fe-doped sites to inactive Fe-rich side-phases. Test results from 0.1 M KOH at room temperature. Reproduced from [67].

It is therefore highly likely that the observed degradation of the NiFe, NiFeAl, and NiFeCr LDH electrocatalysts was due to inactive, Iron-rich side-phases. The origin of these side-phases is the nominal composition of 50% Iron, which does not allow for a full incorporation of Iron into the LDH structure, according to the SEM/EDS-analysis and to the literature. This hypothesis is further supported by the high performance of NiFe LDH in 11.6 M KOH. A fully degraded electrocatalyst would not show such a high performance, with overpotentials as low as 283 and 305 mV for 10 $mA/cm^2_{geometric}$ and Tafel-slopes as low as 40-43 mV/Dec.

In conclusion, NiFe LDH electrocatalysts show very promising, high activities. However, it is crucial to further investigate on the origin of the obvious degradation. In this light, DTU Energy will focus on the stability of these well-performing electrocatalysts under technologically relevant conditions and during prolonged measurement times.

As an example, the findings by Chen et al [78] reveal that a higher acidity of the electrolyte causes dissolution of Nickel and Iron, as shown by inductively coupled plasma mass spectrometry. Vice versa, an increased electrolyte alkalinity (e.g. pH $>$ 14 for technical electrolytes), serving as proton acceptor, should rather increase the stability of layered double hydroxide electrocatalysts. The authors further show the stability of exfoliated LDH in 1 M KOH at 80 $°C$ over a measurement time of 20 h. These findings, together with the testing results by DTU Energy in 11.6 M KOH, promise a high stability of LDH OER electrocatalysts, if the origin of the observed degradation is known and avoided. It is therefore necessary to exclude that the degradation is an intrinsic problem, or a problem of the interconnection with the substrate, or if inactive side-phases are the cause.

One major working objective is the focus on the nominal composition of Iron, as it is expected that Iron-contents above 20% cause the observed degradation. Since the literature shows that Iron-compositions of 10-50% show very promising activities, the focus will be set on Iron-contents between 10% (lowest high performing value) and 30% (expected to be just above the incorporation limit) of Iron. A remarkable loss of intrinsic activity is unexpected compared to the 50% NiFe LDH, but the absence of inactive side-phases is expected to increase the stability and therefore the reliability of the LDH electrocatalyst.

4.3 Characterization of the NiFe LDH electrocatalysts

The as-synthesized NiFe LDH electrocatalysts have been investigated by means of Scanning Electron Microscope, coupled with Energy-Dispersive X-ray spectroscopy. The images, as illustrated in fig. 44, show well dispersed nanoplatelets. For comparison, fig. 45 shows SEM images of the reference for the hydrothermal synthesis at 120 $°C$ [73].

The comparison of the images further reveals the success of the synthesized LDH-structure. Both synthesis-methods, the hot plate synthesis at 90 $°C$ and the hydrothermal synthesis at 120 $°C$, result in a full surface coverage of the LDH electrocatalyst, which is responsible for the high electrochemical performance shown in chap. 4.2.2.

In addition, the images indicate a reason for the observed electrolyte-discoloration. As indicated with green crossbars and summarized in tab. 2, EDX displays local differences in the Nickel to

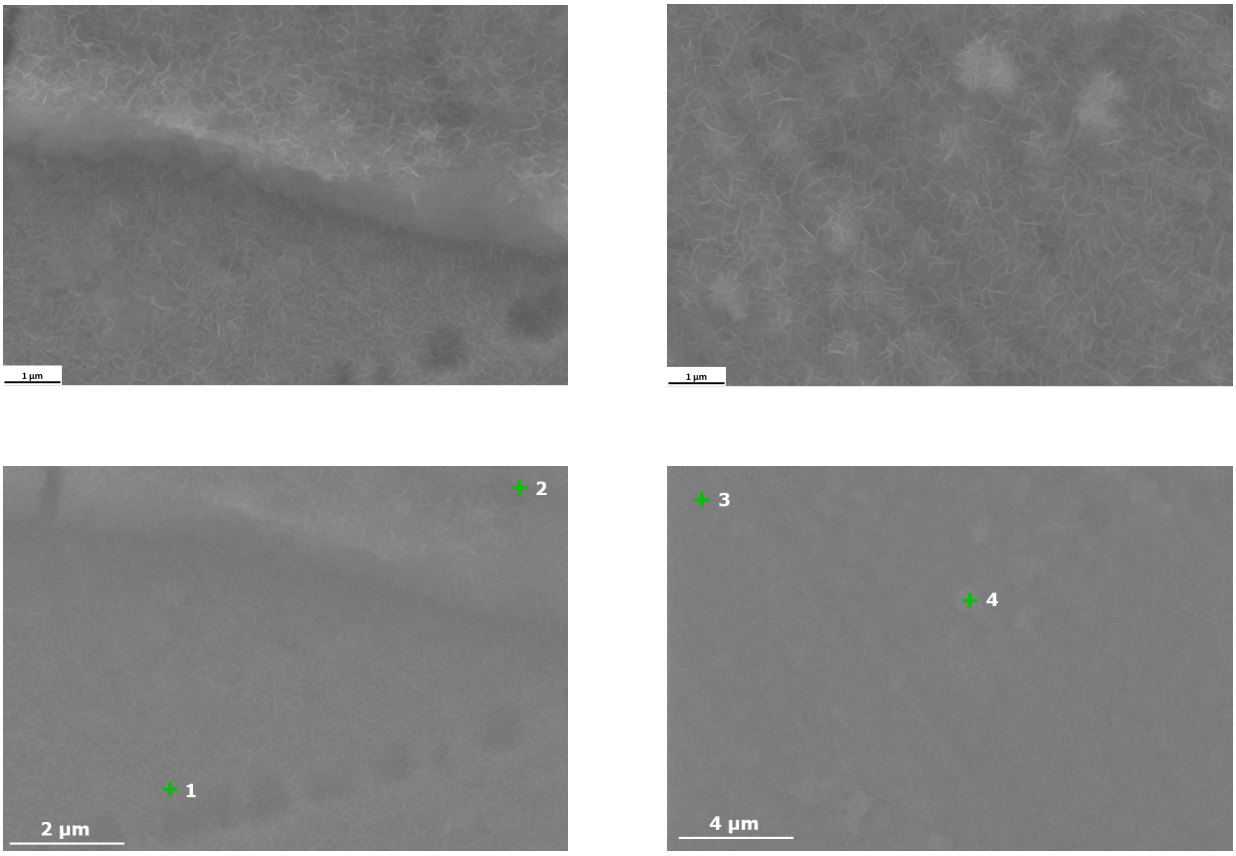

fig. 44: Scanning Electron Microscope images of the pristine NiFe LDH thin-film electrodes, produced by the hotplate synthesis at 90 $°C$ (left) and the hydrothermal synthesis at 120 $°C$ (right). Green crossbars indicating the positions of the EDS measurements, which are shown in tab. 2.

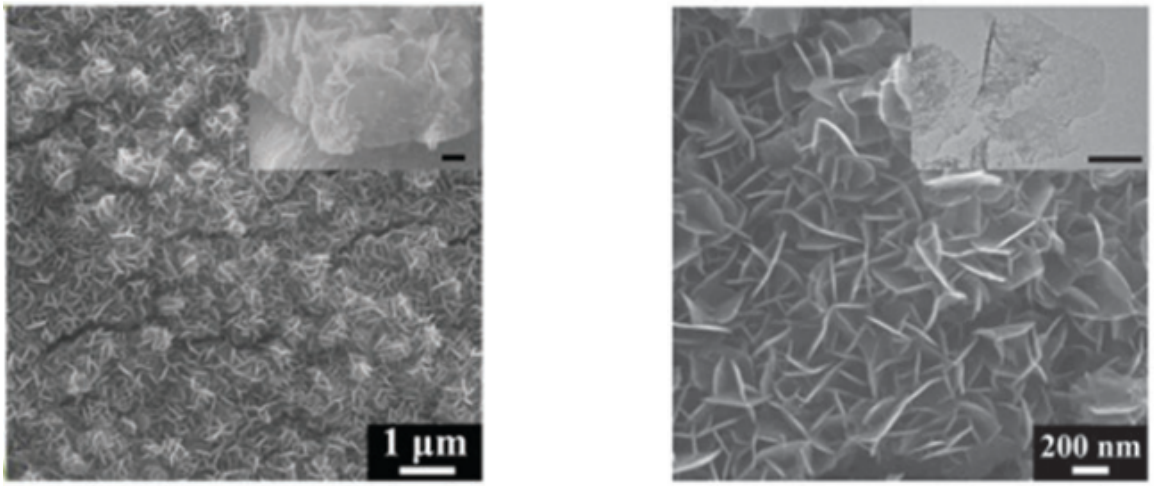

fig. 45: Reference Scanning Electron Microscope images of as-synthesized NiFe LDH by hydrothermal synthesis at 120 $°C$, reproduced from [73].

tab. 2: The EDS results from fig. 44

position	Nickel (at.-%)	Iron (at.-%)	Oxygen (at.-%)	Iron in Ni:Fe (%)
1	94.87	0.36	4.77	0.4
2	40.89	6.45	57.57	13.6
3	78.71	3.36	42.24	4.1
4	65.06	8.45	26.50	11.5

Iron ratio, which are due to unintentionally produced side-phases. As the thin-films are produced on a Nickel-substrate, the measured Iron-content with EDX, due to the measurement depth of this technique, is expected to be low. EDX does not only measure the thin-film, but the Nickel-substrate as well.

The side-phases are particularly Iron-rich, which is backed by the literature, as previously shown in fig. 43. The nominal Iron-content of 50% results in the formation of Iron-rich side-phases, which are mostly Ironoxides and Ironoxihydroxides. These bulk-sized Iron-rich phases are highly inactive.

As a matter of their inactivity and of the electrolyte-pollution, further work will focus on avoiding these Iron-rich phases. Besides the aforementioned change of the nominal Nickel to Iron ratio, the amount of loaded electrocatalyst will be considered as well. It is possible that too high catalyst loadings result in a fragile interconnection, as parts of the electrocatalysts might not directly be interconnected to the substrate but to further electrocatalyst. A second approach can be a mild pretreatment of the nominal 50% electrocatalysts. A pretreatment, e.g. exfoliation, pre-electrolysis or chemical etching, with for instance KOH, can dissolve the problem-causing side-phases before the electrodes are placed in an electrolyzer. This method is of interest, as the studied electrocatalysts in this report are very well-performing. However, this approach would add another manufacturing step. Therefore, the first approach with alterations of the synthesis-method is preferred, unless this approach results in a tremendous, yet unexpected, loss of electrochemical performance.

5 Conclusion

The electrocatalyst testing resulted in the finding of two succesful synthesis methods for each of the water splitting reactions. These four facile, and moreover cost-effective, synthesis methods are conducted with all earth-abundant elements: Nickel, and Molybdenum, and Iron, with a view on further elements, such as Aluminum and Chromium.

NiMo HER electrocatalysts show a benefit from Molybdenum. In comparison to a fresh Nickel electrocatalyst, which is well-performing but degrading quickly, NiMo electrocatalysts display a high performance, with Tafel-slopes reaching 70 mV/Dec and overpotentials at an intrinsic current density of 10 mA/cm^2 of 380 mV, without obvious degradation. The testing results further indicate that the primary descriptor for the high activity is the high electrochemical surface area, which can exceed a surface enhancement factor of 100. Furthermore, the presence of Molybdenum undoubtfully increases the intrinsic electrochemical performance of the electrocatalysts.

Although it remains elusive, if the intrinsic gain is due to the electrochemical activity of Molybdenum, or due to the production of highly active Nickel sites, NiMo electrocatalysts are clearly of higher interest than a pure Nickel electrocatalyst. This is further seen in the higher robustness against a hydrogen-influenced degradation, which has been observed on fresh Nickel, but not on NiMo. These electrocatalysts further allow future adaptions. While the highest performance is gathered for low temperature reduced (400-600 $°C$) NiMo electrocatalysts, with the copresence of Nickelmoybdenumoxide/Molybdenumoxide, a better catalyst interconnection and thus robustness is observed for high temperature reduced (700-800 $°C$) NiMo electrocatalysts, in the absence of oxides. The performance difference between low and high temperature reduced NiMo is marginal, which allows for a trade-off between high performance and electrocatalyst-interconnection, without the loss of the benefits from Molybdenum.

NiFe OER electrocatalysts are high performing in both, low electrolyte concentration (1 M KOH) and high electrolyte concentration (11.6 M KOH). The addition of a third element, specifically Aluminium or Chromium, did not appear to increase the electrochemical performance. However, the high electrolyte case has revealed a technological challenge, which has not been sufficiently addressed in the literature; the electrocatalysts appeared to degrade.

This degradation can be due to three different causes. Firstly, it can be an intrinsic corrosion problem. Secondly, the interconnection of the electrocatalyst with the substrate, or the interconnection

between electrocatalyst, might be insufficient in highly alkaline solutions. Thirdly, the observed degradation can be due to side-phases.

As DTU Energy has observed very high performances in these electrocatalysts, with Tafel-slopes as low as 35-40 mV/Dec and overpotentials at 10 $mA/cm^2_{geometric}$ as low as 283-305 mV, which reach benchmarking literature values, the intrinsic corrosion possibility does not account for the degradation. This is further backed by recent literature.

Furthermore, Iron-rich side-phases have been observed on the high-performing NiFe LDH electrocatalysts by coupled Scanning Electron Microscope/Energy-dispersive X-ray spectroscopy-analysis. These side-phases did not allow for a sufficient surface area correction, as an addition of a pseudocapacitance on the surface area proportional double layer capacitance cannot be outruled. In this perspective, the presumably highly inactive Iron-rich side-phases are expected to cause the observed degradation.

Ultimately, the testing results unquestionably display the benefits of both, NiMo HER and NiFe LDH OER electrocatalysts, over state-of-the-art Nickel. The literature is lacking studies under technological relevant conditions, but the results made by DTU Energy show promisingly high performances in a technologically relevant electrolyte of 11.6 M KOH.

6 Outlook

The electrocatalyst screening results reveal that further studies are required. It is important to understand the behavior of NiMo HER electrocatalysts, in particular if Nickel is the active site. This knowledge will help in a further improvement of the synthesis methods and therefore in increasing the performance and the reliability of the electrocatalyst. For the OER electrocatalysts, it is important to understand their stability and the role of the Iron-rich side-phases.

In both cases, it is of importance for the technical-scale to understand these electrocatalysts on a fundamental level. Thus, DTU Energy has developed a holder that allows to measure electrocatalysts during operating conditions spectroscopically. The holder and its schematic cross-section are shown in fig. 46.

The advantage of this holder is the use of non-model electrodes; any findings can directly be correlated to technical electrodes. Furthermore, the symmetric construction allows for a homogeneous potential distribution, which can be measured with a third electrode. Due to the capillary forces of the working electrode, the electrocatalyst is wetted at all times. The void above the working electrode is further a huge benefit, as any electrode and electrolyte contacting material is suitable for the use with KOH. Furthermore, the use of a gas diffusion electrode as counter electrode avoids gas-crossover and therefore side reactions.

The literature only shows setups for low electrolyte concentrations and room temperature in situ measurements, as the materials in contact with the electrolyte are not KOH corrosion resistant. The holder made by DTU Energy uses KOH resistant materials for electrolyte contacting parts only, which makes spectroelectrochemical measurements under technologically relevant conditions, e.g. 11.6 M KOH and elevated temperatures of up to 100 $^{\circ}C$, possible.

The holder can be used for several spectroscopic techniques, e.g. Raman spectroscopy, X-ray diffraction, and Ambient Pressure X-ray photoelectron spectroscopy. fig. 47 shows the holder operated in Raman spectroscopy and X-ray diffraction as an examploratory application, with a Nickel working electrode and 11.6 M KOH electrolyte.

Furthermore, it is of high importance to study the corrosion resistance of the electrocatalysts over longer measurement times. The catalyst screening results alone cannot address the requirement of a decade-long high performance in technical conditions. In addition, the literature is neglecting this part, which demands these studies to ensure the necessary long-term reliability of the electrocatalysts for the technical application.

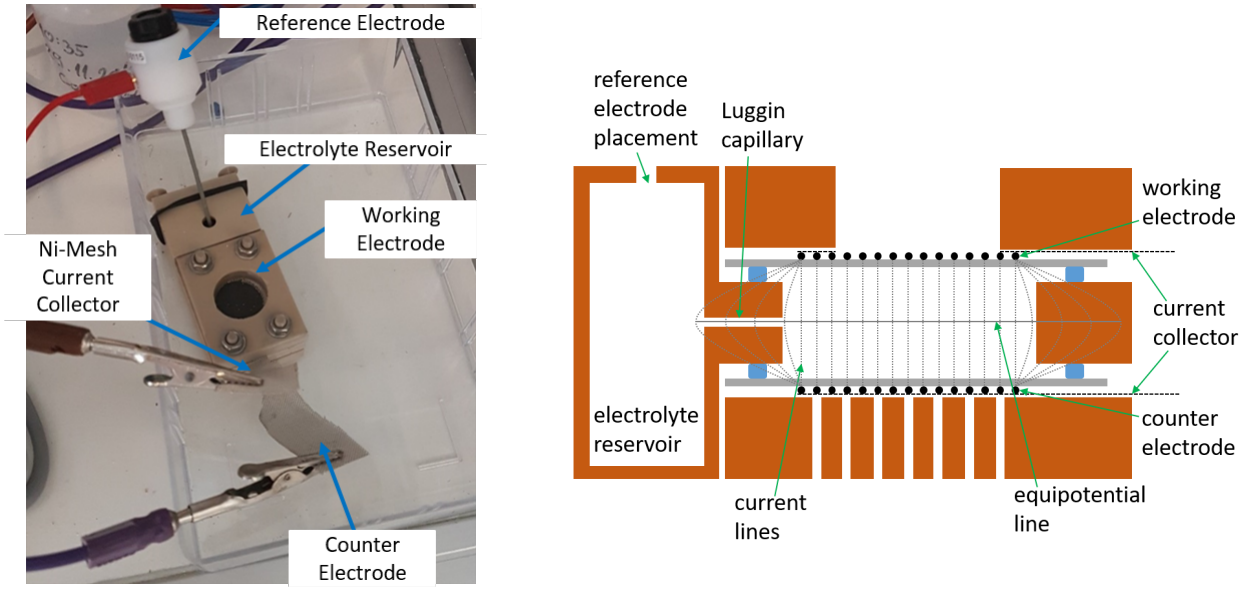

fig. 46: The self-constructed In Operando holder (left) and its schematic cross-section (right).

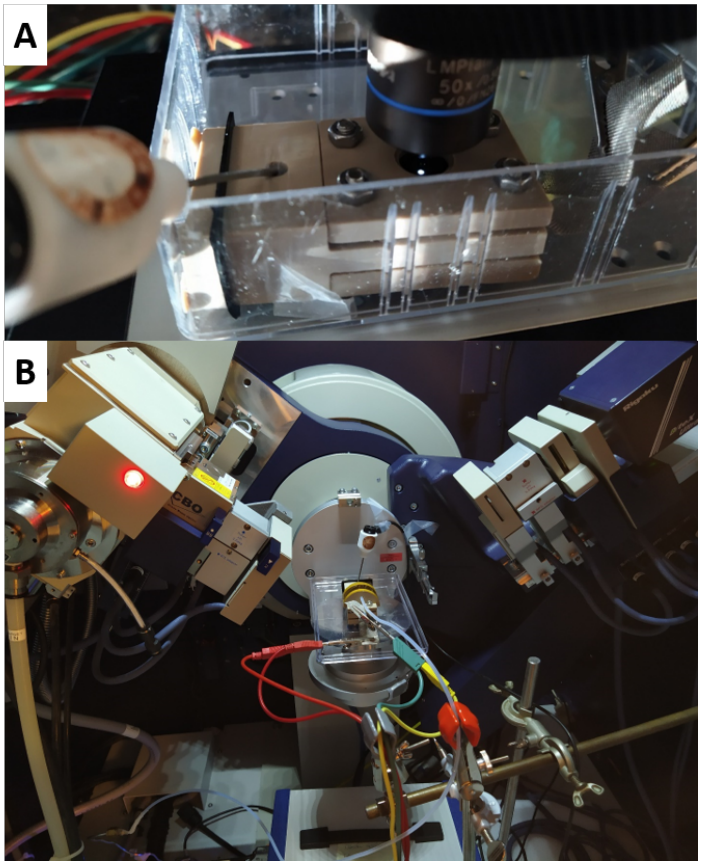

fig. 47: The Operando setup during operation in A: Raman spectroscopy and B: X-ray diffraction. The Raman configuration has a Quartz glas window above the working electrode. The XRD configuration has a round dome with Kapton foil above the working electrode. The gaseous void between the respective lids and the working electrode is inertized with nitrogen.

References

[1] C. C. L. McCrory, S. Jung, I. M. Ferrer, S. M. Chatman, J. C. Peters, and T. F. Jaramillo, Benchmarking hydrogen evolving reaction and oxygen evolving reaction electrocatalysts for solar water splitting devices. Journal of the American Chemical Society, vol. 137, no. 13, pp. 4347–57, 2015.

[2] S. M. Alia and B. S. Pivovar, Evaluating hydrogen evolution and oxidation in alkaline media to establish baselines, Journal of the Electrochemical Society, vol. 165, no. 7, F441–F455, 2018.

[3] J. H. Barber and B. E. Conway, Structural specificity of the kinetics of the hydrogen evolution reaction on the low-index surfaces of Pt single-crystal electrodes in 0.5 M dm-3 NaOH, Journal of Electroanalytical Chemistry, vol. 461, no. 1-2, pp. 80–89, 1999.

[4] P. J. Rheinländer, S. Henning, J. Herranz, and H. A. Gasteiger, Comparing Hydrogen Oxidation and Evolution Reaction Kinetics on Polycrystalline Platinum in 0.1M and 1M KOH, ECS Transactions, vol. 50, no. 2, pp. 2163–2174, 2012.

[5] B. E. Conway and L. Bai, Determination of adsorption of OPD H species in the cathodic hydrogen evolution reaction at Pt in relation to electrocatalysis, Journal of Electroanalytical Chemistry, vol. 198, no. 1, pp. 149–175, 1986.

[6] H. Bode, K. Dehmelt, and J. Witte, Zur Kenntnis der Nickelhydroxidelektrode-I. Uber das Nickel (II)-Hydroxidhydrat, Electrochimica Acta, vol. 11, pp. 1079–1087, 1966.

[7] S. Klaus, Y. Cai, M. W. Louie, L. Trotochaud, and A. T. Bell, Effects of Fe electrolyte impurities on Ni(OH)2/NiOOH structure and oxygen evolution activity, Journal of Physical Chemistry C, vol. 119, no. 13, pp. 7243–7254, 2015.

[8] S. R. Mellsop, A. Gardiner, B. Johannessen, and A. T. Marshall, Structure and transformation of oxy-hydroxide films on Ni anodes below and above the OER potential in alkaline electrolytes, Electrochimica Acta, vol. 168, pp. 356–364, 2015.

[9] D. S. Hall, D. J. Lockwood, C. Bock, B. R. Macdougall, and D. J. Lockwood, Nickel hydroxides and related materials : a review of their structures , synthesis and properties Author for correspondence : Proc. R. Soc. A, vol. 471, 2014.

[10] A. J. Appleby, G. Crepy, and J. Jacquelin, High efficiency water electrolysis in alkaline solution, International Journal of Hydrogen Energy, vol. 3, no. 1, pp. 21–37, 1978.

[11] J. O. Bockris and E. C. Potter, The mechanism of hydrogen evolution at nickel cathodes in aqueous solutions, The Journal of Chemical Physics, vol. 20, no. 4, pp. 614–628, 1952.

[12] E. A. Franceschini, G. I. Lacconi, and H. R. Corti, Kinetics of the hydrogen evolution on nickel in alkaline solution: New insight from rotating disk electrode and impedance spectroscopy analysis, Electrochimica Acta, vol. 159, pp. 210–218, 2015.

[13] A. Gomez Vidales and S. Omanovic, Evaluation of nickel-molybdenum-oxides as cathodes for hydrogen evolution by water electrolysis in acidic, alkaline, and neutral media, Electrochimica Acta, vol. 262, pp. 115–123, 2018.

[14] C. González-Buch, I. Herraiz-Cardona, E. Ortega, J. García-Antón, and V. Pérez-Herranz, Study of the catalytic activity of 3D macroporous Ni and NiMo cathodes for hydrogen production by alkaline water electrolysis, Journal of Applied Electrochemistry, vol. 46, no. 7, pp. 791–803, 2016.

[15] I. Herraiz-Cardona, E. Ortega, J. G. Antón, and V. Pérez-Herranz, Assessment of the roughness factor effect and the intrinsic catalytic activity for hydrogen evolution reaction on Ni-based electrodeposits, International Journal of Hydrogen Energy, vol. 36, no. 16, pp. 9428–9438, 2011.

[16] J. .-.-Y. Huot, Hydrogen Evolution and Interface Phenomena on a Nickel Cathode in 30 w/o KOH, Journal of The Electrochemical Society, vol. 136, no. 7, p. 1933, 2006.

[17] J. M. Jakšić, M. V. Vojnović, and N. V. Krstajić, Kinetic analysis of hydrogen evolution at Ni-Mo alloy electrodes, Electrochimica Acta, vol. 45, no. 25-26, pp. 4151–4158, 2000.

[18] M. F. Kibria, M. S. Mridha, and A. H. Khan, Electrochemical Studies of a Nickel Electrode for the Hydrogen Evolution Reaction, International Journal of Hydrogen Energy, vol. 20, no. 6, pp. 435–440, 1995.

[19] G. Kreysa, B. Håkansson, and P. Ekdunge, Kinetic and Thermodynamic Analysis of Hydrogen Evolution at Nickel Electrodes, Electrochimica Acta, vol. 33, no. 10, pp. 1351–1357, 1988.

[20] N. Krstajić, M. Popović, B. Grgur, M. Vojnović, and D. Šepa, On the kinetics of the hydrogen evolution reaction on nickel in alkaline solution: Part II. Effect of temperature, Journal of Electroanalytical Chemistry, vol. 512, no. 1–2, pp. 27–35, 2001.

[21] Z. Liang, H. S. Ahn, and A. J. Bard, A Study of the Mechanism of the Hydrogen Evolution Reaction on Nickel by Surface Interrogation Scanning Electrochemical Microscopy, Journal of the American Chemical Society, vol. 139, no. 13, pp. 4854–4858, 2017.

[22] S. A. Machado and L. A. Avaca, The hydrogen evolution reaction on nickel surfaces stabilized by H-absorption, Electrochimica Acta, vol. 39, no. 10, pp. 1385–1391, 1994.

[23] A. C. Makrides, Hydrogen Overpotential on Nickel in Alkaline Solution, Journal of The Electrochemical Society, vol. 109, no. 10, p. 977, 2007.

[24] A. G. Oshchepkov, A. Bonnefont, V. N. Parmon, and E. R. Savinova, On the effect of temperature and surface oxidation on the kinetics of hydrogen electrode reactions on nickel in alkaline media, Electrochimica Acta, vol. 269, pp. 111–118, 2018.

[25] R. Palaniappan and G. G. Botte, Effect of ammonia on Pt, Ru, Rh, and Ni cathodes during the alkaline hydrogen evolution reaction, Journal of Physical Chemistry C, vol. 117, no. 34, pp. 17 429–17 441, 2013.

[26] A. G. Oshchepkov, A. Bonnefont, V. A. Saveleva, V. Papaefthimiou, S. Zafeiratos, S. N. Pronkin, V. N. Parmon, and E. R. Savinova, Exploring the Influence of the Nickel Oxide Species on the Kinetics of Hydrogen Electrode Reactions in Alkaline Media, Topics in Catalysis, vol. 59, no. 15-16, pp. 1319–1331, 2016.

[27] M. Alsabet, M. Grden, and G. Jerkiewicz, Electrochemical Growth of Surface Oxides on Nickel. Part 1: Formation of α-(NiOH)2 in Relation to the Polarization Potential, Polarization Time, and Temperature, Electrocatalysis, vol. 2, pp. 317–330, 2011.

[28] M. Grdeń, K. Klimek, and A. Czerwiński, A quartz crystal microbalance study on a metallic nickel electrode, Journal of Solid State Electrochemistry, vol. 8, no. 6, pp. 390–397, 2004.

[29] Z. Liang, H. S. Ahn, and A. J. Bard, Supporting Information for: A Study of the Mechanism of the Hydrogen Evolution Reaction on Nickel by Surface Interrogation Scanning Electrochemical Microscopy, Journal of the American Chemical Society, vol. 139, no. 13, pp. 4854–4858, 2017.

[30] S. L. Medway, C. A. Lucas, A. Kowal, R. J. Nichols, and D. Johnson, In situ studies of the oxidation of nickel electrodes in alkaline solution, Journal of Electroanalytical Chemistry, vol. 587, no. 1, pp. 172–181, 2006.

[31] W. Visscher and E. Barendrecht, Absorption of hydrogen in reduced nickel oxide, Journal of Applied Electrochemistry, vol. 10, no. 2, pp. 269–274, 1980.

[32] A. Pătru, P. Antitomaso, R. Sellin, N. Jerez, P. L. Taberna, and F. Favier, Size and strain dependent activity of Ni nano and micro particles for hydrogen evolution reaction, International Journal of Hydrogen Energy, vol. 38, no. 27, pp. 11 695–11 708, 2013.

[33] N. Takano and S. Kaida, Crack Initiation by Cathodic Hydrogen Charging in Nickel Single Crystal, ISIJ International, vol. 52, no. 2, pp. 263–266, 2012.

[34] D. S. Hall, C. Bock, and B. R. MacDougall, The Electrochemistry of Metallic Nickel: Oxides, Hydroxides, Hydrides and Alkaline Hydrogen Evolution, Journal of The Electrochemical Society, vol. 160, no. 3, F235–F243, 2013.

[35] D. M. Soares, M. U. Kleinke, I. Torriani, and O. Teschke, Deactivation Mechanism of Nickel Cathodes in Alkaline Media, Science, vol. 19, no. 7, 1994.

[36] B. Baranowski, Electrochemical formation of nickel hydride in alkaline solutions, Journal of Electroanalytical Chemistry, vol. 472, no. 2, pp. 182–184, 1999.

[37] D. M. Soares, Hydride Effect on the Kinetics of the Hydrogen Evolution Reaction on Nickel Cathodes in Alkaline Media, Journal of The Electrochemical Society, vol. 139, no. 1, p. 98, 2006.

[38] R. M. Abouatallah, D. W. Kirk, and J. W. Graydon, Long-term electrolytic hydrogen permeation in nickel and the effect of vanadium species addition, Electrochimica Acta, vol. 47, no. 15, pp. 2483–2494, 2002.

[39] M. Grdeń, M. Alsabet, and G. Jerkiewicz, Surface science and electrochemical analysis of nickel foams, ACS Applied Materials and Interfaces, vol. 4, no. 6, pp. 3012–3021, 2012.

[40] A. Lasia, Mechanism and kinetics of the hydrogen evolution reaction, International Journal of Hydrogen Energy, vol. 44, no. 36, pp. 19 484–19 518, 2019.

[41] D. S. Hall, C. Bock, and B. R. MacDougall, An oxalate method for measuring the surface area of nickel electrodes, Journal of the Electrochemical Society, vol. 161, no. 12, H787–H795, 2014.

[42] M. Schalenbach, A. R. Zeradjanin, O. Kasian, S. Cherevko, and K. J. Mayrhofer, A perspective on low-temperature water electrolysis - Challenges in alkaline and acidic technology, International Journal of Electrochemical Science, vol. 13, no. 2, pp. 1173–1226, 2018.

[43] B. E. Conway and L. Bai, Determination of the adsorption behaviour of 'overpotential-deposited' hydrogen-atom species in the cathodic hydrogen-evolution reaction by analysis of potential-relaxation transients, Journal of the Chemical Society, Faraday Transactions 1: Physical Chemistry in Condensed Phases, vol. 81, no. 8, pp. 1841–1862, 1985.

[44] M. Grdeń and G. Jerkiewicz, Influence of Surface Treatment on the Kinetics of the Hydrogen Evolution Reaction on Bulk and Porous Nickel Materials, Electrocatalysis, vol. 10, no. 2, pp. 173–183, 2019.

[45] A. Seyeux, V. Maurice, L. H. Klein, and P. Marcus, In situ scanning tunnelling microscopic study of the initial stages of growth and of the structure of the passive film on Ni(111) in 1 mM NaOH(aq), Journal of Solid State Electrochemistry, vol. 9, no. 5, pp. 337–346, 2005.

[46] B. S. Yeo and A. T. Bell, In situ raman study of nickel oxide and gold-supported nickel oxide catalysts for the electrochemical evolution of oxygen, Journal of Physical Chemistry C, vol. 116, no. 15, pp. 8394–8400, 2012.

[47] D. S. Hall, D. J. Lockwood, S. Poirier, C. Bock, and B. R. MacDougall, Applications of in situ Raman spectroscopy for identifying nickel hydroxide materials and surface layers during chemical aging, ACS Applied Materials and Interfaces, vol. 6, no. 5, pp. 3141–3149, 2014.

[48] D. S. Hall, C. Bock, and B. R. Macdougall, Surface Layers in Alkaline Media: Nickel Hydrides on Metallic Nickel Electrodes, ECS Transactions, vol. 50, no. 31, pp. 165–179, 2013.

[49] T. Shinagawa, A. T. Garcia-Esparza, and K. Takanabe, Insight on Tafel slopes from a microkinetic analysis of aqueous electrocatalysis for energy conversion, Scientific Reports, vol. 5, no. September, pp. 1–21, 2015.

[50] M. E. G. Lyons and M. P. Brandon, The Oxygen Evolution Reaction on Passive Oxide Covered Transition Metal Electrodes in Aqueous Alkaline Solution Part I - Nickel, International Journal of Electrochemical Science, vol. 3, pp. 1425–1462, 2008.

[51] P. W. T. Lu and S. Srinivasan, Electrochemical-Ellipsometric Studies of Oxide Film Formed on Nickel during Oxygen Evolution, Journal of The Electrochemical Society, vol. 125, no. 9, p. 1416, 2006.

[52] J. Kang, Y. Yang, F. Jiang, and H. Shao, Study on the anodic reaction of Ni in an alkaline solution by transient pH detection based on SECM, Surface and Interface Analysis, vol. 39, pp. 877–884, 2007.

[53] M. E. G. Lyons, R. L. Doyle, I. Godwin, M. O'Brien, and L. Russell, Hydrous Nickel Oxide: Redox Switching and the Oxygen Evolution Reaction in Aqueous Alkaline Solution, Journal of The Electrochemical Society, vol. 159, no. 12, H932–H944, 2012.

[54] D. A. Corrigan, The Catalysis of the Oxygen Evolution Reaction by Iron Impurities in Thin Film Nickel Oxide Electrodes, Journal of The Electrochemical Society, vol. 134, no. 2, p. 377, 2006.

[55] T. Rauscher, C. I. Bernäcker, U. Mühle, B. Kieback, and L. Röntzsch, The effect of Fe as constituent in Ni-base alloys on the oxygen evolution reaction in alkaline solutions at high current densities, International Journal of Hydrogen Energy, vol. 44, no. 13, pp. 6392–6402, 2019.

[56] L. Trotochaud, S. L. Young, J. K. Ranney, and S. W. Boettcher, Nickel-Iron oxyhydroxide oxygen-evolution electrocatalysts: The role of intentional and incidental iron incorporation, Journal of the American Chemical Society, vol. 136, no. 18, pp. 6744–6753, 2014.

[57] J. O. Bockris and T. Otagawa, The Electrocatalysis of Oxygen Evolution on Perovskites, Journal of Electrochemical Society, vol. 131, no. 2, pp. 290–302, 1984.

[58] J. Zhang, T. Wang, P. Liu, Z. Liao, S. Liu, X. Zhuang, M. Chen, E. Zschech, and X. Feng, Efficient hydrogen production on MoNi 4 electrocatalysts with fast water dissociation kinetics, Nature Communications, vol. 8, no. May, pp. 1–8, 2017.

[59] V. Umapathy, P. Neeraja, A. Manikandan, and P. Ramu, Synthesis of NiMoO4 nanoparticles by sol-gel method and their structural, morphological, optical, magnetic and photocatalytic properties, Transactions of Nonferrous Metals, vol. China 27, pp. 1785–1793, 2017.

[60] J. R. McKone, B. F. Sadtler, C. A. Werlang, N. S. Lewis, and H. B. Gray, Ni-Mo nanopowders for efficient electrochemical hydrogen evolution, ACS Catalysis, vol. 3, no. 2, pp. 166–169, 2013.

[61] N. Danilovic, R. Subbaraman, D. Strmcnik, K. C. Chang, A. P. Paulikas, V. R. Stamenkovic, and N. M. Markovic, Enhancing the alkaline hydrogen evolution reaction activity through the bifunctionality of Ni(OH)2/metal catalysts, Angewandte Chemie - International Edition, vol. 51, no. 50, pp. 12 495–12 498, 2012.

[62] X. Liu, K. Ni, C. Niu, R. Guo, W. Xi, Z. Wang, J. Meng, J. Li, Y. Zhu, P. Wu, Q. Li, J. Luo, X. Wu, and L. Mai, Upraising the O 2p Orbital by Integrating Ni with MoO 2 for Accelerating Hydrogen Evolution Kinetics, ACS Catalysis, vol. 9, no. 3, pp. 2275–2285, 2019.

[63] T. Wang, X. Wang, Y. Liu, J. Zheng, and X. Li, A highly efficient and stable biphasic nanocrystalline Ni-Mo-N catalyst for hydrogen evolution in both acidic and alkaline electrolytes, Nano Energy, vol. 22, pp. 111–119, 2016.

[64] E. S. Davydova, F. D. Speck, M. T. Y. Paul, D. R. Dekel, and S. Cherevko, Stability Limits of Ni-Based Hydrogen Oxidation Electrocatalysts for Anion Exchange Membrane Fuel Cells, ACS Catalysis, vol. 9, pp. 6837–6845, 2019.

[65] M. Schalenbach, F. D. Speck, M. Ledendecker, O. Kasian, D. Goehl, A. M. Mingers, B. Breitbach, H. Springer, S. Cherevko, and K. J. Mayrhofer, Nickel-molybdenum alloy catalysts for the hydrogen evolution reaction: Activity and stability revised, Electrochimica Acta, vol. 259, pp. 1154–1161, 2018.

[66] P. M. Csernia, J. R. McKone, C. R. Mulzer, W. R. Dichtel, H. D. Abruna, and F. J. DiSalvo, Electrochemical Hydrogen Evolution at Ordered Mo7Ni7, ACS Catalysis, vol. 7, pp. 3375–3383, 2017.

[67] D. Friebel, M. W. Louie, M. Bajdich, K. E. Sanwald, Y. Cai, A. M. Wise, M.-J. Cheng, D. Sokaras, T.-C. Weng, R. Alonso-Mori, R. C. Davis, J. R. Bargar, J. K. Nørskov, A. Nilsson, and A. T. Bell, Identification of highly active Fe sites in (Ni,Fe)OOH for electrocatalytic water splitting. Journal of the American Chemical Society, vol. 137, no. 3, pp. 1305–13, 2015.

[68] K. Zhu, X. Zhu, and W. Yang, Application of In Situ Techniques for the Characterization of NiFe-Based Oxygen Evolution Reaction (OER) Electrocatalysts, Angewandte Chemie - International Edition, vol. 58, no. 5, pp. 1252–1265, 2019.

[69] M. B. Stevens, C. D. Trang, L. J. Enman, J. Deng, and S. W. Boettcher, Reactive Fe-Sites in Ni/Fe (Oxy)hydroxide Are Responsible for Exceptional Oxygen Electrocatalysis Activity, Journal of the American Chemical Society, vol. 139, no. 33, pp. 11 361–11 364, 2017.

[70] F. Dionigi and P. Strasser, NiFe-Based (Oxy)hydroxide Catalysts for Oxygen Evolution Reaction in Non-Acidic Electrolytes, Advanced Energy Materials, vol. 6, no. 23, 2016.

[71] M. W. Louie and A. T. Bell, An investigation of thin-film Ni-Fe oxide catalysts for the electrochemical evolution of oxygen, Journal of the American Chemical Society, vol. 135, no. 33, pp. 12 329–12 337, 2013.

[72] A. S. Batchellor and S. W. Boettcher, Pulse-Electrodeposited Ni-Fe (Oxy)hydroxide Oxygen Evolution Electrocatalysts with High Geometric and Intrinsic Activities at Large Mass Loadings, ACS Catalysis, vol. 5, no. 11, pp. 6680–6689, 2015.

[73] Z. Lu, W. Xu, W. Zhu, Q. Yang, X. Lei, J. Liu, Y. Li, X. Sun, and X. Duan, Three-dimensional NiFe layered double hydroxide film for high-efficiency oxygen evolution reaction, Chemical Communications, vol. 50, no. 49, pp. 6479–6482, 2014.

[74] F. Song and X. Hu, Exfoliation of layered double hydroxides for enhanced oxygen evolution catalysis, Nature Communications, vol. 5, no. 4477, 2014.

[75] R. Li, Z. Hu, X. Shao, P. Cheng, S. Li, W. Yu, W. Lin, and D. Yuan, Large scale synthesis of NiCo layered double hydroxides for superior asymmetric electrochemical capacitor, Scientific Reports, vol. 6, no. September 2015, pp. 1–9, 2016.

[76] T. Li, G. H. Li, L. H. Li, L. Liu, Y. Xu, H. Y. Ding, and T. Zhang, Large-Scale Self-Assembly of 3D Flower-like Hierarchical Ni/Co-LDHs Microspheres for High-Performance Flexible Asymmetric Supercapacitors, ACS Applied Materials and Interfaces, vol. 8, no. 4, pp. 2562–2572, 2016.

[77] J. B. Gerken, S. E. Shaner, R. C. Massé, N. J. Porubsky, and S. S. Stahl, A survey of diverse earth abundant oxygen evolution electrocatalysts showing enhanced activity from Ni-Fe oxides containing a third metal, Energy and Environmental Science, vol. 7, no. 7, pp. 2376–2382, 2014.

[78] R. Chen, S. Hung, D. Zhou, J. Gao, C. Yang, H. Tao, H. B. Yang, L. Zhang, L. Zhang, Q. Xiong, H. M. Chen, and B. Liu, Layered Structure Causes Bulk NiFe Layered Double Hydroxide Unstable in Alkaline Oxygen Evolution Reaction, Advanced Materials, vol. 1903909, p. 1 903 909, 2019.

List of Figures

List of Tables

Appendices

A Kinetic Literature Values for the HER on Nickel

tab. 3: The kinetic values plotted in chap. 2.2. Bold marked sources show the as "intrinsic" denoted values. The overpotential at 10 mA/cm^2 (η_{10}) is either given by the authors, or otherwise calculated with the Tafel-equation.

Electrolyte	Concentration	Tafel-slope $[mV/Dec]$	$i_0[mA/cm^2]$	pH	$\eta_{10}[mV]$	Source
KOH	34%	103	0.00009	14.9	520	[10]
NaOH	0.1 M	101	0.000398	13	444	[11]
KOH	1 M	249	0.000121	14	n/a	[12]
KOH	1 M	167	0.000000691	14	n/a	[12]
NaOH	1 M	145	0.0013	14	563	**[13]**
KOH	30%	95	0.11	14.8	186	[14]
KOH	30%	98	0.00007	14.8	505	**[15]**
KOH	30%	115	0.0355	14.8	282	[16]
NaOH	1 M	121	0.0033	14	421	**[17]**
KOH	30%	80	n/a	14.8	177	[18]
KOH	1 M	136	n/a	14	n/a	[19]
KOH	1 M	87	n/a	14	n/a	[19]
NaOH	1 M	116	0.00076	14	478	[20]
NaOH	1 M	122	0.0019	14	454	[20]
KOH	0.01 M	120	0.266	12	189	[21]
NaOH	0.5 M	123	0.00344	13.7	426	**[22]**
NaOH	0.1 M	90	0.0095	13	272	[23]
NaOH	0.1 M	130	0.025	13	338	[23]
NaOH	0.1 M	115	0.0022	13	421	**[24]**
KOH	5 M	95	0.0005	14.7	409	**[25]**

B Cleaning of Nickel substrates

Nickel substrates, foils in case of thin-film electrodes, are cleaned in three steps. Firstly, a mild mechanical polishing with sandpaper is conducted. Secondly, chemical etching is conducted in an ultrasound bath for five minutes in 5 M HCl. Thirdly, after rinsing with deionized water, another five minutes ultrasound treatment are added, with Ethanol as solvent.

C Synthesis methods of NiMo electrocatalysts

All three different Nickelmolybdenumoxides are drop-casted on Nickel-foils utilizing Isopropanol as solvent to produce thin-film electrodes. As a matter of processability, several iterative approaches resulted in different mass loadings in the drop-casting solutions and on the final thin-film electrodes to produce fully covered, homogeneous electrocatalyst surfaces.

C.1 NiMo Cuboids - hydrothermal synthesis

The hydrothermal synthesis of Nickelmolybdenumoxide, denoted as Cuboids, is based on the publication of Zhang et al [58]. A Teflon-lined autoclave of 100 mL is washed with concentrated nitric acid and thoroughly rinsed with distilled water. After drying, solutions of $Ni(NO_3)_2 \cdot 6H_2O$ (0.08 M) and $(NH_4)_6Mo_7O_{24} \cdot 4H_2O$ (0.02 M) are added 50:50 b/v to the autoclave, filling up the entire volume of the autoclave.

The autoclave is placed in a furnace, heated to 150 $°C$ with 120 $°C/h$, held 6 hours at 150 $°C$ and then cooled to room temperature with 120 $°C/h$. The resulting powder is of green/yellow color.

Nickel-foils, in a rectangular shape of $25 \cdot 25\ mm$, are cleaned as described above. A solution of 0.75 wt% Nickelmolybdenumoxides in Isopropanol is prepared with five minutes of ultrasound bath. Sequential drop-casting of $20\ \mu L$ portions of this solution, including tilting of the foils for a homogeneous distribution, up to a total drop-casted amount of $200\ \mu L$ results in a mass loading of $188.64\ \mu g/cm^2$.

C.2 NiMo Solgel - solgel synthesis

The Solgel synthesis method, denoted as Solgel, is based on the publication of Umapathy et al [59]. 3 g ethyl cellulose (DS 1.2) is sprinkled slowly under continuous stirring into deionized water at 50 $°C/h$. 17.7 g of $(NH_4)_6Mo_7O_{24} \cdot 4H_2O$, and 29.1 g of $Ni(NO_3)_2 \cdot 6H_2O$, and 10 g of citric acid are each dissolved seperately in 50 mL deionized water. These three solutions are slowly added under stirring to the ethyl cellulose solution at 50 $°C/h$ to form the sol. Slow heating to 90 $°C/h$ results in a wet gel. The wet gel is dried at 105 $°C/h$ for 1 h in hot air, and then calcined at 650 $°C/h$ for 2 h.

The drop-casting was done with a 1 wt% solution in Isopropanol, and a total amount of $300\ \mu L$ results in a mass loading of $377.28\ \mu g/cm^2$.

C.3 NiMo Coprecip - coprecipitation synthesis

The Coprecipitation synthesis, denoted as Coprecip, is based on the publication of McKone et al [60]. 5.2 mmol of $Ni(NO_3)_2 \cdot 6H_2O$ and 3.4 mmol (calculated on Molybdenum) of $(NH_4)_6Mo_7O_{24} \cdot 4H_2O$ were added to 5 mL deionized water. 2 mL of ammonium hydroxide (30%) are added, forming a deep blue solution. The resulting solution was added at once into 45 mL diethylene glycol, and heated to about $110\ ^\circ C$. The resoluting suspension was centrifuged, while still being hot. The obtained solid fraction is washed with deionized water and sonicated once. This procedure has been repeated with acetone as solvent. The final solid is added to a crystallization dish and wetted with methanol. After several hours of crystallization at $60\ ^\circ C$, a green solid is gathered.

The drop-casting was done with a 2 wt% solution in Isopropanol, and a total amount of $300\ \mu L$ results in a mass loading of $754.56\ \mu g/cm^2$.

D Synthesis methods of NiFe LDH electrocatalysts

D.1 NiFe 120C - hydrothermal synthesis at 120C

The hydrothermal synthesis at 120 $°C$ is based on the publication of Lu et al [73]. A Teflon-lined autoclave of 100 mL is washed with concentrated nitric acid and thoroughly rinsed with distilled water. After drying, the autoclave is filled with 80 mL of deionized water and degassed with high purity Argon for a minimum of 5 minutes. A total of 10 mM of transition-metals and 40 mM of urea are added to the autoclave. For an autoclave of 100 mL, this reflects 145.4 mg of $Ni(NO_3)_2 \cdot 6H_2O$, and 202.0 mg of $Fe(NO_3)_3 \cdot 9H_2O$, and 240.0 mg of $CO(NH_2)_2$. The cleaned Nickel-substrate is added to the solution and the residual empty volume of the autoclave filled with deionized water. The autoclave is closed and placed in a furnace, where the hydrothermal synthesis takes place at 120 $°C$ for 12 h (heating ramp: 120 $°C/h$).

D.2 NiFe 90C - precipitation synthesis at 90C

The precipitation synthesis at 90 $°C$ is based on the publication of Li et al [75]. In a similar fashion to the hydrothermal synthesis at 120 $°C$, 5 mM of $Ni(NO_3)_2 \cdot 6H_2O$ and 5 mM of $Fe(NO_3)_3 \cdot 9H_2O$ are dissolved in a mixture of 30 mL deionized water and 75 mL ethylene glycol. Under continuous stirring, 40 mM of $CO(NH_2)_2$ and the cleaned Nickel-substrate are added. The solution is sealed to the ambient to avoid oxygen intake. Heating to 90 $°C$ for 3 h results in the formation of a brownish film on the Nickel-substrate. This method has been conducted on a hot plate at first, in a second approach the synthesis was conducted in an oven, to ensure a homogeneous temperature distribution. For the second approach, the amounts were 6.66 mM of $Ni(NO_3)_2 \cdot 6H_2O$ and 3.33 mM of $Fe(NO_3)_3 \cdot 9H_2O$.

D.3 NiFe 55C - precipitation synthesis at 55C

The precipitation synthesis at 55 $°C$ is based on the publication of Li et al [76]. In a similar fashion to the precipitation synthesis at 90 $°C$, the precipitation at 55 $°C$ was conducted in an oven, with the

Nickel-substrate immersed in the reactant solution. 0.45 mM of $NiCl_2$, 0.30 mM of $FeCl_2$, 4 mM of NH_4Cl, and 1.375 mmol of $NaOH$ are added to deionized water. The synthesis takes place at 55 $°C$ for 15 h.

D.4 NiFe 150C - hydrothermal synthesis at 150C

The hydrothermal synthesis at 150 $°C$ is based on the publication of Song and Hu [74]. The synthesis is, in principal, similar to the hydrothermal synthesis at 120 $°C$. A deviation, besides the reaction temperature of 150 $°C$ and the reaction time of 2 days, is the addition of 12.5 mM of triethanolamine (TEA).